

Dual transcriptomic and proteomic analysis of
intestinal epithelial cell response to *Citrobacter*
rodentium infection in mice

Thesis presented by

Teresa Paradell Gil

In candidature for the degree of Doctor of Philosophy

Microbiomes, Microbes and Informatics Group,

School of Biosciences,

Cardiff University

September 2024

Acknowledgements

I'd like to give a huge thank you to everyone who supported and encouraged me throughout this PhD journey.

First off, a big shoutout to my supervisor, Dr Cedric Berger. Thank you for giving me the opportunity to start this journey, believing in me from the start (even when my English was still a work in progress), teaching me invaluable lab skills, and offering daily encouragement. Despite the many challenges over the years, your steady support made everything much easier. I'm very grateful to have had you as my supervisor.

I would like to thank Dr. Daniel Pass for his invaluable assistance and support with the bioinformatics analysis, which was essential to this work.

A huge thanks to everyone in the Microbes, Microbiomes, and Informatics (MMI) group, both past and present. Special thanks to Dr Kasia Parfitt and Dr Yoana Petrova, for always being there with your unconditional support, both in and out of the office. To Dr Katherine Smith, Dr Laura Rushton, Ms Ella Reed, Dr Alex Mullins and Dr Franek Bydalek, for all the help in the lab, the lunchtime and tea breaks, and the friendly chats.

Doyle, thank you for taking care of my cells, keeping me entertained with your singing and chats in Spanish, and just being such a great person to be around. It's been a pleasure working with you!

To my family and friends in Spain—thank you for believing in me, making the trips to Cardiff, and letting me unwind during my visits to Vigo. To my friends Rosiña and Juan, thank you for all the visits to Coruña, Vigo, and Santiago, and for always making time for each other. A special thanks to my parents for their constant support, even from thousands of kilometres away, and for always being there to lift my spirits over the phone. ¡Gracias!

Last but certainly not least, to my partner and favourite person, Nico Bruyniks. Thank you for making me laugh every day, for all the silliness, and for comforting me when I needed it most. Your support has been invaluable during this adventure, and I hope I can be just as supportive when it's your turn.

Thank you all so much!

Abstract

Citrobacter rodentium is a natural mouse pathogen and the etiological agent of transmissible murine colonic hyperplasia (CCH). As a member of the Attaching and Effacing (AE) pathogens, *C. rodentium* shares a similar infection strategy with Enteropathogenic *Escherichia coli* (EPEC) and Enterohemorrhagic *E. coli* (EHEC), two human pathogens responsible for diarrhoeal diseases that contribute significantly to morbidity and mortality worldwide. Since mice are resistant to EPEC and EHEC infections, *C. rodentium* provides an ideal surrogate model for in vivo studies to better understand the mechanisms of infection of AE pathogens.

In this study, we aimed to elucidate the infection mechanisms of *C. rodentium* by investigating the transcriptome and proteome profiles of infected intestinal epithelial cells (IECs) in mice. Through the combined analysis of gene expression and protein patterns, we identified key regulatory pathways related to immune responses, inflammation, and metabolism. These included the upregulation of the pentose phosphate pathway, the ubiquitin-proteasome system, and the prostaglandin biosynthesis pathway. Additionally, the dual analysis demonstrated that the disruption of microvilli and mitochondria in infected IECs was due to the active destruction of these structures, as evidenced by a marked reduction in their protein levels, despite no changes being observed at the RNA levels. Additionally, we investigated the mRNA and protein targets of altered microRNA (miRNA) during *C. rodentium* infection. Our findings revealed no correlation between the miRNA levels, their corresponding mRNA targets, and the resulting protein levels. This lack of correlation suggests that the bacteria target the miRNA system potentially to promote disease progression.

In summary, this research provides significant insights into the complex host-pathogen interactions during *C. rodentium* infection, contributing to a deeper understanding of similar AE pathogens such as EPEC and EHEC. This study enhances our understanding of infectious diseases by identifying crucial pathways that could be explored for diagnostic or therapeutic innovation.

Table of Contents

1	CHAPTER 1: Introduction.	1
1.1	Foodborne diseases.	1
1.2	<i>Escherichia coli</i>	2
1.2.1	Pathotypes.	3
1.2.2	Enteropathogenic <i>E. coli</i>	3
1.2.3	Enterohemorrhagic <i>E. coli</i>	4
1.2.4	EPEC and EHEC differences.	5
1.3	Attaching and effacing pathogens.	6
1.4	Type three secretion system.	7
1.5	T3SS Effectors.	9
1.6	<i>Citrobacter rodentium</i>	11
1.6.1	<i>C. rodentium</i> and host cell metabolism.	13
1.6.2	Host miRNome and <i>C. rodentium</i>	15
1.6.3	Host immune response to <i>C. rodentium</i>	17
1.6.4	Host microbiome and <i>C. rodentium</i> infection.	20
1.7	Aims and Objectives.	22
2	CHAPTER 2: Materials and Methods.	24
2.1	Microbial strains and growth conditions.	24
2.1.1	Microbial strains.	24
2.1.2	Bacterial media.	24
2.1.3	Storage.	24
2.1.4	Growth conditions.	24
2.2	In vivo experiments.	25
2.2.1	Mouse husbandry.	25

2.2.2	Preparation of culture and infection of mice.	25
2.2.3	Aspirin preparation and administration.	26
2.2.4	<i>C. rodentium</i> faecal enumeration.	26
2.2.5	Tissue sample collection.	26
2.2.5.1	Intestinal epithelial cell isolation.	26
2.2.5.2	Histological analyses.	27
2.3	RNA sequencing and bioinformatic analysis.	27
2.3.1	RNA sequencing sample preparation.	27
2.3.2	RNA sequencing.	27
2.3.3	Bioinformatic analysis.	28
2.4	Proteome.	29
2.5	Lipocalin-2 ELISA assay.	30
2.6	Molecular biology techniques.	30
2.6.1	Plasmids.	30
2.6.2	Plasmid DNA extraction.	31
2.6.3	Expression vector - pMMLV-Puro-HA-Ago proteins.	31
2.7	Cell culture techniques.	33
2.7.1	Cell culture media.	33
2.7.2	Cell line subculturing.	33
2.7.3	Cell line cryopreservation.	34
2.7.4	Recovery of cryopreserved cells.	34
2.8	Transfection assay.	34
2.9	Transduction assay.	35
2.10	Infection of cells.	37
2.11	Immunofluorescence.	38
2.12	Western Blot.	39

2.12.1	Cell sample preparation.....	39
2.12.2	Protein BCA assay.	39
2.12.3	SDS-PAGE.	40
2.12.4	Membrane transference.....	41
2.13	Statistical analysis.....	41
3	CHAPTER 3: Intestinal epithelial cells response to <i>Citrobacter rodentium</i> infection at the RNA level.....	43
3.1	Introduction.....	43
3.2	Aims and Objectives.....	44
3.3	Results.....	45
3.3.1	Mice colonisation and crypt hyperplasia development.	45
3.3.2	RNA sequencing analysis of <i>C. rodentium</i> -infected cells.....	46
3.3.3	Transcriptome analysis of <i>C. rodentium</i> -infected intestinal epithelial cells.....	48
3.3.4	Subcellular location of the products of differentially expressed genes.	52
3.3.5	Pathway alterations during <i>C. rodentium</i> infection.....	53
3.4	Discussion.....	59
3.4.1	Transcriptome of <i>C. rodentium</i> -infected intestinal epithelial cells.	59
3.4.2	Pathway analysis and novel findings during <i>C. rodentium</i> infection.....	60
3.4.3	Identification of secreted proteins in response to infection.	60
3.4.4	<i>C. rodentium</i> induces metabolic changes in intestinal epithelial cells.	62
3.4.5	Ubiquitin-Proteasome system and <i>C. rodentium</i>	63
3.5	Conclusions.....	66
4	CHAPTER 4: Comparative analysis - Understanding transcriptome and proteome of <i>C. rodentium</i> -infected intestinal epithelial cells.....	68
4.1	Introduction.....	68
4.2	Aims and Objectives.....	69

4.3	Results.....	70
4.3.1	Transcriptome and proteome of <i>C. rodentium</i> -infected enterocytes.....	70
4.3.2	Antimicrobial response of intestinal epithelial cells during <i>C. rodentium</i> infection.....	73
4.3.3	Cholesterol metabolism of intestinal epithelial cells during <i>C. rodentium</i> infection.....	74
4.3.4	Impact of <i>C. rodentium</i> infection on microvilli of intestinal epithelial cells.....	76
4.3.5	Effects of <i>C. rodentium</i> on the mitochondria of intestinal epithelial cells.....	78
4.4	Discussion.....	83
4.4.1	Integrative analysis of transcriptome and proteome of <i>C. rodentium</i> -infected enterocytes.....	83
4.4.2	<i>C. rodentium</i> infection induces changes in the host enterocyte.....	84
4.4.3	Cell proliferation and DNA replication molecules are enhanced during <i>C. rodentium</i> infection.....	86
4.5	Conclusions.....	88
5	CHAPTER 5: Prostaglandin biosynthesis regulation during <i>Citrobacter rodentium</i> infection.....	90
5.1	Introduction.....	90
5.2	Aims and Objectives.....	91
5.3	Results.....	92
5.3.1	The prostaglandin biosynthesis pathway is altered during <i>Citrobacter rodentium</i> infection.....	92
5.3.2	Effect of prostaglandin metabolism pathway on <i>C. rodentium</i> infection.....	97
5.4	Discussion.....	101
5.4.1	Prostaglandin profile of <i>C. rodentium</i> -infected enterocytes.....	101
5.4.2	Annexin A1 effects on <i>C. rodentium</i> infection.....	102
5.4.3	Prostaglandin metabolism is reduced during <i>C. rodentium</i> infection.....	103

5.4.4	Aspirin effects on <i>C. rodentium</i> infection.	104
5.5	Conclusions.....	107
6	CHAPTER 6: Establish how the RNA-induced Silencing Complex (RISC) is regulated during <i>C. rodentium</i> infection.	109
6.1	Introduction.....	109
6.2	Aims and Objectives.....	110
6.3	Results.	111
6.3.1	Changes in miRNA during <i>C. rodentium</i> infection.	111
6.3.2	<i>C. rodentium</i> and the RNA-induced Silencing Complex (RISC).	115
6.3.3	<i>C. rodentium</i> and the Ago1 and Ago2 proteins.	117
6.4	Discussion.....	121
6.4.1	miRNA system and <i>C. rodentium</i>	121
6.4.2	Argonaute proteins and <i>C. rodentium</i>	122
6.5	Conclusions.....	125
7	CHAPTER 7: General conclusions and future directions.....	127
7.1	General conclusions.	127
7.2	Overall discussion.....	130
7.2.1	Manipulation of the Ubiquitin-Proteasome System.....	130
7.2.2	Exploitation of the Pentose Phosphate Pathway.	130
7.2.3	Prostaglandins in pathogen-mediated immune modulation.	131
7.2.4	miRNA system in host-pathogen interactions.	132
7.3	Future directions.	132
7.4	Final summary.	135
	REFERENCES.....	137

List of Figures

Figure 1.1. Pedestal formation in AE pathogens.....	7
Figure 1.2. Structure of the Type Three Secretion System.....	8
Figure 1.3. Locus of Enterocyte Effacement of EPEC.	9
Figure 1.4. miRNA synthesis and functions.....	15
Figure 1.5. Phases of <i>Citrobacter rodentium</i> infection.....	18
Figure 2.1. pMMLV-Puro-HA-Ago vector structure.	32
Figure 2.2. Viral transduction.	36
Figure 3.1. <i>Citrobacter rodentium</i> colonisation in infected mice.	45
Figure 3.2. Histological analysis and crypt length comparison of <i>C. rodentium</i> -infected and non-infected colon tissue.....	46
Figure 3.3. Cluster dendrogram showing separation of samples into groups.....	48
Figure 3.4. Differential regulation of intestinal epithelial cell genes during <i>C. rodentium</i> infection.....	49
Figure 3.5. Top 20 upregulated and downregulated genes during infection.	51
Figure 3.6. Subcellular location of detected proteins.....	52
Figure 3.7. Percentage of associated genes per pathway affected during <i>C. rodentium</i> infection.....	54
Figure 3.8. Altered pathways during mice infection with <i>Citrobacter rodentium</i>	55
Figure 3.9. Upregulation of the pentose phosphate pathway during infection.....	56
Figure 3.10. Proteasome subunits structure and expression during infection.....	57
Figure 3.11. Ubiquitin-proteasome system and <i>C. rodentium</i> infection.	58
Figure 4.1. Transcriptome and proteome of <i>C. rodentium</i> -infected enterocytes.....	70
Figure 4.2. Comparison of gene expression and protein abundance changes in <i>C. rodentium</i> -infected enterocytes.	72
Figure 4.3. Infection with <i>C. rodentium</i> triggers antimicrobial gene expression and antimicrobial protein production.	74
Figure 4.4. <i>C. rodentium</i> induces upregulation of cholesterol metabolism.	75
Figure 4.5. Microvilli structure of intestinal epithelial cells during <i>C. rodentium</i> infection.	77
Figure 4.6. Key components of mitochondrial structure.....	78

Figure 4.7. Mitochondrial gene expression and protein abundance.	79
Figure 4.8. Effects of <i>C. rodentium</i> infection on mitochondrial OXPHOS proteins.	80
Figure 4.9. Effects of <i>Citrobacter rodentium</i> infection on mitochondrial morphology.	82
Figure 5.1. Prostaglandin metabolism regulation in <i>C. rodentium</i> infection.	92
Figure 5.2. Modulation of prostaglandin biosynthesis in <i>C. rodentium</i> infection: integration of transcriptome and proteome data.	94
Figure 5.3. Regulation of prostaglandins biosynthesis in <i>C. rodentium</i> infection.	96
Figure 5.4. <i>C. rodentium</i> colonisation and mice weight at day 7 and day 8 post-infection.	98
Figure 5.5. Impact of aspirin treatment on colonic crypt hyperplasia development.	99
Figure 5.6. Lipocalin-2 levels during <i>C. rodentium</i> infection at 5 and 8 days post-infection.	100
Figure 6.1. Post-transcriptional regulation: impact of microRNAs and pathogenic bacteria.	109
Figure 6.2. miRNAs and <i>C. rodentium</i> infection.	111
Figure 6.3. Diagram showing the effect of miRNAs on mRNA and protein abundance.	112
Figure 6.4. <i>C. rodentium</i> and miRNA targets.	113
Figure 6.5. Integrated transcriptome and proteome heatmaps of predicted targets of mmu-miR-92a-2-5p and mmu-miR-361-3p.	115
Figure 6.6. Overview of miRNA synthesis process.	116
Figure 6.7. Gene expression and protein abundance of miRNA system proteins.	117
Figure 6.8. Western Blot result shows HA-Ago 1 and HA-Ago2 expression in HeLa and CMT93 cells.	118
Figure 6.9. Western Blot analysis of HA-Ago1/Ago2 levels in CMT93 cells after 6h infection.	119

List of Tables

Table 1.1. STEC cases in England and Wales.	5
Table 2.1. Bacterial strains used in this study.	24
Table 2.2. Dilutions used for Lipocalin-2 ELISA assay.	30
Table 2.3. Plasmids used in this study.	30
Table 2.4. Cell culture media.	33
Table 2.5. Antibodies and stains used for immunostaining.	39
Table 2.6. 10% SDS-PAGE gel composition.	40
Table 2.7. Antibodies used for Western Blot.	41
Table 3.1. RNA concentration of samples from experiments 1 and 2.	47
Table 5.1. Daily water and aspirin consumption across experimental groups.	97
Table 6.1. Number of predicted targets for mmu-miR-92a-2-5p and mmu-miR-361-3p in transcriptome and proteome.	114

List of abbreviations

aEPEC – Atypical Enteropathogenic *Escherichia coli*

AIEC – Adherent-Invasive *E. coli*

AE – Attaching and Effacing

Amp – Ampicillin

ASA – Aspirin

BFP – Bundle-Forming Pilus

CCH – Colonic Crypt Hyperplasia

CFC – Colonisation Factor *Citrobacter*

CFU – Colony Forming Units

DAEC – Diffusely Adherent *E. coli*

DE – Differentially Expressed

DPI – Days Post-Infection

EAEC – Enteroaggregative *E. coli*

EHEC – Enterohemorrhagic *E. coli*

EIEC – Enteroinvasive *E. coli*

ELISA – Enzyme-Linked Immunosorbent Assay

ETEC – Enterotoxigenic *E. coli*

ExPEC – Extraintestinal Pathogenic *E. coli*

H&E – Haematoxylin and Eosin

HCP – Haemorrhagic Coli Pilus

HUS – Haemolytic Uremic Syndrome

IEC – Intestinal Epithelial Cells

InPEC – Intestinal Pathogenic *E. coli*

Kn – Kanamycin

LB – Luria-Bertani

LEE – Locus of Enterocyte Effacement

LPS – Lipopolysaccharide

Mbp – Million base pairs

miRNA – microRNA

MTS – Mitochondrial Targeting Signal

MW – Molecular Weight

Nal – Nalidixic acid

Nle – Non-LEE Encoded

NMEC – Neonatal meningitis *E. coli*

NSAIDs – Non-Steroidal Anti-Inflammatory Drugs

OXPHOS – Oxidative Phosphorylation

PAI – Pathogenicity Island

PAMPS – Pathogen-Associated Molecular Patterns

PBS – Phosphate-Buffered Saline

pEAF – Plasmid-Encoding Adherence Factor

PEPEC – Porcine-Enteropathogenic *E. coli*

PPP – Pentose Phosphate Pathway

Pre-miRNA – Precursor-miRNA

Pri-miRNA – Primary-miRNA

PRR – Pattern Recognition Receptor

PTM – Post-Translational Modifications

PUFA – Polyunsaturated Fatty Acid

Puro – Puromycin

REPEC – Rabbit-Enteropathogenic *E. coli*

RIN – RNA Integrity Number

RISC – RNA-Induced Silencing Complex

RNAseq – RNA Sequencing

rpm – revolutions per minute

SDS-PAGE – Sodium Dodecyl Sulphate-Polyacrylamide Gel Electrophoresis

SEPEC – Sepsis-associated *E. coli*

STEC – Shiga Toxin-Producing *E. coli*

TA – Transit Amplifying

tEPEC – Typical Enteropathogenic *E. coli*

T3SS – Type Three Secretion System

T4P – Type IV Pilus

T6SS – Type VI Secretion System

TLR – Toll-Like Receptor

UTI – Urinary Tract Infections

UPEC – Uropathogenic *E. coli*

UPS – Ubiquitin-Proteasome System

WT – Wild Type

CHAPTER 1: Introduction

1 CHAPTER 1: Introduction.

1.1 Foodborne diseases.

Foodborne diseases arise from consuming food contaminated with viruses, bacteria, parasites, or chemicals, with diarrhoeal disease being the most common outcome. Although foodborne diseases are a global concern, affecting all countries, they disproportionately impact low-income and middle-income countries, particularly vulnerable populations and children under 5 years old, killing around 450000 children annually (WHO 2024).

Common pathogens responsible for foodborne disease outbreaks worldwide include bacteria such as *Salmonella*, *Campylobacter*, *Listeria monocytogenes* (*L. monocytogenes*), *Vibrio cholerae*, *Shigella* or *Escherichia coli* (*E. coli*), along with the virus rotavirus, adenovirus and norovirus and the parasites *Giardia*, *Cryptosporidium* and *Entamoeba spp* (WHO 2024). In low-income countries, *E. coli* and viruses in the genus *Rotavirus* are the most common etiological agents (WHO 2024). Bacterial cases are frequently linked to unpasteurised or raw milk, undercooked meat products, and contaminated fresh fruit and vegetables (WHO 2018). Conversely, viral infections are typically associated with raw or undercooked seafood or contaminated raw produce (WHO 2022). Infections can also be transmitted from person to person, particularly under poor hygiene conditions.

While the symptoms of both bacterial and viral infections are very similar, bacterial infections commonly present with fever, headache, nausea, vomiting, abdominal pain, and diarrhoea. In contrast, viral infections are characterised by explosive vomiting and watery diarrhoea (WHO 2022). Dehydration, a significant consequence of diarrhoea, leaves the body depleted of water and salts. Therefore, the primary treatment for diarrhoea involves oral rehydration salts (ORS) solution, a mixture of clean water, salt and sugar, or intravenous rehydration in severe cases (WHO 2024).

Effectively treating and preventing diarrhoea is crucial for reducing mortality and morbidity, including the risk of malnutrition. Preventive measures include access to safe drinking water, good personal and food hygiene, hand washing with soap, and health education (WHO 2024). Vaccination also plays a significant role in preventing diarrheal diseases. The rotavirus vaccine is widely used and effective in preventing rotavirus infections. Similarly, the cholera vaccine

is vital in areas prone to cholera outbreaks. Additionally, ongoing vaccine development targets pathogens like *Shigella*, norovirus, invasive non-typhoidal *Salmonella*, and enterotoxigenic *E. coli* (ETEC). According to the latest WHO information, there are currently 23 candidates in various stages of clinical trials (WHO 2023).

The lack of preventative therapies emphasises the importance of developing safe and effective strategies. Understanding the infection dynamics of key enteropathogens is a critical step towards creating such therapies with the potential to impact public health significantly. This research project aims to comprehend the mechanisms of infection, providing valuable insights that could benefit global health outcomes.

1.2 *Escherichia coli*.

E. coli is a facultative anaerobe that belongs to the *Enterobacteriaceae* family (Nataro and Kaper 1998). This Gram-negative bacillus is a commensal found in the environment, food, and the mammalian intestine. It is a crucial component of the healthy human intestinal microflora and usually colonises the mammalian gut within hours of birth (Kaper et al. 2004). Most commensal *E. coli* are harmless and live in symbiosis in the gut of humans and animals. However, in immunocompromised individuals or patients with damaged gastrointestinal barriers, *E. coli* can cause disease (Tenailon et al. 2010).

E. coli strains share a core genome of approximately 4.2 to 6.0 million base pairs (Mbp) (Denamur et al. 2021). While most *E. coli* are harmless to their host, some can cause disease and are referred to as pathotypes. The ability to cause disease is conferred by the acquisition of mobile genetic elements, such as large virulence gene clusters like pathogenicity islands (PAIs), plasmids, bacteriophages and transposons (Robins-Browne et al. 2016; Denamur et al. 2021). Horizontal gene transfer of these mobile genetic elements facilitates the acquisition of virulence factors, contributing to the pathogenicity of some *E. coli* strains (Tenailon et al. 2010). Consequently, pathogenic *E. coli* strains have significantly larger genomes than commensal strains (Denamur et al. 2021).

1.2.1 Pathotypes.

The different pathotypes can be differentiated into two groups: intestinal pathogenic *E. coli* (InPEC), which causes intestinal infections in humans and animals, and extraintestinal pathogenic *E. coli* (ExPEC), which causes extraintestinal infections in mammals (Kaper et al. 2004; Köhler and Dobrindt 2011).

Extraintestinal *E. coli* strains include uropathogenic *E. coli* (UPEC), neonatal meningitis *E. coli* (NMEC), and sepsis-associated *E. coli* (SEPEC), which are responsible for urinary tract infections (UTI), neonatal meningitis and sepsis (Köhler and Dobrindt 2011; Sora et al. 2021). Intestinal infections, on the other hand, mainly cause diarrhoea. Intestinal pathogenic *E. coli* can be separated into several types: enteropathogenic *E. coli* (EPEC), Shiga toxin-producing *E. coli* (STEC) which includes enterohemorrhagic *E. coli* (EHEC), enteroinvasive *E. coli* (EIEC), enteroaggregative *E. coli* (EAEC), diffusely adherent *E. coli* (DAEC), adherent-invasive *E. coli* (AIEC), and enterotoxigenic *E. coli* (ETEC) (Kaper et al. 2004; Croxen and Finlay 2010; Rojas-Lopez et al. 2018; Pakbin et al. 2021).

Although most pathotypes have their specific mechanism of infection, some mechanisms are shared among pathogenic *E. coli* strains. Once the bacteria attach to host cells, these bacteria hijack and manipulate host cell processes, allowing them to colonise the host, evade the immune response, and ultimately lead to disease (Bhavsar et al. 2007; Croxen and Finlay 2010).

1.2.2 Enteropathogenic *E. coli*.

First described in 1945, EPEC is a type of *E. coli* known for causing infantile diarrhoea, particularly prevalent in low-income countries, and is associated with traveller's diarrhoea (Croxen and Finlay 2010; Rojas-Lopez et al. 2018; Pakbin et al. 2021).

EPEC is further classified based on its pathogenicity into two subgroups: typical EPEC (tEPEC) and atypical EPEC (aEPEC), each exhibiting distinct adherence patterns. Localised adherence is characteristic of tEPEC, whereas a diffuse or aggregative adherence pattern characterises aEPEC (Kaur and Dudeja 2023). This variation in adhesion patterns is attributed to the presence (tEPEC) or absence (aEPEC) of the adherent factor plasmid (pEAF) (Trabulsi 2002; Kaur and Dudeja 2023). The pEAF plasmid contains two operons, which include *bfp*, a type

IV bundle-forming pilus, and *per*, a plasmid-encoded regulator. These operons play an essential role as transcriptional activators for the Locus of Enterocyte Effacement (LEE) PAI (Kaur and Dudeja 2023).

The LEE pathogenicity island encodes the genetic elements required for the Type Three Secretion System (T3SS), which is essential for the formation of attaching and effacing (AE) lesions, the hallmark of EPEC pathogenesis (Yerushalmi et al. 2014). EPEC is classified as an AE pathogen due to its ability to induce these lesions, a trait it shares with EHEC. Both pathogens exhibit many genetic and phenotypic similarities (Goosney et al. 2000; Trabulsi 2002; Platenkamp and Mellies 2018; Kaur and Dudeja 2023).

1.2.3 Enterohemorrhagic *E. coli*.

While EPEC is endemic in low-income countries and causes traveller's diarrhoea, EHEC is responsible for outbreaks worldwide, causing gastroenteritis and haemorrhagic diarrhoea (Rojas-Lopez et al. 2018; Pakbin et al. 2021). Cattle serve as the primary reservoir for EHEC (Croxen and Finlay 2010; Pakbin et al. 2021). Initially identified as a causative agent of human disease in 1982 (Kaper et al. 2004; Welinder-Olsson and Kaijser 2005; Pakbin et al. 2021), the EHEC serotype is classified under the Shiga-toxin-producing *E. coli* subgroup (STEC) and contains adhesin and attachment virulence factors encoded by the LEE PAI (Kaper et al. 2004; Welinder-Olsson and Kaijser 2005; Croxen and Finlay 2010; Pakbin et al. 2021).

The Shiga-toxin (Stx), also known as Verocytotoxin (VT), can be divided into two serogroups, *stx1* and *stx2*, and can be present in various combinations in EHEC. Stx is an AB5 toxin comprising a pentamer of the subunit B and the enzymatically active subunit A. Subunit B binds to glycolipid globotriaosylceramide (Gb3) receptors on target cells such as Paneth cells and kidney epithelial cells, while subunit A disrupts protein synthesis by cleaving ribosomal RNA, inhibiting protein synthesis (Kaper et al. 2004; Croxen and Finlay 2010; Pakbin et al. 2021). These toxins are initially produced in the colon, then translocated across the gut and enter the bloodstream, where they can reach the kidneys, and potentially induce neurological complications (Frankel et al. 1998; Kaper et al. 2004; Welinder-Olsson and Kaijser 2005; Hunt 2010; Tran et al. 2018). Once in the kidney, the Stx damages endothelial cells and obstructs microvasculature, leading to thrombosis, which contributes to

Haemolytic Uremic Syndrome (HUS), a severe and life-threatening condition characterised by acute renal insufficiency, thrombocytopenia, and hemolytic anaemia (Kaper et al. 2004; Jokiranta 2017). Moreover, Stx induces apoptosis in intestinal epithelial cells (IECs), causing local damage in the colon, resulting in haemorrhagic colitis, bloody diarrhoea, necrosis, and intestinal perforation (Kaper et al. 2004).

EHEC serotype O157:H7, a significant Shiga-toxin-producing *E. coli* strain, notably impacts public health. In 2021, England reported 365 confirmed STEC O157 and 1234 cases of STEC non-O157. **Table 1.1** shows that STEC O157 cases have reduced over the last 4 years; however, non-O157 cases have almost doubled (Public Health England 2024). Across all years, one-third of confirmed STEC O157 cases in England required hospital admission, with 2%-3% developing HUS (Public Health England, 2024). Understanding the virulence and pathogenicity of EHEC strains is crucial in addressing associated health risks.

Year	STEC O157 cases	non-O157 STEC cases
2018	607	612
2019	539	768
2020	402	690
2021	365	1234

Table 1.1. STEC cases in England and Wales.

1.2.4 EPEC and EHEC differences.

Although both pathotypes belong to the AE pathogens group and share common virulence mechanisms, they exhibit distinct characteristics. Notably, the infectious dose required for EHEC infection is significantly lower (between 1 and 100 bacteria) compared to EPEC (10^6 and 10^8 bacteria) (Kaper et al. 2004; Welinder-Olsson and Kaijser 2005; Croxen et al. 2013). The tropism is also different, with EHEC predominantly colonising the Peyer's patches and large bowel, while EPEC primarily colonising the small intestine (Armstrong et al. 1996; Fitzhenry 2002; Gaytan et al. 2016). Perhaps the most crucial difference lies in Shiga toxin production, which is unique to enterohemorrhagic *E. coli* as it belongs to the STEC family (Kaper et al. 2004; Wong et al. 2011). This distinction emphasises the diverse pathogenic mechanisms and clinical implications associated with EPEC and EHEC infections.

1.3 Attaching and effacing pathogens.

EPEC and EHEC are categorised as attaching and effacing pathogens (AE pathogens) due to their ability to induce AE lesions within the intestinal epithelial cells. These lesions are characterised by the intimate attachment of the bacteria to the surface of intestinal epithelial cells followed by the effacement of microvilli and the formation of actin-rich pedestals beneath the bacteria (Hall et al. 1990; Trabulsi 2002; Gaytan et al. 2016; Pakbin et al. 2021). In HeLa cells, these pathogens form pedestal-like structures where they remain attached, further emphasising their role in disrupting the host cell's structure and function (Scaletsky et al. 1996; Gaytan et al. 2016; Cepeda-Molero et al. 2017).

However, this classification of pathogens extends beyond human pathogens to include others causing diseases in animals, such as rabbit-enteropathogenic *E. coli* (REPEC), porcine-enteropathogenic *E. coli* (PEPEC), *Escherichia albertii* (both avian and human pathogen), and the mouse pathogen *Citrobacter rodentium* (*C. rodentium*) (Goosney et al. 2000; Kaper et al. 2004; Mundy et al. 2005; Croxen and Finlay 2010; Wong et al. 2011; Gomes et al. 2020; Pakbin et al. 2021).

EPEC, EHEC and *C. rodentium* are all extracellular Gram-negative enteric pathogens with similar infection strategies (Mundy et al. 2005; Wong et al. 2011). While EPEC and EHEC are responsible for causing diarrheal diseases with global morbidity and mortality implications (WHO, 2018), *C. rodentium* is a natural pathogen in mice, acting as the etiological agent of transmissible murine crypt hyperplasia, also known as colonic crypt hyperplasia (CCH) (Collins et al. 2014a; Collins et al. 2014b; Cepeda-Molero et al. 2017). Given that mice are naturally resistant to EPEC/EHEC infection, in vivo research on AE pathogens was impeded for a long time (Law et al. 2013). However, the infection of mice with *C. rodentium* now provides an ideal surrogate model for in vivo studies to understand the mechanisms of infection of AE pathogens (Mundy et al. 2005; Law et al. 2013).

The development of the AE lesion occurs in three stages. Initially, bacteria adhere to the host cells in a non-intimate manner through a type IV pilus (T4P), referred to as bundle-forming pilus (BFP) in tEPEC, haemorrhagic coli pilus (HCP) in EHEC and colonisation factor *Citrobacter* (CFC) in *C. rodentium* (Mundy et al. 2003; Wales et al. 2005; Xicohtencatl-Cortes et al. 2007; Kaur and Dudeja 2023). Next, bacteria disrupt signal transduction pathways

within the host cell by translocating effector proteins through the T3SS (Garmendia et al. 2005; Wales et al. 2005). Finally, bacteria establish an intimate attachment to the host cell via the interaction between the adhesin intimin and its receptor Tir (Translocated Intimin Receptor), translocated through the T3SS into the host cell membrane. These phases collectively result in the recruitment of actin from the host cell, forming a pedestal-like structure (**Error! Reference source not found.**) (Frankel and Phillips 2008; Croxen and Finlay 2010; Gaytan et al. 2016).

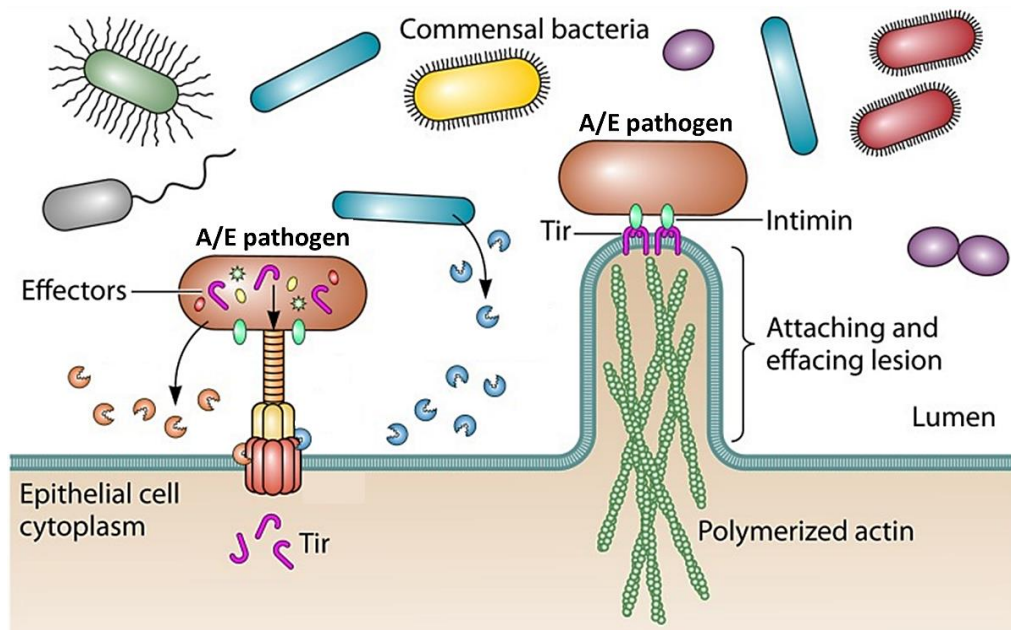


Figure 1.1. Pedestal formation in AE pathogens.

The T3SS of AE pathogens injects Translocated Intimin Receptor (Tir) into host intestinal epithelial cells upon infection. Tir integrates into the host cell membrane, binding bacterial intimin and initiating actin cytoskeleton rearrangement. This process forms actin pedestals around the bacteria, crucial for their attachment and colonisation of the intestinal epithelium. Figure adapted from Palmer and Skaar (2019).

1.4 Type three secretion system.

AE pathogens employ a T3SS to promote disease. This system acts as a macromolecular syringe, creating a continuous channel from the bacterial cytoplasm to the cell exterior. The T3SS consists of several key components: the extracellular components, including a filament/needle (EscF/EspA) and a translocation pore (EspB/EspD), which penetrate the host cell membrane to facilitate protein delivery; a basal body, which consists of an outer membrane ring, an inner membrane ring, an inner rod, and an export apparatus, all crucial for the assembly and function of the T3SS; and the cytoplasmic protein complexes, including

the cytoplasmic ring and an ATPase (EscN), which provide the necessary energy for the secretion process (**Figure 1.2**) (Vallance and Finlay 2000; Gaytan et al. 2016; Slater et al. 2018; Slater and Frankel 2020; Ruano-Gallego et al. 2021).

EspA forms the filament of the T3SS, creating a channel between the bacterial cytoplasm and the host cell. Together with the translocation pore units EspB and EspD, it constitutes the translocon. Mutants lacking these translocon components can secrete proteins but fail to translocate them into host cells. This defect affects adhesion, AE lesion formation, and overall virulence, highlighting the importance of these secreted proteins (Knutton 1998; Crepin et al. 2005; Gaytan et al. 2016).

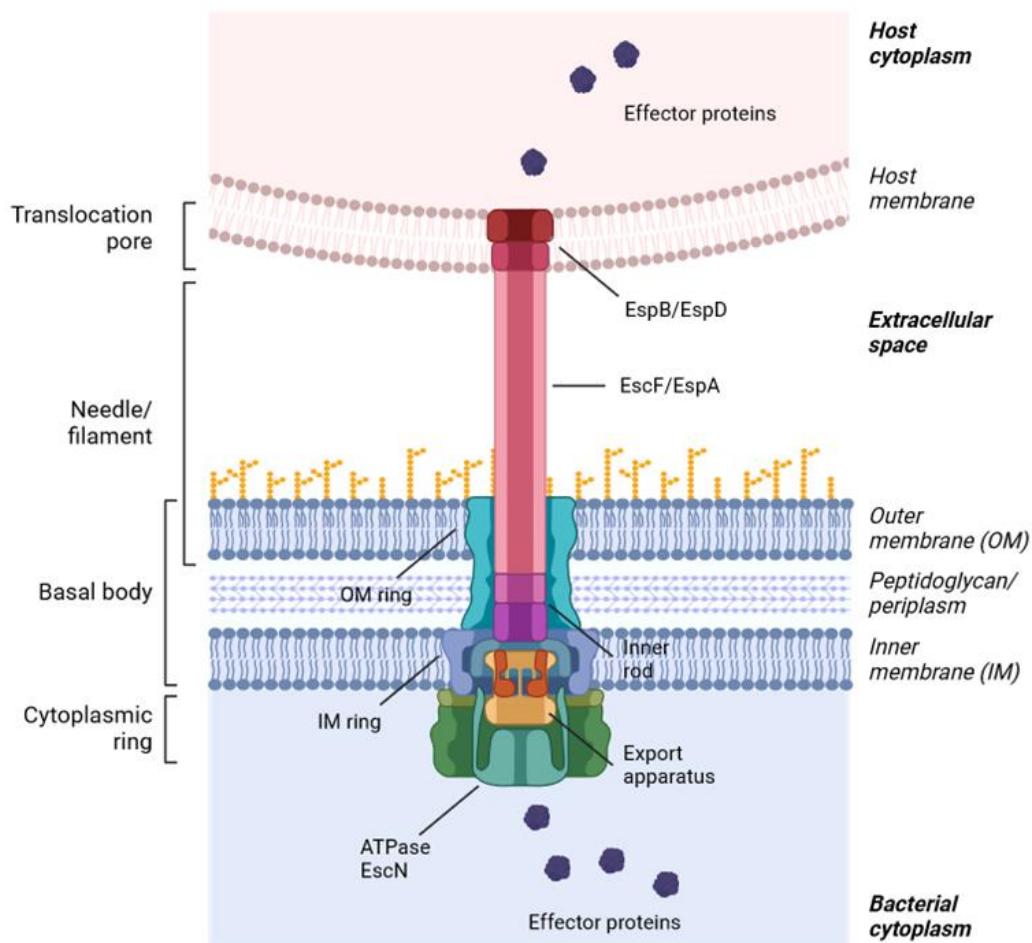
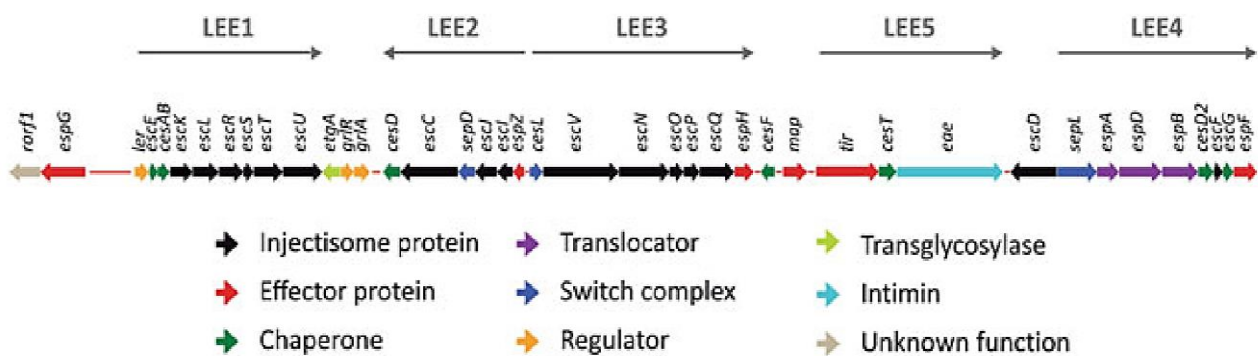


Figure 1.2. Structure of the Type Three Secretion System.

The figure illustrates the T3SS structure, highlighting four main components: the translocation pore, the filament/needle (which extends from the bacterial membrane), the basal body (embedded in the bacterial membranes), and the cytoplasmic ring. Figure created with BioRender.com.

The genes necessary for the formation of the T3SS are encoded in the LEE pathogenicity island (**Figure 1.3**), a 35.6 kb region inserted in the genome of AE pathogens (Perna et al. 1998; Kaper et al. 2004; Franzin and Sircili 2015; Furniss and Clements 2018). These genes are organised in 5 operons: LEE1 to LEE5. The LEE1, LEE2, and LEE3 operons encode the structural components of the T3SS, inner and outer membrane components of the T3SS (*E. coli* secretion gene, *Esc*), gene regulators (like *Ler*), chaperones (chaperone for *E. coli* secreted protein, *Ces*), and secreted proteins (*E. coli* secreted protein, *Esp*). The LEE4 encodes for the needle proteins *EscF* and *EspA*, the translocators *EspB* and *EspD*, and effector proteins. The LEE5 operon encodes the adhesin intimin (encoded by the *eae* gene), its translocated receptor *Tir*, and the chaperone *CesT* (Elliott et al. 1998; Elliott et al. 2000; Deng et al. 2004; Deng et al. 2005; Serapio-Palacios and Finlay 2020).



AE pathogens have 22 core effectors, including those encoded within the LEE and non-LEE encoded (Nle) effectors. Nle effectors are found on mobile genetic elements or other pathogenicity islands, and while they are not necessary for pedestal formation in EPEC, they are required for AE lesions and colonisation (Collins et al. 2014b; Cepeda-Molero et al. 2017). The LEE-encoded effectors are Tir, Map, EspZ, EspF, EspH, EspG and EspB each with distinct functions (Iguchi et al. 2009).

The T3SS effector protein targets different parts of the host to create an environment that allows the pathogens to thrive (Slater et al. 2018; Serapio-Palacios and Finlay 2020). For instance, Tir (translocated intimin receptor) is a protein translocated into the plasma membrane of host cells, where it serves as a receptor for the adhesin intimin. The interaction between Tir and intimin is essential for triggering a signalling cascade that leads to the forming of actin pedestals and intimate attachment of bacteria in host cells. Additionally, Tir plays a role in downregulating Map-dependent filopodia formation (Nancy L. Freeman et al. 2000; Dean et al. 2006; Berger et al. 2009; Stevens and Frankel 2015).

Map (mitochondrial-associated protein) is another multifunctional effector that regulates diverse processes in the host cell. Upon infection, Map localises to the mitochondria via the mitochondrial targeting signal (MTS), disrupting membrane potential and impacting oxygen availability in the colon (Ma et al. 2006). Additionally, Map induces the formation of filopodia (long finger-like structures) and causes the rapid inactivation of the sodium-glucose-transporter SGLT-1, leading to rapid watery diarrhoea (Berger et al. 2009; Berger et al. 2017; Shenoy et al. 2018).

EspZ plays a significant role during infection inhibiting apoptosis and reducing the cytotoxic effect of bacterial infection, preventing rapid cell death during infection. Moreover, it targets the mitochondria of infected cells (Shames et al. 2010; Shames et al. 2011). Additionally, EspZ regulates the translocation of other effector proteins during infection, ensuring that effectors are delivered in a regulated and timely manner to maximize their impact on host cell functions (Berger et al. 2012; Serapio-Palacios and Finlay 2020).

EspF is a multifunctional effector that interacts with multiple host proteins and modulates several processes. Along with the effector proteins Map and EspZ, EspF targets mitochondria, disrupting the membrane potential and inducing the release of cytochrome c

(Dean et al. 2006; Holmes et al. 2010). Its effects include disruption of the epithelial barrier, microvillus effacement, modulation of the cytoskeleton, targeting and disruption of the nucleolus, and inhibition of several epithelial transporters, which impairs water reabsorption and induces diarrhoea (Holmes et al. 2010; Stevens and Frankel 2015).

EspH interferes with actin cytoskeleton dynamics. It represses filopodia formation, enhances pedestal length and inhibits phagocytosis (Tu et al. 2003; Dong et al. 2010; Shenoy et al. 2018). EspH directly binds to and inactivates mammalian RhoGEFs, preventing their activity toward RhoGTPases and thereby modulating actin dynamics (Dong et al. 2010).

EspG 's cellular function aims to disrupt microtubules and form actin stress fibres. Moreover, EspG has been implicated in disrupting tight junctions in epithelial cells, thereby altering cell permeability (Matsuzawa et al. 2004; Tomson et al. 2005; Shenoy et al. 2018).

EspB is the only secreted protein that functions as a component of the T3SS translocation pore and is also a translocated effector. EspB disrupts adherens junctions and interacts with the actin-binding domain of myosins, impairing their function and inhibiting phagocytosis (Kodama et al. 2002; Iizumi et al. 2007).

In summary, the diverse functions and targeted actions of T3SS effector proteins underscore their pivotal role in bacterial pathogenesis and illustrate the complex strategies AE pathogens employ to manipulate host cell processes. *C. rodentium*, a natural intestinal pathogen in mice, is a valuable model for studying these mechanisms.

1.6 *Citrobacter rodentium*.

C. rodentium shares 67% of its genes and key virulence factors with related human pathogens EPEC and EHEC (Collins et al. 2014b; Silberger et al. 2017). These shared factors include the LEE pathogenicity island, which encodes for the T3SS. Additionally, it encodes a type IV pilus and two type VI secretion systems (T6SS). Notably, although *C. rodentium* does not express the Shiga toxin, researchers have developed a *C. rodentium* strain that expresses the Shiga toxin, enabling studies on its impact on pathogenesis in vivo (Collins et al. 2014b). Interestingly, *C. rodentium* is also used as a model for studying ulcerative colitis and colon cancer (Hopkins and Frankel 2021).

A hallmark of infection is CCH, characterised by the elongation of crypts, increased colonic thickness, goblet cell loss and an increase in proliferating cells, particularly transit amplifying (TA) cells at the base of the crypt (Silberger et al. 2017; Hopkins and Frankel 2021). This hyperplasia arises from excessive epithelial regeneration and repair mechanisms (Mundy et al. 2005; Ahmed et al. 2012; Roy et al. 2015). Under normal conditions, intestinal epithelial cells are renewed from Lgr5+ stem cells, which are stimulated by Wnt signalling to produce TA cells that eventually differentiate into mature epithelial cells. However, during *C. rodentium* infection, the proliferation of TA cells is excessively stimulated by mitogens and cytokines. This heightened proliferation, coupled with reduced shedding of enterocytes, leads to the elongation of colonic crypts and contributes to the severity of colitis. The severity can vary depending on the genetic background of the mouse, with outcomes ranging from fatal to self-limiting (Collins et al. 2014b; Mullineaux-Sanders et al. 2019).

In C57BL/6 mice, the infection typically progresses through four phases. In the establishment phase (1-3 days post-infection, DPI), *C. rodentium* colonises the caecal patch. In the expansion phase (4-8 DPI), the bacteria attach intimately to the distal part of the colon and proliferate. During this phase, the effector protein Tir is injected into the IEC via the T3SS. Tir integrates into the IEC plasma membrane and interacts with the bacterial adhesin intimin, forming an intimate attachment. In the steady-state phase (8-12 DPI), *C. rodentium* reaches the peak of infection, with colonisation levels reaching a plateau at 10^8 to 10^9 colony former units (CFU)/g of faeces (Hopkins et al. 2019). Finally, in the clearance phase (from 12 DPI onward), bacterial levels rapidly decrease as the host begins to clear the infection (Mullineaux-Sanders et al. 2019; Hopkins and Frankel 2021). Throughout infection, mice develop colitis and dysbiosis is induced in the large intestine, which results in a reduction of the abundance and diversity of commensal bacteria (Lupp et al. 2007; Hopkins et al. 2019).

The interaction between the bacteria and the host cell leads to significant changes in the enterocyte. *C. rodentium* infection triggers notable changes, including an enhanced antimicrobial response and host defence mechanisms, changed colonic microbiome, altered cellular metabolism, and significant modifications in the miRNome profile of infected IECs

(Collins et al. 2014b; Berger et al. 2017; Hopkins et al. 2019; Mullineaux-Sanders et al. 2019; Wen et al. 2019; Hopkins and Frankel 2021). These changes are critical for understanding how *C. rodentium* manipulates host cell functions to facilitate its survival and proliferation.

1.6.1 *C. rodentium* and host cell metabolism.

C. rodentium infection triggers colonic crypt hyperplasia by increasing the proliferation of TA cells, which reduces the number of differentiated IECs such as enterocytes, goblet cells, and deep crypt secretory cells (Hopkins et al. 2019). This loss disrupts Notch, Wnt, and EGF signalling pathways, disturbing cellular homeostasis. The decrease in differentiated enterocytes, marked by fewer ion exchangers, obstructs ion absorption and contributes to infection-induced diarrhoea (Papapietro et al. 2013; Hopkins et al. 2019). These shifts in cellular turnover likely affect cellular metabolism, increasing energy demands within the crypt.

Cholesterol, a crucial lipid constituent of biological membranes, plays a vital role in maintaining the epithelium integrity to prevent pathogen dissemination. Its homeostasis is regulated by the expression of transcription factors such as liver X receptors (LXRs) and sterol regulatory element-binding protein 2 (SREBP2), which control the expression of efflux transporters and cholesterol biosynthesis, respectively. In conditions of cholesterol excess, LXR transcription factors are activated to promote the expression of efflux transporters such as ATP-binding cassette transporter A1 (ABCA1), ATP-binding cassette sub-family G member 5 (ABCG5), and ATP-binding cassette sub-family G member 8 (ABCG8) to facilitate cholesterol removal. Conversely, biogenesis pathways are stimulated under low cholesterol conditions to maintain cellular cholesterol levels (Luo et al. 2020).

During infection, IECs experience significant changes in cholesterol metabolism. *C. rodentium* infection leads to an upregulation of the uptake and biosynthesis of cholesterol. 3-Hydroxy-3-methylglutaryl-coenzyme A reductase (HMGCR), a key enzyme in cholesterol biosynthesis, is upregulated, and the levels of low-density lipoprotein receptor (LDLR) and proprotein convertase subtilisin/kexin type 9 (PCSK9), which regulates LDL and cholesterol synthesis, are increased. Interestingly, cholesterol efflux is also enhanced, with transporters like ABCA1 in higher abundance, leading to elevated cholesterol levels in serum and faeces

during infection (Berger et al. 2017; Hopkins et al. 2019). These changes indicate a complex interaction between cholesterol biosynthesis and efflux in response to infection.

Under normal conditions, IECs metabolise butyrate in the mitochondria via the β -oxidation process, producing acetyl-CoA. This process consumes oxygen and promotes an anaerobic environment in the lumen. The acetyl-CoA enters the tricarboxylic acid (TCA) cycle to produce high-energy molecules, fueling oxidative phosphorylation (OXPHOS) for ATP production. This efficient energy production is crucial for maintaining normal cellular functions in the intestine (Szrok-Jurga et al. 2023).

During infection with *C. rodentium*, there is a downregulation of pathways like OXPHOS, TCA cycle and β -oxidation, coupled with the upregulation of the glycolysis pathway (Berger et al. 2017; Hopkins et al. 2019). This phenomenon mirrors the Warburg effect, which is characterised by an increased reliance on glycolysis for energy production even in the presence of sufficient oxygen. Typically observed in cancer and proliferative cells, the Warburg effect allows cells to rapidly generate ATP and biosynthetic precursors necessary for cell growth and proliferation (Vander Heiden et al. 2009; Escoll and Buchrieser 2018).

Disruption of β -oxidation reduces mitochondrial energy production and oxygen consumption through OXPHOS, leading to increased oxygenation of the colonic epithelium. These alterations in the oxygenation of the intestinal mucosa are likely attributed to mitochondrial disruption caused by effector proteins like Map, EspF, and EspZ (Nougayrede and Sonnenberg 2004; Nagai et al. 2005; Ma et al. 2006; Shames et al. 2011; Hua et al. 2018). Simultaneously, the abundance of the Sodium-Glucose Co-Transporter 4 (SGLT4) increases, facilitating more glucose transport into the cells for glycolysis. Additionally, phosphocreatine, a molecule that helps rapidly regenerate adenosine triphosphate (ATP), is found at higher levels in infected IECs (Berger et al. 2017). This indicates that these cells are mobilising more ATP to meet heightened energy demands. Overall, these changes suggest that infected IECs adjust their metabolic pathways to cope with the stress of infection, relying more on glycolysis and enhancing their capacity to regenerate ATP.

1.6.2 Host miRNome and *C. rodentium*.

Moreover, *C. rodentium* induces a change in the microRNA (miRNA) profile of infected cells in mice. miRNAs are small, non-protein-coding RNAs, approximately 21-25 nucleotides in length, that regulate gene expression by targeting mRNAs for degradation or translation repression (Wahid et al. 2010). The synthesis of the miRNA begins in the nucleus, where DNA is transcribed to primary miRNA (pri-miRNA) by RNA polymerase II (**Figure 1.4**) (Lee et al. 2002; Bartel 2004). This pri-miRNA is then processed by Drosha, an RNase III enzyme, to precursor-microRNA (pre-miRNA). The pre-miRNA is subsequently transported to the cytoplasm by exportin-5 (Xpo5), where it is further processed into mature miRNA by Dicer (Lee et al. 2002; Wahid et al. 2010).

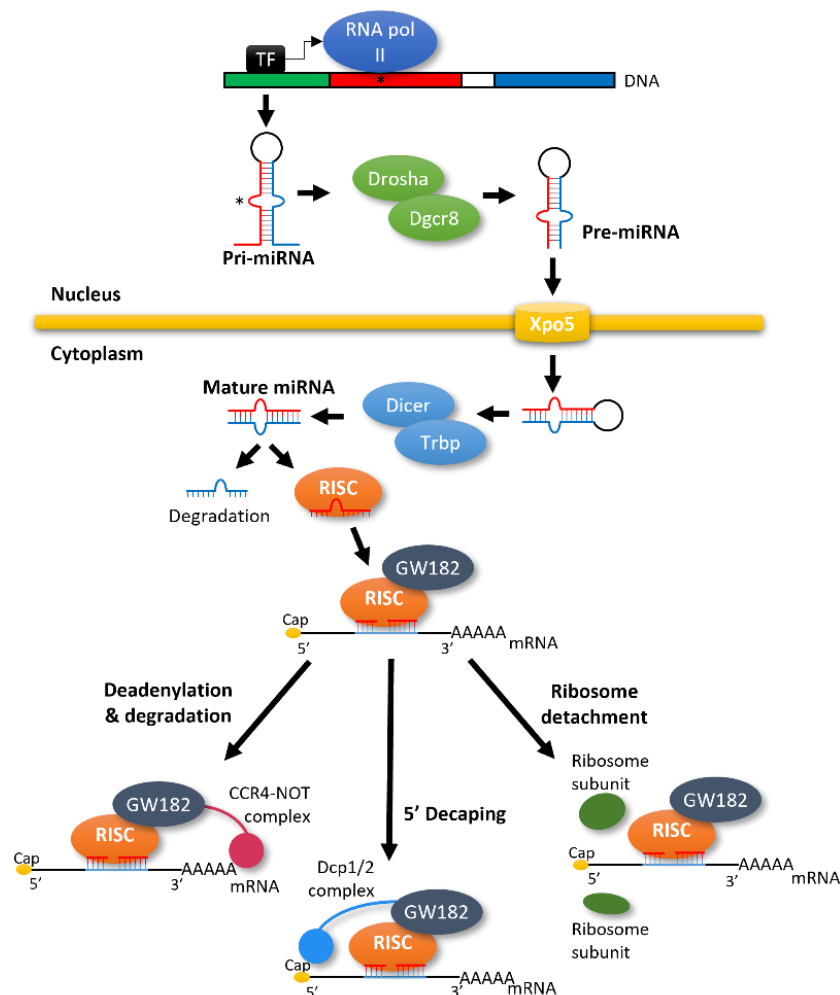


Figure 1.4. miRNA synthesis and functions.

Pri-miRNA is transformed into *pre-miRNA* in the nucleus of the cell. Then, is exported through exportin 5 to the cytoplasm, where it is transformed into mature miRNA by Dicer. Mature miRNA is loaded in the RISC, forming the active complex. RISC promote gene silencing via deadenylation and degradation of mRNA, 5' decapping, or promoting ribosome detachment from the target mRNA.

In the cytoplasm, mature miRNAs are incorporated into the RNA-induced silencing complex (RISC). This complex includes Argonaute proteins such as Argonaute 1 (Ago 1) and Argonaute 2 (Ago 2), as well as p54 and the fragile X protein (FRAX) (Wahid et al. 2010; Saliminejad et al. 2019). RISC regulates gene expression through diverse mechanisms. Typically, miRNA binds to complementary regions in the 3' untranslated region of target mRNA, leading Ago2 to promote mRNA degradation (Lee et al. 2002). In cases of imperfect complementarity between the miRNA and its target mRNA, the catalytic function of Ago is altered, and the GW182 protein is recruited (Niaz and Hussain 2018). GW182 acts as a scaffold for recruiting catalytic proteins or the CCR4-NOT complex, which leads to deadenylation of the mRNA's polyA tail (Wahid et al. 2010; Niaz and Hussain 2018). Additionally, RISC recruits Dcp1/2 proteins to induce mRNA 5' decapping and degradation. Another mechanism involves the RISC complex causing ribosome stalling, which interferes with protein translation and leads to premature termination (Wahid et al. 2010). Through these diverse mechanisms, RISC effectively silences gene expression.

MiRNAs regulate different physiological processes in animals, including cell death, cell proliferation, metabolic pathways, immune response, antiviral defence, adipocyte differentiation, and insulin secretion (Wahid et al. 2010; Das et al. 2016; Saliminejad et al. 2019). Dysregulation of miRNA expression is associated with various disease pathologies, such as myocardial infarction to cancers, highlighting their potential as diagnostic markers and therapeutic targets (Saliminejad et al. 2019). Furthermore, miRNAs are integral to the host's response to both viral and bacterial infections and are often exploited by pathogens to manipulate host cell pathways (Wahid et al. 2010; Das et al. 2016).

Several intestinal pathogens, such as the Gram-negative bacteria *Salmonella*, *Campylobacter concisus*, *Helicobacter pylori*, and the Gram-positive bacterium *Listeria monocytogenes*, have been reported to modify host miRNAs (Maudet et al. 2014; Das et al. 2016). Notably, *C. rodentium* infection also induces a change in the miRNome profile of IEC in mice. Wen et al. (2019) investigated the impact of infection on the miRNome of IECs and found that 24 miRNAs were significantly deregulated during infection. These deregulated miRNAs were associated with pathways related to cell cycle regulation, immune response, and cancer development. This change in the miRNome of infected cells emphasises the complex

interplay between miRNAs and host responses to pathogenic infections, highlighting their importance in understanding and managing these interactions.

1.6.3 Host immune response to *C. rodentium*.

C. rodentium infection triggers a complex host immune response, involving both innate and adaptive mechanisms to combat the pathogen. Inflammation is a critical aspect of this response, essential to eliminate affected cells and harmful factors, and restore tissue and physiological function (Ricciotti and Fitzgerald 2011; Wautier and Wautier 2023).

Initially, *C. rodentium* infection depletes goblet cells, which are responsible for secreting mucins that protect the gut and maintain epithelial barrier integrity (Bergstrom et al. 2008; Chan et al. 2013). This depletion compromises the barrier, allowing bacteria to penetrate and trigger inflammatory signalling pathways (Mullineaux-Sanders et al. 2019).

The innate immune response is initiated through the recognition of pathogen-associated molecular patterns (PAMPs) (Collins et al. 2014b; Silberger et al. 2017; Mullineaux-Sanders et al. 2019). Epithelial cells respond by releasing antimicrobial proteins and reactive oxygen species to contain the pathogen. This is followed by activating antigen-presenting cells and phagocytes, including macrophages, monocytes, and neutrophils. These immune cells use pattern recognition receptors (PRRs) such as toll-like receptors (TLR) or nucleotide-binding oligomerisation domain-like receptors (NOD) to recognise and respond to the pathogen (Hopkins and Frankel 2021). TLR2, TLR4, and NOD2 detect components such as peptidoglycan and lipopolysaccharides (LPS). While TLR2 helps maintain mucosal integrity, TLR4 intensifies inflammation and tissue damage, and NOD2 aids bacterial clearance by recruiting inflammatory monocytes (Gibson et al. 2010; Kim et al. 2011).

The activation of these PRRs triggers adaptor proteins, leading to the activation of pro-inflammatory transcription factors such as NF- κ B and interferon regulatory factors. This cascade results in the production of cytokines (such as IL-6) and chemokines (for instance CXCL1 and CCL2), as well as nitric oxide, all of which contribute to inflammation and pathogen clearance (Kim et al. 2011; Mullineaux-Sanders et al. 2019). Phagocytes also engulf and destroy *C. rodentium* while releasing additional pro-inflammatory cytokines. Dendritic cells migrate to the lymph nodes, where they activate and guide circulating

lymphocytes to the colonic lamina propria. Importantly, dendritic cells produce IL-23 (**Error! Reference source not found.**), which boosts the immune response by stimulating the production of interleukin-22 (IL-22) from group 3 innate lymphoid cells (ILC3) and T-helper (Th) cells (Collins et al. 2014b; Mullineaux-Sanders et al. 2019). Notably, mice lacking IL-22 or IL-23 are highly susceptible to *C. rodentium* infection (Koroleva et al. 2015; Silberger et al. 2017).

The adaptive immune response to *C. rodentium* is predominantly driven by Th1 cells. CD4+ T cells are central in this process, producing key cytokines such as IL-22, IL-17A, and IFN γ (**Error! Reference source not found.**) (Silberger et al. 2017; Mullineaux-Sanders et al. 2019). Early in the infection, the attachment of *C. rodentium* to IECs triggers a strong Th17 response. Initially, Th17 cells mainly produce IL-17A and IL-22. However, as the infection

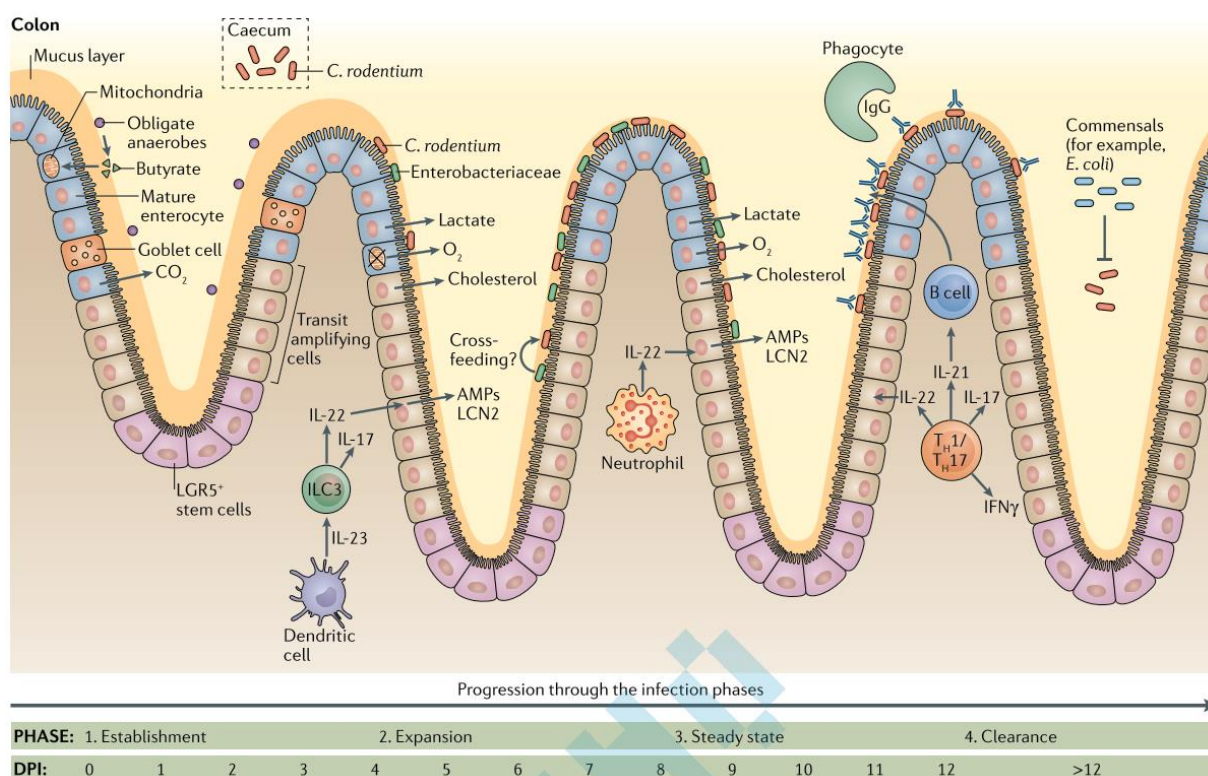


Figure 1.5. Phases of *Citrobacter rodentium* infection.

The image illustrates the changes occurring during the different phases of *C. rodentium* infection. Initially, the mucus layer of the colon diminishes as goblet cells are depleted. Host cell metabolism shifts, leading to increased cholesterol release into the lumen. Oxygen levels in the lumen rise due to mitochondrial destruction and reduced cellular respiration. Both innate and adaptive immune cells, such as dendritic cells, neutrophils, and T-helper (Th) cells, activate an immune response, stimulating the production of various molecules to combat the infection. Figure from Mullineaux-Sanders et al. (2019).

progresses, they increase their production of IFN γ and the transcription factor T-bet, adopting a more Th1-like phenotype (Collins et al. 2014b; Silberger et al. 2017; Mullineaux-Sanders et al. 2019).

IL-17A plays a key role in inflammation by recruiting neutrophils, which are vital for controlling bacterial infections (Collins et al. 2014b; Silberger et al. 2017; Mullineaux-Sanders et al. 2019). IL-22, a pro-inflammatory cytokine from the IL-10 family, acts on IECs to promote the secretion of antimicrobial peptides such as RegIII γ and RegIII β , as well as nutritional immunity proteins like calprotectin (a heterodimer of S100A8 and S100A9) and lipocalin 2 (Lcn2) (Hood and Skaar 2012). These molecules help limit *C. rodentium* colonisation (Collins et al. 2014b).

Additionally, Gamma-Delta ($\gamma\delta$)-T cells contribute to the production of IL-17A and IFN γ (Collins et al. 2014b). IFN γ enhances epithelial cell responses and promotes pro-inflammatory lymphocyte phenotypes, reinforcing the Th1 bias typical of responses to AE pathogens. Th17 cells also produce IL-21, which works alongside IFN γ to activate STAT1 and induce the expression of interferon-stimulated genes in T cells (Mullineaux-Sanders et al. 2019).

In the clearance phase, starting from 12 days post-infection, *C. rodentium* associated with mucosal tissues is opsonized by immunoglobulin G (IgG) produced by B cells and engulfed by phagocytes (Mullineaux-Sanders et al. 2019). Meanwhile, luminal *C. rodentium* is outcompeted by commensal bacteria, such as *E. coli*, resulting in clearance of the pathogen in approximately three weeks (Collins et al. 2014b; Silberger et al. 2017; Mullineaux-Sanders et al. 2019).

Moreover, prostaglandins (PGs), derived from the fatty acid arachidonic acid, play a significant role in the inflammatory response. The principal bioactive PGs are prostaglandin E₂ (PGE₂), prostaglandin I₂ (PGI₂), prostaglandin F_{2 α} (PGF_{2 α}), and prostaglandin D₂ (PGD₂). While these molecules are ubiquitously produced, their expression level and production profiles change during inflammation (Ricciotti and Fitzgerald 2011; Aoki and Narumiya 2012; Allaj et al. 2013). For example, during *C. rodentium* infection, there is an increase in PGE₂ production in the colonic tissue, which inhibits T-helper 17 (Th17) cell differentiation. Th17 cells are crucial for mucosal defence, as they secrete cytokines that enhance the

antimicrobial response and promote the recruitment of immune cells to infection sites. Interestingly, targeting the prostaglandin E₂ receptor EP4 enhances intestinal defence against *C. rodentium* by leading to increased Th17 cells, boosting antimicrobial peptide production and a decreased number of bacteria in the colon (Dejani et al. 2018). While this highlights the complex regulation of immune responses during infection, the precise role of PGE₂ and the prostaglandin pathway during *C. rodentium* infection is not yet fully understood.

1.6.4 Host microbiome and *C. rodentium* infection.

The composition of the commensal bacteria significantly influences *C. rodentium*-host interactions. During homeostasis, the microbiota is formed by obligate anaerobic bacteria, including *Firmicutes* and *Bacteroidetes*. These bacteria play crucial roles in modulating host metabolism, aiding digestion, and stimulating the development of mucosal immune and lymphatic systems (Hopkins and Frankel 2021).

IECs differentiate commensal bacteria from pathogens via TLR. For instance, a surface polysaccharide of *Bacteroides fragilis* triggers TLR2 activation, which stimulates T cells and secretion of the anti-inflammatory IL-10 and inhibits pro-inflammatory Th-17 response (Hopkins and Frankel 2021). Moreover, *Lactobacillus* and *Bacteroides* spp. promote the mucus barrier, while Clostridia produce butyrate, an energy source for host colon cells (**Error! Reference source not found.**) (Mullineaux-Sanders et al. 2019; Hopkins and Frankel 2021).

Commensal bacteria limit infections through three primary strategies: blocking pathogen growth by releasing antibacterial metabolites and competing for nutrients and oxygen, priming the host's immune defences, and out-competing pathogens during the resolution of infection (Stecher and Hardt 2011; Hopkins and Frankel 2021).

Diet significantly influences microbiota composition and can affect the progression of infection (Mullineaux-Sanders et al. 2019; Hopkins and Frankel 2021). For example, omega-6 polyunsaturated fatty acids (PUFAs) derived from dietary oils increase the levels of *Enterobacteriaceae*, segmented filamentous bacteria (SFB) and *Clostridium* spp., which are implicated in pro-inflammatory responses in the colon. Furthermore, a low-fibre diet can

lead commensal bacteria to degrade the mucus layer, increasing susceptibility to infection (Mullineaux-Sanders et al. 2019). Additionally, dietary compounds can also modify immune responses in the colon. For example, vitamin D suppresses Th17 responses, reducing ILC3 and IL-22 production, and increasing susceptibility to *C. rodentium* infection (Hopkins and Frankel 2021).

IEC metabolism changes during *C. rodentium* infection affects the microbiota by promoting a shift from obligate anaerobes (which thrive in oxygen-free environments) to facultative anaerobes (which can survive with or without oxygen) (Lupp et al. 2007; Berger et al. 2017; Hopkins et al. 2019; Mullineaux-Sanders et al. 2019; Caballero-Flores et al. 2021). *C. rodentium* uses metabolites from the microbiota to adjust its virulence gene expression. For instance, butyrate produced by obligate anaerobes in the colon induces the expression of the T3SS. Conversely, fucose liberated from host glycans by *Bacteroides thetaiotaomicron* (*B. thetaiotaomicron*) is sensed by *C. rodentium* and represses T3SS. This is a mechanism by which the pathogen conserves energy in expressing virulence factors until it is close to the mucosa. Moreover, *B. thetaiotaomicron* produces 1,2-propanediol, which is metabolised by *C. rodentium* to propionate and induces the expression of the LEE1 operon, encoding the regulator Ler, crucial for virulence. In addition, *C. rodentium* degrades the mucus layer via mucinases. This degradation induces the secretion of succinate by *B. thetaiotaomicron*, which is sensed by *C. rodentium* and leads to the expression of T3SS.

These interactions illustrate how *C. rodentium* exploits the microbiota to regulate its virulence and adapt to the host environment.

1.7 Aims and Objectives.

Previous studies have shown the impact of *C. rodentium* infection on host cells, revealing significant alterations in the molecular profile of intestinal epithelial cells. These changes affect cellular metabolism, cellular respiration, inflammatory responses, the microbiome, and the miRNome. Despite these findings, the specific regulatory mechanisms and pathways involved in the IEC response are not fully understood. This PhD aimed to understand how IECs respond to *C. rodentium* at a molecular level to provide valuable insights into host-pathogen interactions. The following objectives were outlined:

1. Investigate how intestinal epithelial cells respond to *C. rodentium* infection at the RNA level (Chapter 3).
2. Understanding transcriptome and proteome of *C. rodentium*-infected intestinal epithelial cells (Chapter 4).
3. Investigate the prostaglandin biosynthesis regulation during *C. rodentium* infection (Chapter 5).
4. Establish how the RNA-induced silencing complex (RISC) is regulated during *C. rodentium* infection (Chapter 6).

CHAPTER 2: Materials and Methods

2 CHAPTER 2: Materials and Methods.

2.1 Microbial strains and growth conditions.

2.1.1 [Microbial strains.](#)

All bacterial strains used in this study are detailed in **Table 2.1**.

Bacterial strains	Antibiotic resistance	Reference
<i>Citrobacter rodentium</i> ICC169	Nal ^a	Schauer and Falkow (1993)
<i>C. rodentium</i> ΔEspA	Nal ^a – Kn ^b	Petty et al. (2010)

^aNalidixic acid, ^bkanamycin.

Table 2.1. Bacterial strains used in this study.

2.1.2 [Bacterial media.](#)

Luria-Bertani (LB) Agar Miller (Fisher Scientific, 12821660) and LB Broth Miller (Fisher Scientific, 11345992) were prepared with double-distilled water and sterilised by autoclaving at 121 °C for 15 minutes, following the manufacturer's instructions. When necessary, media was supplemented with the appropriate antibiotics at the following concentrations: nalidixic acid (Nal) (Alfa Aesar, J67194.8=), 50 µg/mL; kanamycin (Kn) (Sigma Aldrich, K4000-25G), 50 µg/mL.

2.1.3 [Storage.](#)

All bacterial strains in this study were stored at -80 °C in Microbank™ cryovials (Pro Lab Diagnostics, PL.170/M). Cryovials were first inoculated with an overnight bacterial culture under an aseptic technique, labelled, and placed in a -80 °C freezer for long-term storage.

2.1.4 [Growth conditions.](#)

Bacterial strains were streaked into LB agar Petri dishes, with or without antibiotics when needed, from frozen stock and incubated at 37 °C overnight. Then, a colony from a plate was taken and cultured overnight in LB broth media at 37 °C with shaking at 150 rpm.

2.2 In vivo experiments.

2.2.1 Mouse husbandry.

All animal experiments adhered to the Animals (Scientific Procedures) Act 1986 (Home Office 2014) and were approved by the local Ethical Review Committee, with Project Licence (PPL) number P42814957 and Personal Licence (PIL) number I041F3CC0.

Pathogen-free female C57BL/6 mice (18-20 g; purchased from Charles River Ltd., UK) were housed in individually ventilated, HEPA-filtered cages with sterile bedding and nesting materials, with sterilised food and water freely available. Upon arrival, the mice were randomised using a random number generator and tagged for identification before each experiment. Different colour markers (blue, green, red, black, or no tag) were used to mark the animals' tails. Before initiating the experiments, the mice were acclimatised to the new environment for 6 days. Independent single-infection experiments were conducted with 4-6 mice per group. Mice were humanely euthanised by cervical dislocation.

2.2.2 Preparation of culture and infection of mice.

Mice were infected with *C. rodentium* strain ICC169 (Wild Type, WT) or PBS-treated. To prepare the inoculum, bacteria were cultured overnight (37 °C, 150 rpm shaking) from frozen stock in 50 mL tubes containing 20 mL of LB broth supplemented with nalidixic acid (50 µg/mL). On the day of infection, bacteria were pelleted (4000 rpm for 10 minutes) and resuspended in 2 mL of sterile PBS.

In the main experimental groups, the *C. rodentium* experiment was conducted twice to assess transcriptomic changes. Mice received 200 µL of *C. rodentium* WT ($6.3E^{+09}$ f CFU) by oral gavage (treatment group) or 200 µL of PBS (control group) in these experiments. In a separate experiment, aspirin (ASA) (Sigma Aldrich, A5375-100G) was used to investigate Lcn 2 production and phenotype changes, including crypt hyperplasia development. This experiment was performed once and included four conditions: (1) mice receiving 200 µL of *C. rodentium* WT alongside ASA, (2) mice receiving 200 µL of PBS alongside ASA, (3) mice receiving 200 µL of *C. rodentium* WT without ASA, and (4) mice receiving 200 µL of PBS without ASA. After infection, all mice were weighed and monitored daily until the end of the experiment.

2.2.3 Aspirin preparation and administration.

The aspirin concentration given to mice was 25 mg/kg/day. Considering that the average mice weight was around 20 g and that mice drink an average of 4 mL of water daily, 125 mg of aspirin was dissolved in 1 L of tap water and placed in the drinking water holder. The aspirin solution was prepared fresh and replaced every two days.

2.2.4 *C. rodentium* faecal enumeration.

Infected mice were separated into individual boxes to be weighed and to collect faeces. In the main experimental group, faeces from the treatment group were collected, and for the ASA experiment, from both the *C. rodentium*-ASA treatment group and the *C. rodentium*-treatment group.

Faeces from infected mice were collected, weighed, and resuspended in PBS (1 mL of PBS per 0.1 g of stool). The suspension was then serially diluted and plated in LB agar supplemented with nalidixic acid (50 µg/mL). Plates were incubated at 37 °C overnight, and colonies were counted the following day. Each dilution was plated in triplicates.

2.2.5 Tissue sample collection.

Tissue samples were collected at eight days post-infection (DPI), the peak of infection. Four centimetres of the terminal colon were collected. Of these, 3.5 cm were cut longitudinally for enterocyte extraction; to preserve the integrity of the tissue, stools were removed using forceps. An additional 0.5 cm was collected for tissue fixation and Haematoxylin and Eosin (H&E) staining.

2.2.5.1 Intestinal epithelial cell isolation.

Colon samples were placed in a 50 mL Falcon tube containing 4 mL of intestinal epithelial cells (IEC) isolation reagent (5 mL 10x HBSS; 0.5 mL HEPES; 100 µL EDTA 0.5M; 250 µL β-mercaptoethanol; to 50 mL H₂O). Then, the tissue was incubated at 37 °C with shaking at 200 rpm. for 40 min. Next, the tissue was removed, and the lifted enterocytes were centrifuged at 4 °C for 10 min (2500 g). Finally, cells were washed twice with PBS, 4 ml of PBS and 0.5 mL of PBS, respectively, and centrifuged at 4 °C for 10 min (2500 g). The supernatant was discarded, and the enterocyte pellet was stored at –80 °C for further RNA extraction.

2.2.5.2 *Histological analyses.*

0.5 cm of the distal colon was collected and fixed in 4% paraformaldehyde (Thermo Scientific, 28908) diluted in PBS for at least 48 hours. After fixation, samples were transferred to PBS and were Haematoxylin and Eosin (H&E) stained by the Bioimaging Hub, Histology department at Cardiff University Bioimaging Hub Core Facility.

Histological images were captured using the Leica DMRB microscope at the Cardiff University Bioimaging Hub. Crypt length was measured with Image J software for all animals and all conditions, and the results were analysed using GraphPad Prism.

2.3 RNA sequencing and bioinformatic analysis.

2.3.1 RNA sequencing sample preparation.

RNA was extracted from IEC samples stored at -80°C using the RNeasy mini kit (Qiagen, 74104). RNA concentration was quantified using the NanoDrop spectrophotometer (samples with concentrations higher than $100\text{ ng}/\mu\text{L}$ were considered for further steps). Next, RNA was treated with RQ1 RNase-Free DNase (Promega, M6101) and the quality of the samples was determined using TapeStation and Qubit technologies. DNase treatment was repeated twice due to the high concentration of DNA in the samples. Then, TapeStation and Qubit were repeated, and samples with an RNA concentration higher than $88.4\text{ ng}/\mu\text{L}$ and RNA Rin higher than 2.7 were selected. Three samples for each condition (Infected and Control) from two independent experiments were selected.

2.3.2 RNA sequencing.

The RNA extracted from IEC samples was subjected to polyA tail purification. PolyA selection is often used to enrich mRNA by capturing the polyadenylated tails that are characteristic of eukaryotic mRNA, minimising the presence of bacterial RNA, which typically lacks polyA tails. To ensure biological replicates and account for inter-individual variability, mRNA was extracted and processed separately for each mouse. The RNA samples were assessed for quality and purity, including checking ribosomal RNA (rRNA) content, to ensure minimal rRNA contamination prior to library preparation.

The polyA-purified mRNA was used to create RNAseq libraries. Single-end RNA sequencing was performed on an Illumina NextSeq500 platform with a read configuration of 1x75 base

pairs, generating approximately 30 million reads per sample. Sequencing depth was optimised to provide sufficient resolution for transcriptomic analysis. Sequencing was performed by the Genome Hub, School of Biosciences, Cardiff University. The raw sequencing reads were aligned to the reference genome (*Mus_musculus*.GRCm38.101) using the STAR aligner, and gene expression levels were quantified with FeatureCounts by counting the reads mapped to each gene.

2.3.3 Bioinformatic analysis.

Transcriptomic analysis was carried out using the Linux operating system and R software, with Bioconductor packages including DESeq2 for normalisation and differential analysis, and SARTools for quality control (Varet et al. 2016). Differentially expressed genes were annotated using Ensembl and cross-referenced against the UniProt Reference Proteomes of 17102 reviewed mouse protein entries. Variance Stabilising Transformation (VST) was applied to transform count data, followed by hierarchical clustering to assess variability across samples.

The analysis began with the identification of differentially expressed genes using an adjusted p-value threshold of <0.05 , calculated using the Benjamini-Hochberg (BH) method to control for the false discovery rate. Genes with a $-\log_{10}$ adjusted p-value >1.30 were considered significant, and a \log_2 fold change (\log_2FC) threshold of ± 0.58 was applied to classify genes as upregulated ($\log_2FC > 0.58$) or downregulated ($\log_2FC < -0.58$).

Following the identification of differentially expressed genes, a comprehensive manual curation process was conducted. All differentially expressed genes were linked to their corresponding protein names, functions, associated pathways, and subcellular locations using the UniProt database. This step was crucial for accurate functional classification and for grouping genes into relevant pathways. Additionally, the top 20 upregulated and downregulated genes were further examined in detail to assess their subcellular localisation and specific biological roles.

Pathway analysis for the transcriptome data was conducted using Ingenuity Pathway Analysis (IPA, QIAGEN Inc., <https://digitalinsights.qiagen.com/IPA>) (Kramer et al. 2014) and ClueGO, a Cytoscape plugin (Bindea et al. 2009). IPA was employed to identify over-

represented canonical pathways, cellular functions, and upstream regulators. ClueGO provided a network-based visualisation of gene ontology (GO) terms, which were used to validate and cross-check the pathways identified by IPA. For each pathway selected for further analysis, the associated genes were examined in detail, including their Log2FC values and the adjusted p-value, to ensure the robustness and biological significance of the findings.

After completing the transcriptome analysis, an integrated analysis of both the transcriptome and proteome datasets was performed. The two datasets were combined to identify common entries as well as those unique to either the transcriptome or proteome. Differentially expressed genes and proteins were then compared to discern patterns of regulation across both levels. Common entries were analysed to determine their contributions to specific biological pathways, while unique entries were explored for their involvement in distinct pathways not captured in the other dataset. This integrative approach provided a comprehensive view of the molecular changes occurring during infection.

Finally, PathVisio was employed to map the differentially expressed genes and proteins from both the transcriptome and proteome data onto curated and custom biological pathways. This allowed for a deeper exploration of the molecular interactions disrupted during *C. rodentium* infection. The combination of manual curation, detailed transcriptome analysis, integration of transcriptome and proteome data, and the use of advanced bioinformatics tools provided a robust and nuanced understanding of the altered pathways.

2.4 Proteome.

The proteome data used in this study (PXD005004) was deposited in the ProteomeXchange Consortium via the PRIDE database and was originally published Berger et al. (2017). This dataset comprises the proteome of infected enterocytes, collected 8 days post-*C. rodentium* infection. The proteome data was utilised to complement the transcriptomic analysis by identifying and integrating protein-level changes during infection. This integration allowed for a comprehensive exploration of the molecular pathways and biological processes affected during *C. rodentium* infection.

2.5 Lipocalin-2 ELISA assay.

Additional stool samples were collected for the ASA experiment for an ELISA assay to detect Lipocalin-2 (Bio Techne, DY1857) concentration. These samples were placed in the -80 °C freezer until analysis.

Samples of mice from all groups from 5 DPI and 8 DPI were analysed in duplicates. Frozen stool pellets were resuspended in PBS-0.1% Tween 20 at a ratio of 0.1 g of stool per 1 mL PBS. The samples were shaken for 20 min and then centrifuged at maximum speed for 10 min before freezing the supernatant. Supernatants were kept at the -80 °C freezer or processed on the same day.

Faecal Lipocalin-2 was measured using Mouse Lipocalin-2/NGAL DuoSet ELISA according to the manufacturer's instructions. The dilutions used for the different samples are shown in

Table 2.2:

<i>Treatment</i>		<i>Dilution</i>	
<i>C. rodentium</i>	<i>Aspirin</i>	<i>5 DPI</i>	<i>8 DPI</i>
Infected	No aspirin	1:500	1:2000
	Aspirin	1:500	1:2000
No infected	No aspirin	1:50	1:100
	Aspirin	1:50	1:100

Table 2.2. Dilutions used for Lipocalin-2 ELISA assay.

2.6 Molecular biology techniques.

2.6.1 Plasmids.

All plasmids used in this study are detailed in **Table 2.3**

Plasmids	Antibiotic resistance	Origin/Reference
pCMV-VSV-G-env	Amp ^a	Stewart et al. (2003)
pCMV-MMLV- <i>gag-pol</i>	Amp ^a	Buchsacher et al. (1999)
pMMLV-Puro-HA-Ago 1	Amp ^a – Puro ^b	This study
pMMLV-Puro-HA-Ago 2	Amp ^a – Puro ^b	This study
^a Ampicillin, ^b puromycin.		

Table 2.3. Plasmids used in this study.

2.6.2 Plasmid DNA extraction.

Plasmids expressed in *E. coli* were stored at -80 °C for long-term storage. For plasmid extraction, bacteria were streaked in LB Agar plates supplemented with ampicillin (Amp) (Melford, A0104-25G), 100 µg/mL, and incubated at 37 °C overnight. The next day, a single colony was picked and placed in LB broth and incubated at 37 °C overnight, shaking 150 rpm. Finally, the plasmid was extracted following the instructions from the Monarch® Plasmid Miniprep Kit (New England Biolabs (NEB), T1010S) and stored at -20 °C. DNA concentration was measured using a Nanodrop spectrophotometer.

2.6.3 Expression vector - pMMLV-Puro-HA-Ago proteins.

The Gibson technique was selected to prepare the desired expression vector; however, after unsuccessful attempts, the vectors were designed and purchased from Vector Builder. The MMLV Retrovirus Gene Expression Vector, derived from Moloney murine leukaemia virus, was selected as it is an efficient vehicle for introducing genes permanently into mammalian cells.

The following genes were introduced in the vector (**Figure 2.1**):

Puromycin resistance gene: allows cells to be resistant to puromycin and the selection of cells expressing this gene by adding the antibiotic to the media.

Self-cleaving 2A peptide: causes co-translational cleavage of the encoded polypeptide.

HA/hAGO2[NM_012154.5]: HA refers to the hemagglutinin (HA) epitope tag, a small protein tag added to the target protein to facilitate detection and purification; hAGO2 refers to the human Argonaute 2 (Ago2).

HA/hAGO1[NM_012199.5]: HA refers to the HA epitope tag, and hAGO1 refers to the human Argonaute 1 (Ago1).

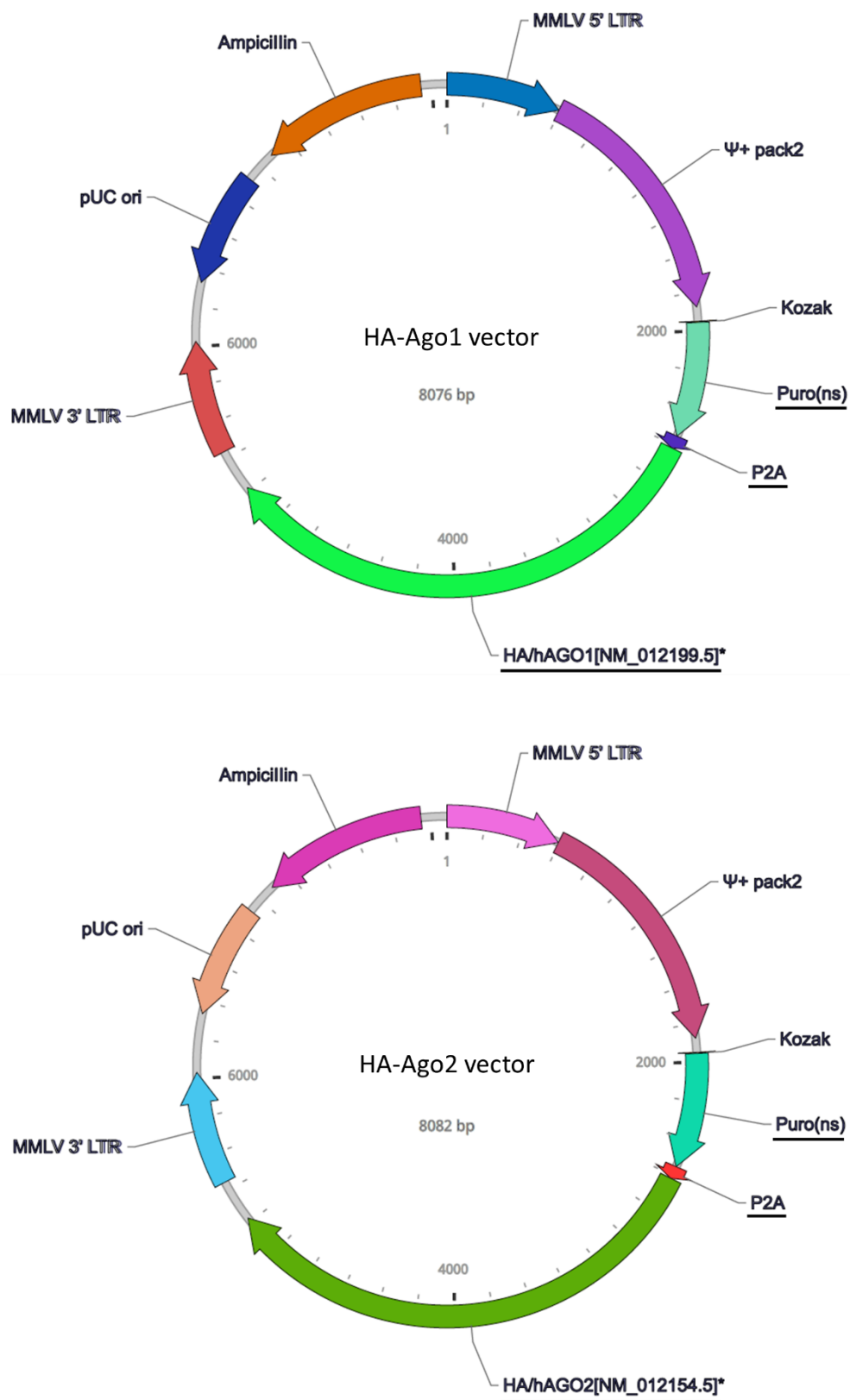


Figure 2.1. pMMLV-Puro-HA-Ago vector structure.
Schematic representation of the parts of the pMMLV-Puro-HA-Ago vector. Image from Vector Builder.

2.7 Cell culture techniques.

2.7.1 Cell culture media.

The cell lines in this study were cultured in different media combinations (**Table 2.4**). Media was purchased from Sigma or Fisher Scientific. Fetal Bovine Serum (FBS), Glutamax (L-alanyl-L-glutamine), and non-essential amino acids (NEAA) were purchased from Fisher Scientific (11550356, 11574466, and 11350912, respectively). Puromycin was purchased from VWR (J67236.XF).

Cell Line	Media type	Glucose concentration	Supplements
HeLa	DMEM	1000 mg/L	FBS (10%), Glutamax (1%), NEAA (1%)
HeLa (HA-Ago1 or HA-Ago2)	DMEM	1000 mg/L	FBS (10%), Glutamax (1%), NEAA (1%), Puromycin (2 µg/mL)
HEK293E	DMEM	4500 mg/L	FBS (10%), Glutamax (1%), NEAA (1%)
CMT93	DMEM-F12	4500 mg/L	FBS (5%), Glutamax (1%), NEAA (1%)
CMT93 (HA-Ago1 or HA-Ago2)	DMEM-F12	4500 mg/L	FBS (5%), Glutamax (1%), NEAA (1%), Puromycin (2 µg/mL)

Table 2.4. Cell culture media.

2.7.2 Cell line subculturing.

Cell subculturing was performed every 2-4 days depending on the cell line, when cells reached 70%-80% confluence. All reagents and media were pre-warmed to 37 °C (or room temperature for trypsin-EDTA 0.05%) before use. The procedure began with the removal and discarding of the cell culture medium, followed by a DPBS (Sigma, D8537-100ML) wash to remove any residual media, which was then also discarded. Trypsin-EDTA 0.05% (Fisher Scientific, 11580626) was added to the tissue culture flask to detach cells from the flask and disaggregate cells and incubated at 37 °C for 5-15 minutes, depending on the cell line, after which fresh media was added to inactivate the trypsin. The concentrated cell suspension was then transferred to a new T25 tissue culture flask (Fisher Scientific, 10700052) with fresh media according to the routine split ratio. Finally, the tissue culture flask was placed in

an incubator at 37 °C with 5% CO₂ and monitored daily or every other day for standard cell growth.

2.7.3 Cell line cryopreservation.

For long-term storage, all cell lines were cryopreserved in liquid nitrogen. The process began with culturing cells in a T75 tissue culture flask (Falcon, 353136) until they reached 70%-80% confluence. The cells were then washed with DPBS and incubated with trypsin-EDTA 0.05% for 5-15 minutes. After incubation, fresh media was added, and the cell suspension was transferred to a sterile Falcon tube and centrifuged at 1200 rpm for 4 minutes at 20 °C to pellet the cells. The supernatant was aspirated, and the pelleted cells were resuspended in a freezing medium (FBS with 10% DMSO as a cryoprotectant). The cell suspension was aliquoted into 2 mL cryovials (Fisher Brand, 12-567-501), which were labelled with the cell line name, passage number, date, and operator's name. The vials were then placed in a Mr Frosty® Freezing container (Nalgene, 5100-0001) filled with isopropanol to achieve a slow cooling rate of approximately -1 °C per minute, and stored in a -80 °C freezer for at least 24 hours. Finally, the cryovials were transferred to liquid nitrogen for long-term storage at -130 °C.

2.7.4 Recovery of cryopreserved cells.

To recover cryopreserved cells, the cryovial was removed from liquid nitrogen and quickly thawed in a 37 °C water bath. The thawed cells were then resuspended in fresh media and gently centrifuged at 1200 rpm for 4 minutes at 20 °C. The supernatant was discarded, and the pelleted cells were resuspended in complete growth media. Finally, the cells were transferred to a new T25 tissue culture flask and incubated at 37 °C with 5% CO₂.

2.8 Transfection assay.

The transfection assay was used to transfect CMT93 cells with HA-Ago1/Ago2 plasmids. After confirming the expression of the proteins in the CMT93 cells, a more stable cell line was generated.

CMT93 cells were seeded in a 24-well plate (Falcon, 10048760). After two days, when the cells reached approximately 70% confluence, transfection was performed using GeneJuice transfection reagent (Sigma, 70967) according to the manufacturer's instructions. The

transfection mix was prepared by combining 20 μL of OPTIMEM (Fisher Scientific, 11524456) with 0.75 μL of GeneJuice and at least 0.25 μg of plasmid DNA per well. This mixture was then added to the cells, which were incubated for 24 hours before being washed with DPBS. Following transfection, CMT93 cells were treated with puromycin (2 $\mu\text{g}/\text{mL}$) to select cells that successfully incorporated the plasmids.

2.9 Transduction assay.

Permanent cell lines expressing HA-Ago1 and HA-Ago2 were generated following a viral transduction protocol. This protocol allows the delivery of genes of interest into the genome of a target cell in vitro by infecting them with a pseudo-virion (see **Figure 2.2**).

Three different plasmids were used to generate this pseudo-virion: pMMLV-HA-Protein (HA-Ago1 or HA-Ago2), pCMV-VSV-G env, and pCMV-MMLV-gag-pol.

pMMLV HA-Protein (HA-Ago1 or HA-Ago2): this vector is based on the Moloney murine leukaemia virus (MMLV). It contains the Long Terminal Repeats (LTRs) necessary for gene expression and facilitating the integration of the viral genome into the host cell's DNA, the gene of interest (either HA-Ago1 or HA-Ago2), a viral packaging signal essential for the production of viral particles, and resistance marker for puromycin to select successfully transduced cells.

pCMV-MMLV-gag-pol: this plasmid provides essential components for pseudo-virion assembly, including gag proteins for the capsid and pol enzymes (reverse transcriptase and integrase) for reverse transcription and integration of the viral genome.

pCMV-VSV-G env: this plasmid encodes the envelope (env) protein of the Vesicular stomatitis virus (VSV-G), which facilitates the entry of the pseudovirus into target cells.

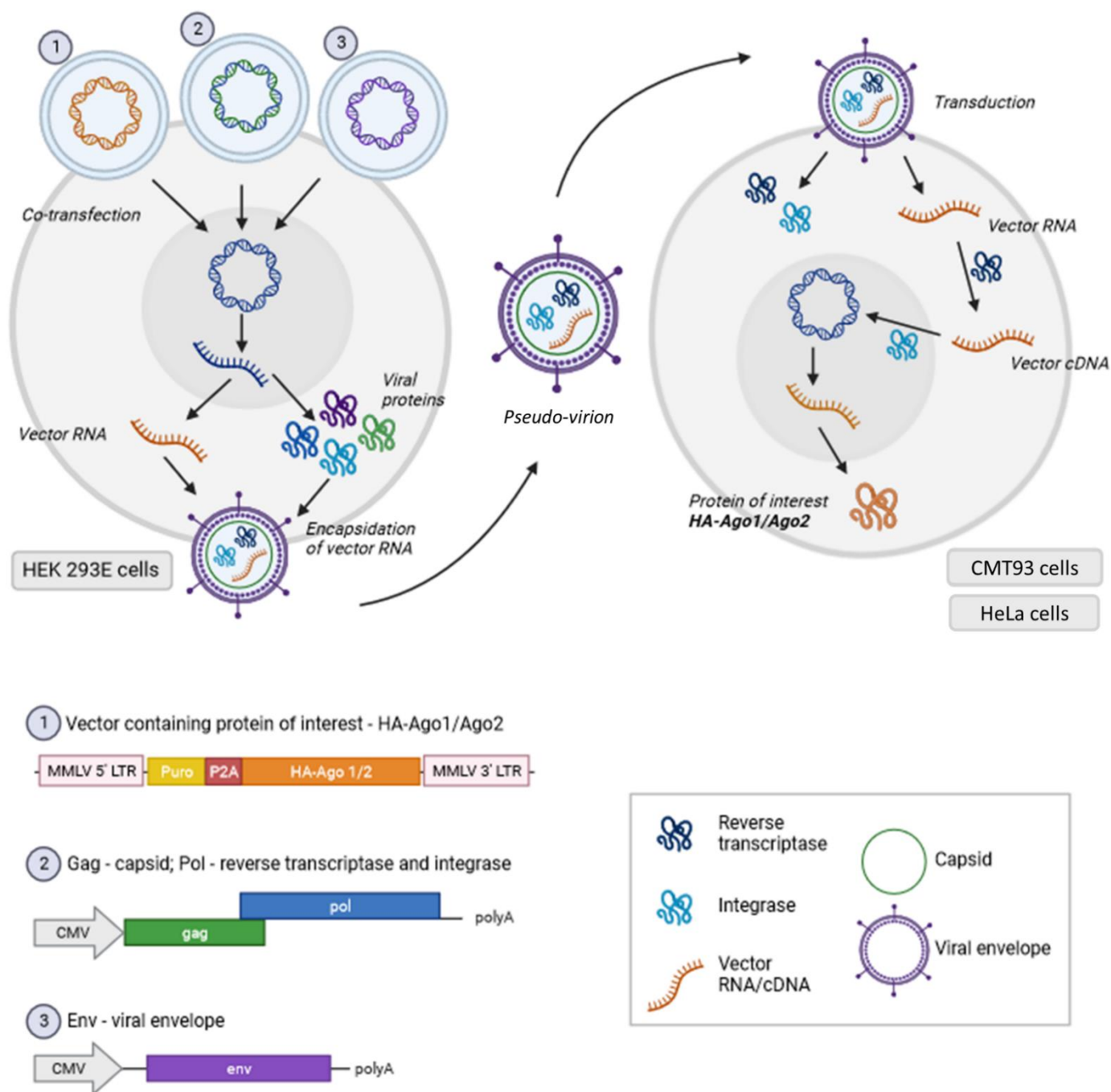


Figure 2.2. Viral transduction.

To generate a permanent cell line expressing a protein of interest, HEK293 cells are co-transfected with plasmids that encode the protein of interest, envelope proteins (*env*), and viral components necessary for virion assembly (such as *gag-pol*). After transfection, the cells are incubated to produce pseudovirions, which are then collected from the supernatant. This virion-containing supernatant is used to infect target cells (for example HeLa or CMT93), leading to the integration of the gene of interest into the host cell genome and resulting in stable expression of the target protein. Figure created with BioRender.com.

To produce the pseudo-virion that carries the gene of interest, these plasmids were co-transfected into HEK293 cells, a cell line that supports high transfection efficiency. The process involves:

1. Seeding and co-transfection:

HEK293 cells were seeded in a 6-well plate (Falcon, 10110151) at a density of 3×10^5 cells per well and grown to 70% confluence. On the day of the reaching confluence, cells were co-transfected with the plasmids using Lipopectamin® 3000 transfection reagent (Thermo Fisher, L3000001), following the manufacturer's instructions. A master mix of the plasmids (1250 ng of pMMLV-HA-Protein; 1000 ng of pCMV-MMLV-gag-pol; and 250 ng of pCMV-VSV-G env) was prepared and added to the HEK293 cells.

Additionally, HeLa and CMT93 cells were seeded in 24-well plates at a density of 5×10^4 cells per well on the same day.

2. Pseudo-virion production:

After 24h, the transfected cells were washed with DPBS and incubated for an additional 24 hours to produce pseudo-virions. The supernatant containing the pseudo-virions was collected, buffered with 20 mM HEPES (Fisher Scientific, BP299-100), and filtered using a 0.45 μ m filter (MCE NON-PVDF membrane) (Sartorius, FC142).

3. Infection and selection:

The filtered supernatant was used to infect 70%-confluent HeLa or CMT93 cells. The viral RNA was reverse-transcribed into DNA and integrated into the host cell genome by the viral integrase enzyme. After 24 hours of infection, cells were washed with DPBS and treated with puromycin (2 μ g/mL) to select cells that have integrated the gene of interest. Puromycin selection was carried out for at least 6 weeks to ensure stable integration and expression of the transgene.

2.10 Infection of cells.

For immunostaining, CMT93 cells were seeded into 24-well plates with coverslips at a density of 5×10^4 cells per well, while for Western Blot, CMT93, CMT93-HA-Ago1, or CMT93-HA-Ago2 cells were seeded into 6-well plates at 3×10^5 cells per well. All cells were grown for

48 hours until they reached approximately 70% confluency for immunostaining and 90% confluency for Western Blot.

To prime the bacteria, *C. rodentium* was cultured in LB broth for 8 hours at 37 °C with shaking at 150 rpm, then diluted 1/500 in pre-warmed DMEM (1g/L glucose, without FBS), and incubated overnight at 37 °C in 5% CO₂ under static conditions. Following bacterial priming, cells were washed with DPBS, and the media was replaced with fresh media appropriate for each cell type before infection.

For Immunostaining, CMT93 cells were infected with 50-100 µL of the primed *C. rodentium*, centrifuged for 5 minutes at 500G, and incubated for 1 to 4 hours at 37 °C in 5% CO₂. After infection, cells were washed with DPBS, treated with fresh media containing gentamicin (100 µg/mL) (Gibco, 11530506) to remove non-adherent bacteria and incubated for an additional 3 to 6 hours. As a positive control, a medium containing 25 µM CCCP (a mitochondrial uncoupler) was added and incubated at 37 °C for 30 minutes. Post-infection, all cells were washed three times with DPBS, fixed in 4% paraformaldehyde for 15 minutes, washed three additional times, and stored at 4 °C wrapped in parafilm until processing for immunostaining.

For Western Blot, CMT93 cells (including CMT93-HA-Ago1 and CMT93-HA-Ago2) were treated similarly after seeding and media replacement. Cells were infected with 250 µL of the primed *C. rodentium* and incubated for 3 hours at 37 °C in 5% CO₂. Post-infection, cells were washed with DPBS, treated with gentamicin-containing media to eliminate non-adherent bacteria and incubated for an additional 3 hours. After this final incubation, cells were washed three times with DPBS, DPBS was aspirated, and the plates were stored at -80 °C until further processing for Western Blot analysis.

2.11 Immunofluorescence.

Fixed coverslips were treated with 50 mM NH₄Cl/PBS for 10 minutes, permeabilised with 0.1% Triton-100 in PBS for 4 minutes, washed 2 times with PBS, and blocked with 0.2% Bovine Serum Albumin (BSA)/PBS for 10 minutes. The primary antibody mix in 0.2% BSA/PBS was added and incubated wet for 1 h, then washed twice with PBS, and the secondary antibody mix was incubated for 45 min. Finally, stained coverslips were washed 3 times in

PBS, dipped in H₂O, and mounted in the microscopic slide (Fisher Scientific, 17224894) using ProLong Gold Antifade reagent (Fisher Scientific, 11559306). The antibodies used are detailed in **Table 2.5**.

Images were acquired using a ZEISS LSM880 Airyscan confocal microscope at Cardiff University Bioimaging Hub Core Facility and processed using ZEN 3.6 (Blue Version) (Carl Zeiss Microscopy GmbH).

Name	Primary/ Secondary/Stain	Produced in	Target	Dilution	Company
Hoechst	Stain	-	DNA	1:500	Sigma
Phalloidin Trit C	Stain	-	Actin	1:500	Sigma
Recombinant Anti-TOMM20	Primary	Rabbit	Tomm20	1:500	Abcam
Alexa Fluor [®] 488-conjugated AffiniPure Donkey Anti-Rabbit IgG (H+L)	Secondary	Donkey	Rabbit antibodies	1:200	Jackson Immuno Research

Table 2.5. Antibodies and stains used for immunostaining.

2.12 Western Blot.

2.12.1 [Cell sample preparation.](#)

Cells stored at -80 °C were lysed using a lysis buffer prepared by diluting a 7X stock solution to a 1X working concentration. The lysis buffer stock (7X) consisted of the following components: Tris pH 7.4, 350 mM; NaCl, 1.05 M; EDTA, 14 mM; NP-40, 7%; H₂O. For lysis, this stock solution was diluted to 1X, and protease inhibitor (Sigma Aldrich, P8340-5ML) was added (25 µL per 7 mL of Lysis buffer 1X).

The lysis buffer was added to the well, and cells were scrapped and transferred to a 1.5 microfuge tube. The samples were homogenised using a 1 mL syringe and a 24G needle and incubated at 4 °C for 30 minutes. Finally, samples were centrifuged at 15000 rpm for 15 minutes at 4 °C, and the supernatant was collected.

2.12.2 [Protein BCA assay.](#)

Protein concentrations were determined using the Pierce[™] BCA Protein Assay Kit (ThermoFischer Scientific, 23227) as recommended by the manufacturer.

2.12.3 SDS-PAGE.

For an even result while running the SDS-polyacrylamide gel electrophoresis (SDS-PAGE), all wells contained the same sample volume and the same protein amount (at least 10 µg). Each gel contained the molecular weight control (Color Prestained Protein Standard, Broad Range (10-250 kDa), NEB, P7719S), a sample containing protein of interest, and a blank (containing lysis buffer 1X and loading buffer 1X).

Samples were prepared by adding loading buffer 4X (final concentration 1X) to a final volume of 50 µL. The 4X loading buffer, also known as Laemmli buffer, consisted of the following components: Tris pH 6.8, 250 mM; glycerol, 25%; 20% SDS, 6%; bromophenol blue, 1%; β-mercaptoéthanol, 8%.

The colour protein standard was mixed with lysis buffer 1X, and blanks were prepared by mixing lysis buffer with loading buffer (final concentration 1X).

The Mini-PROTEAN® Tetra Cell Casting Module (Bio Rad, 1658021) was used to prepare the 10% SDS-PAGE gels (formulation in **Table 2.6**). Samples were denatured for 5 minutes at 100 °C before being loaded into the gel. Then, samples were separated by SDS-PAGE in the Mini-PROTEAN Tetra Vertical Electrophoresis Cell (Bio Rad, 1658004) at 120V for 5 minutes and at 80V for 90-120 minutes in running buffer 1X (Running Buffer 10X: Tris pH 7.4, 0.25 M; SDS, 1%; glycine, 14.4%; H₂O). Acrylamide/Bis-acrylamide was obtained from Sigma (A3699-5X100ML).

10% SDS-PAGE components	Resolving gel 10% (30 mL)	Stacking gel 4% (5 mL)
H ₂ O	12.3 mL	3.075 mL
1.5 M Tris-HCl, pH 8.8	7.5 mL	-
0.5 M Tris-HCl, pH 6.8	-	1.25 mL
20% SDS	0.15 mL	0.025 mL
Acrylamide/Bis-acrylamide (30%/0.8%)	9.9 mL	0.67 mL
10% ammonium persulfate (APS)	0.15 mL	0.025 mL
TEMED	0.02 mL	0.005 mL

Table 2.6. 10% SDS-PAGE gel composition.

2.12.4 Membrane transference.

Gels were transferred to Low Fluorescence-Polyvinylidene Fluoride (LF-PVDF) membrane (from Trans-Blot Turbo RTA Midi 0.45 μm LF PVDF Transfer Kit, BioRad, 1704275) using the Trans-Blot Turbo Blotting System (Bio-Rad, 1704150) according to the manufacturer's instructions. The membrane was activated in methanol for 1 minute before transfer. After the transfer, the membrane was washed once for 5 minutes with TBS 1X (10X stock, pH 7.5: Tris, 0.5 M; NaCl, 1.5 M; H₂O) and incubated with a blocking solution (Tris 10 mM pH 7.4; NaCl, 0.15 M; EDTA, 1 mM; BSA, 3%; gelatine, 0.5%; H₂O) for 30 minutes at room temperature with shaking.

The primary antibody, diluted in blocking solution, was incubated overnight at 4 °C with shaking. The following day, the membrane was washed 3 times for 10 minutes each with TBS-Tween (TBS 1X; Tween 20, 0.2%; H₂O). The secondary antibody was then added and incubated for 1 hour at room temperature, protected from light and shaking. The membrane was washed 3 more times with TBS-Tween for 10 minutes each, followed by a final wash with TBS (without Tween) for 10 minutes. Immunodetection was performed using the LI-COR Odyssey-CLX system, and densitometry analysis was conducted using ImageJ.

The antibodies used for Western Blot are detailed in **Table 2.7**.

Name	Primary/ Secondary	Produced in	Target	Dilution	Company
Purified anti-HA.11 Epitope Tag Antibody	Primary	Mouse	HA tag	1:1000	Biolegend
Anti α-tubulin antibody mouse monoclonal	Primary	Mouse	Tubulin	1:2000	Sigma
Alexa-Fluor anti-mouse 680	Secondary	Goat	Mouse antibodies	1:15000	Jackson Immuno Research

Table 2.7. Antibodies used for Western Blot.

2.13 Statistical analysis.

Statistical analyses and graphical representation of the data were performed using GraphPad Prism version 10.0.0 for Windows, GraphPad Software, Boston, Massachusetts USA, www.graphpad.com. Statistical significance was determined based on the chosen test and significance thresholds, which are specified for each analysis as relevant.

CHAPTER 3: Intestinal epithelial cells response to
Citrobacter rodentium infection at the RNA level

3 CHAPTER 3: Intestinal epithelial cells response to *Citrobacter rodentium* infection at the RNA level.

3.1 Introduction.

C. rodentium is responsible for the induction of transmissible colonic crypt hyperplasia in mice, which is characterised by hyperproliferation of enterocytes, colonic crypt elongation, depletion of goblet cells and mucosal thickening (Collins et al. 2014b; Hopkins and Frankel 2021). Its infection progression is divided into four phases: the establishment phase, occurring 1-3 days post-infection (DPI) when it colonises the caecal patch; the expansion phase, between 4-8 DPI, *C. rodentium* attaches to the distal part of the colon and proliferates; the steady-state phase, between 8-12 DPI, *C. rodentium* reaches the peak of infection; and the clearance phase, from 12 DPI, bacteria rapidly decrease and the host starts to clear the infection (Mullineaux-Sanders et al. 2019; Hopkins and Frankel 2021).

Most information available regarding *C. rodentium*-host interactions describes changes in host metabolism, microbiota, and immune response (Collins et al. 2014b; Silberberger et al. 2017; Mullineaux-Sanders et al. 2019; Hopkins and Frankel 2021; Stockinger 2021).

Recently, publications have shown significant changes in the abundance of proteins in intestinal epithelial cells (IEC) during *C. rodentium* infection in vivo (Berger et al. 2017; Berger et al. 2018), with upregulated pathways such as aerobic glycolysis and cholesterol biosynthetic pathway, alongside the downregulation of mitochondrial proteins biogenesis. These differences in protein abundance could be attributed to post-translational regulation processes or variations in the RNA expression.

While proteomic and metabolomic methods have been typically employed to study the effects of *C. rodentium* infection in the host, transcriptomics analysis offers additional information by detecting early changes in gene expression. This approach can detect regulatory pathways and networks that occur before protein synthesis and post-translational modifications. In this study, we applied a transcriptomic approach to investigate the in vivo effects of *C. rodentium* infection. By focusing on RNA changes, transcriptomic analysis provides a complementary perspective to previous studies, helping to understand how *C. rodentium* modifies cellular processes at the RNA level.

3.2 Aims and Objectives.

This study aims to understand the mechanisms of infection and the induced changes in intestinal epithelial cells during *C. rodentium* infection by characterising the RNA expression profile. To achieve this goal, the specific objectives are:

- To characterise the transcriptomic profile of *C. rodentium*-infected intestinal epithelial cells.
- To analyse the gene expression patterns to identify differentially expressed genes and elucidate the altered pathways in the host during infection.

3.3 Results.

3.3.1 Mice colonisation and crypt hyperplasia development.

Colonisation of mice and hyperplasia development were determined to control for successful infection. Stools from seven infected mice were collected daily to calculate the CFU Maculins et al. 2016 and assess colonisation. The results indicate that for all mice colonisation reaches a plateau at day 6 post-infection (PI) and remains stable until the last day of the experiment, day 8 PI (**Figure 3.1**).

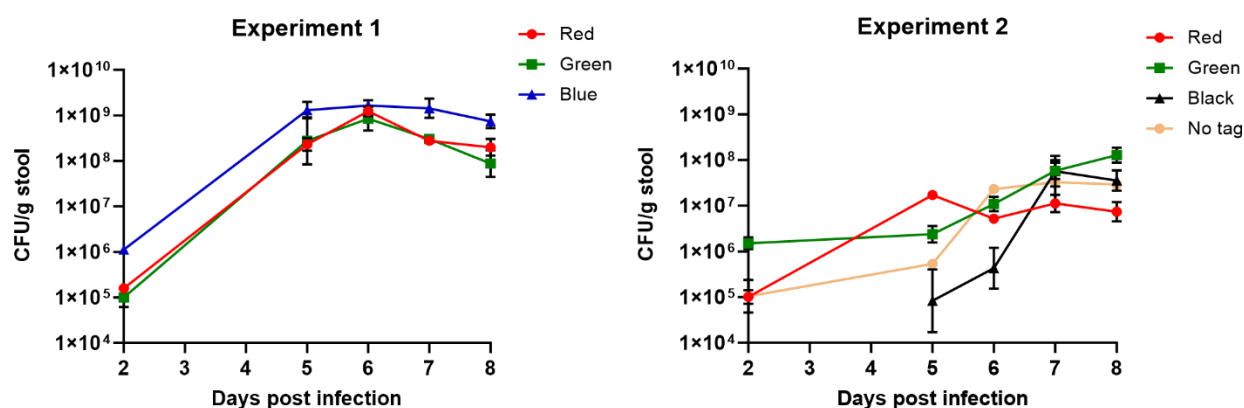


Figure 3.1. *Citrobacter rodentium* colonisation in infected mice.

The results show a consistent pattern across both experiments, with colonisation reaching a plateau between days 5 and 8 post-infection. Each colour in the graph corresponds to a distinct animal identification tag: blue, green, red, black, or untagged (represented as light orange). Graphs were generated using GraphPad Prism.

H&E staining was performed on the distal colon of samples obtained 8 DPI to confirm the presence of hyperplasia. Images from experiments 1 and 2 were analysed, and crypt length was measured for each image. Comparing infected and non-infected enterocytes showed that the former developed crypt hyperplasia during *C. rodentium* infection (**Figure 3.2A**). A Mann-Whitney test revealed a significant difference (p-value < 0.05) in crypt length between infected and non-infected colons (**Figure 3.2B**), confirming that infected mice develop hyperplasia as a consequence of *C. rodentium* infection.

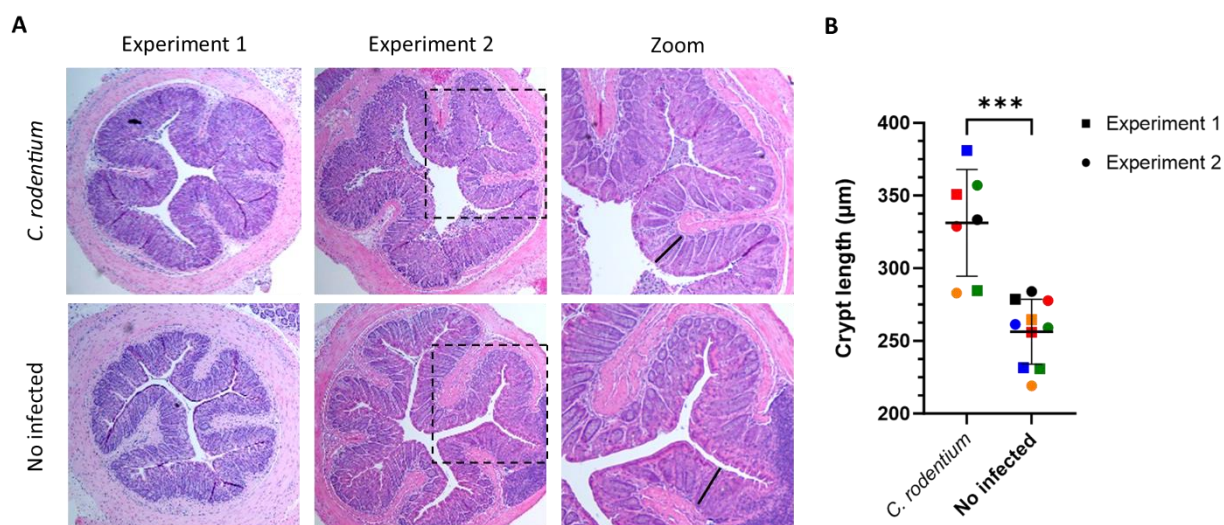


Figure 3.2. Histological analysis and crypt length comparison of *C. rodentium*-infected and non-infected colon tissue.

(A) Distal colon samples were taken at 8 days post-infection (PI) and stained with Haematoxylin and Eosin (H&E) to visualise tissue morphology. The infected colon shows crypt hyperplasia, while the colon of non-infected mice exhibits normal crypt length. The black line on the images represents the measured crypt length. (B) Crypt length analysis reveals a significant difference between infected and non-infected mice. Each colour in the graph corresponds to the animal's identification tag (blue, green, red, black, or untagged, shown as orange). Statistical analysis: Mann-Whitney test. *** p value < 0.05. The graph was generated using GraphPad Prism.

3.3.2 RNA sequencing analysis of *C. rodentium*-infected cells.

Following confirmation of mice colonisation, the subsequent step involved RNA extraction from the IEC isolated from the colon. To prevent DNA contamination, samples were treated with RQ1 DNase twice, and sample quality was assessed using TapeStation and Qubit technologies.

The results for RNA concentration revealed variability across different experiments and conditions (**Table 3.1**). Samples with an RNA concentration higher than 88.4 ng/µL and RNA RIN higher than 2.7 were selected for RNA sequencing. The RIN measures the integrity of RNA on a scale from 1 to 10, with higher numbers indicating better integrity and lower numbers indicating RNA degradation. Three samples from each experiment and condition were selected for RNAseq. Sequencing was conducted by the Genome Hub at the School of Biosciences, Cardiff University. Single-end RNA sequencing was carried out, with 30 million reads per sample.

Experiment	Condition	Sample No	Samples for RNAseq	Qubit RNA (ng/μL)	RNA RIN
Experiment 1	Infected	1	I1.1	95.6	3.1
		2	I1.2	88.4	3.3
		3	I1.3	99.2	3.3
	No Infected	4	-	92.1	2.7
		5	NI1.1	94.7	2.9
		6	NI1.2	101	2.9
		7	NI1.3	96.4	2.8
		8	-	83.8	2.6
Experiment 2	Infected	1	I2.1	97.6	2.7
		2	-	95.1	2.6
		3	I2.2	98.5	3.1
		4	I2.3	106	2.8
	No Infected	5	-	98.7	3.1
		6	NI2.1	109	2.8
		7	NI2.2	107	3.1
		8	-	97.3	2.5
		9	NI2.3	101	2.8
				Std 1 355.82	
				Std 2 7220.69	

Table 3.1. RNA concentration of samples from experiments 1 and 2.

The RNAseq analysis was performed using the Linux operating system and R software, utilising Bioconductor packages such as DESeq2 and the SARTools package, developed at PF2 - Institut Pasteur. Normalisation and differential analysis were performed based on the DESeq2 model and package. The Ensembl annotated genes resulting from this analysis were compared against the UniProt Reference Proteomes, encompassing 17102 mice-reviewed protein entries.

The experiment's variability was examined previous to conducting an in-depth analysis of the RNA sequencing data. As seen in **Figure 3.3**, the dendrogram obtained from Variance Stabilizing Transformation (VST) data effectively separates infected and non-infected conditions, regardless of the experiment they originate from. The separation enabled the joint analysis of the RNA sequencing results from experiments 1 and 2, considering three samples from each experiment and condition, which allowed focus on discerning differences between infected and non-infected mice.

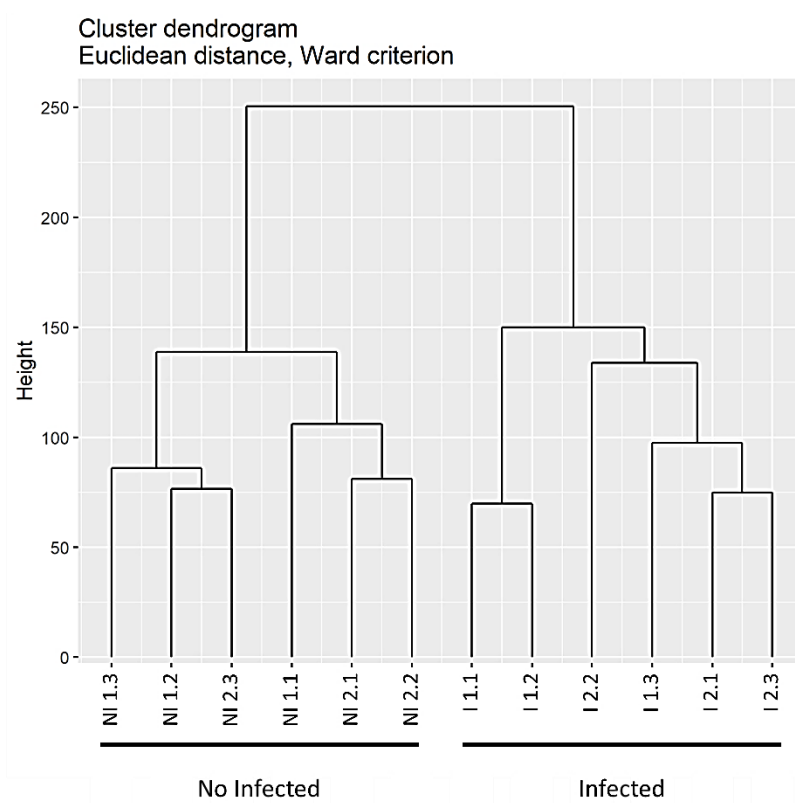


Figure 3.3. Cluster dendrogram showing separation of samples into groups.

The dendrogram illustrates the clustering of samples into distinct infected and non-infected groups. Notably, both experiments 1 and 2 exhibit similar clustering patterns, with samples from each experiment grouped into infected and non-infected groups.

3.3.3 Transcriptome analysis of *C. rodentium*-infected intestinal epithelial cells.

Following the assessment of the variability of the experiment, the next step was to examine the number of transcripts identified in the samples and their differential regulation. After revising and removing entries with no reads, the transcriptomic analysis identified 15116 transcripts, which were subsequently refined to yield 11836 unique mouse genes.

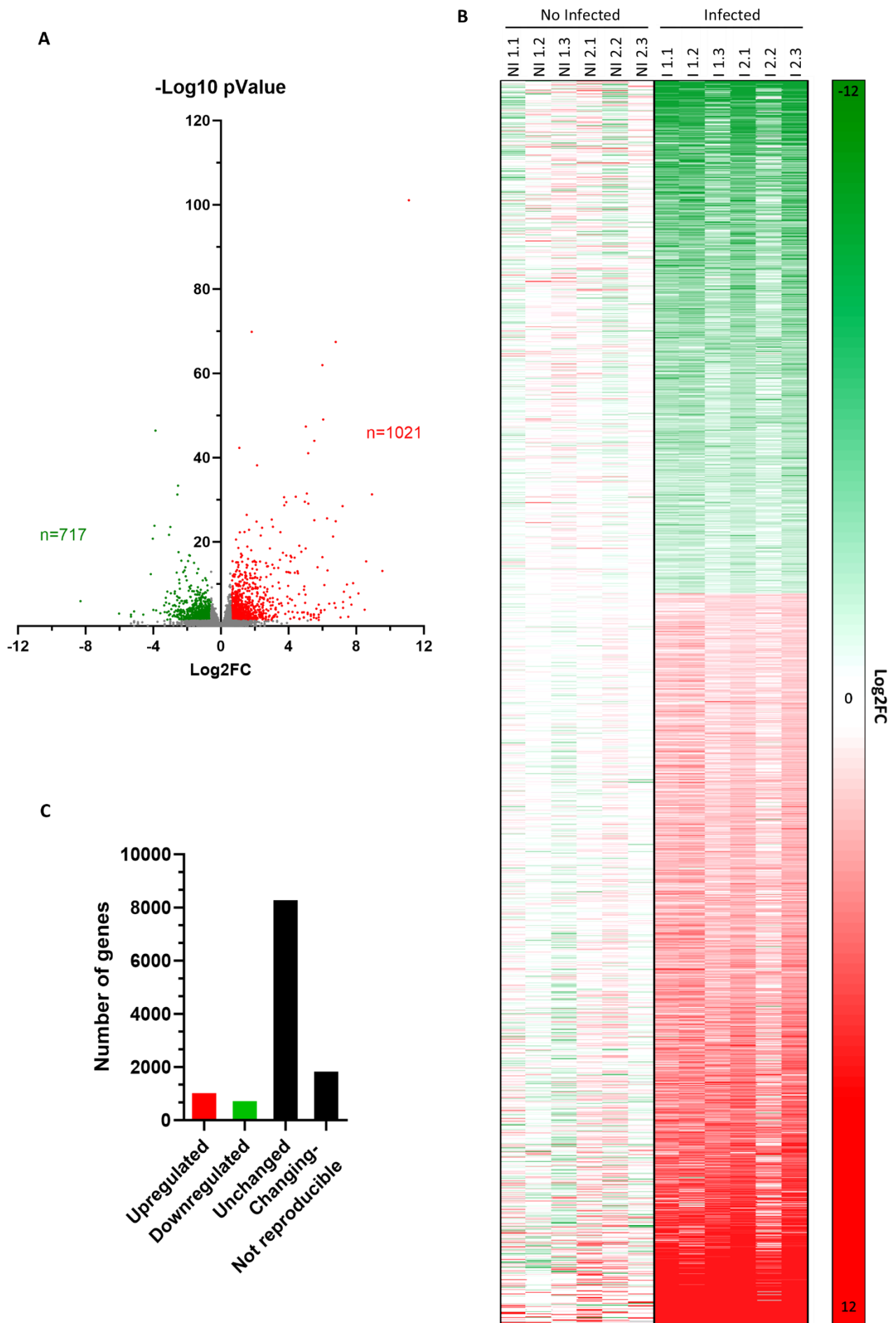
The differential regulation of genes was studied using specific parameters. To identify genes that significantly changed in expression, the mean of each mouse was calculated, and a p-value threshold of less than 0.05 was applied, corresponding to a $-\log_{10}$ p-value > 1.30 . Additionally, a fold-change threshold was used to determine the magnitude of gene expression changes. Specifically, genes with a \log_2 fold change (\log_2FC) greater than 0.58 were considered upregulated, indicating an increase in expression by at least 1.5 times.

Conversely, genes with a log₂FC less than -0.58 were considered downregulated, indicating a decrease in expression by at least 1.5 times.

Based on these parameters, 1738 genes exhibited differential regulation, with 1021 upregulated and 717 downregulated (**Figure 3.4A** and B). Genes with a log₂FC value between -0.58 and 0.58 were considered unchanged, resulting in a total of 8272 genes. Additionally, 1826 genes displayed changes but were not reproducible, having a p-value > 0.05 (**Figure 3.4C**). During infection, significant changes in gene expression were observed; however, these changes may also reflect alterations in the cellular composition of the infected tissue, which can influence the overall transcriptomic profile.

Figure 3.4. Differential regulation of intestinal epithelial cell genes during *C. rodentium* infection. (A) Volcano plot illustrating gene expression changes: 1021 genes were upregulated (highlighted in red), 717 genes were downregulated (green), and 10098 genes showed no significant change (grey). (B) Heatmap of differentially expressed genes. Each column represents one mouse (six mice per group in total). Data are from two separate experiments. (C) Differences in the distribution of the genes. Graphs were generated using GraphPad Prism.

Figure on page 50.



The next step was to study the top 20 upregulated and downregulated genes (**Figure 3.5**). Within the top 20 upregulated genes, there was a notable trend of pro-inflammatory genes. Examples include *S100a8* and *S100a9*, encoding calgranulin-A and B, which increased by 487 times ($p= 5.6E^{-32}$) and 384 ($p= 4.2E^{-16}$), respectively. Additionally, *Lcn2*, encoding lipocalin 2, increased 210 times ($p= 8.2E^{-06}$), and *Mmp9*, encoding matrix metalloproteinase-9, increased by 135 fold ($p= 9.0E^{-03}$). These results confirm a strong inflammatory response in the infected intestinal epithelial cells.

Conversely, the downregulated genes did not show a clear trend, as the different genes belonged to different pathways. Some encoded transporters, such as *Slc20a1* (encoding sodium-dependent phosphate transporter 1) and membrane proteins like *Klb* (encoding a beta-klotho protein), which decreased 14.6 times and 15.2 times, respectively ($p=3.8E^{-47}$ and $p=1.5E^{-24}$, respectively). Additionally, *G6pc2*, which encodes the Glucose-6-phosphatase 2, a molecule involved in hydrolysing glucose-6-phosphate to produce glucose, decreased 65 times ($p= 1.1E^{-03}$).

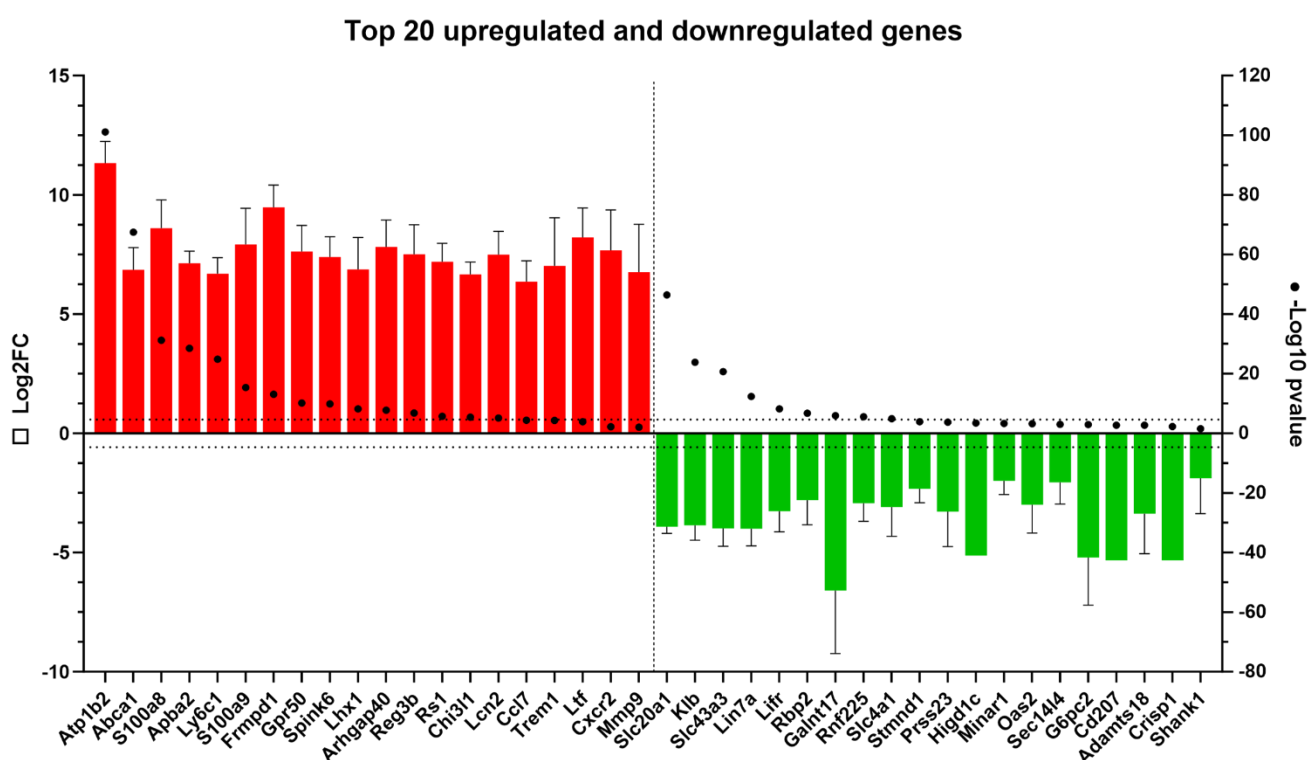


Figure 3.5. Top 20 upregulated and downregulated genes during infection.

Bar chart illustrating the top 20 upregulated and top 20 downregulated genes, represented by log₂ fold change (Log₂FC) values and -log₁₀ p-values. The dotted line represents the cutoff, Log₂FC ± 0.58. Graph generated using GraphPad Prism.

These findings highlight significant alterations in the expression of key genes involved in ion transport, inflammation, and metabolism during infection, setting the stage for further exploration of their roles in disease progression.

3.3.4 Subcellular location of the products of differentially expressed genes.

After conducting a preliminary analysis of the transcriptomic results, the differentially expressed genes were further studied for subcellular localisation using the UniProt database, allowing the grouping of genes based on their primary location.

Interestingly, a significant number of proteins encoded by differentially expressed genes were found to be expressed at the cell membrane (384 genes), followed by the nucleus (243), the endoplasmic reticulum (134 genes), and genes encoding secreted molecules (125) (see **Figure 3.6**). Conversely, the endosome had the lowest number of expressed genes (5), followed by the peroxisome (7 genes) and cell junction (9) (**Figure 3.6**). Notably, except for

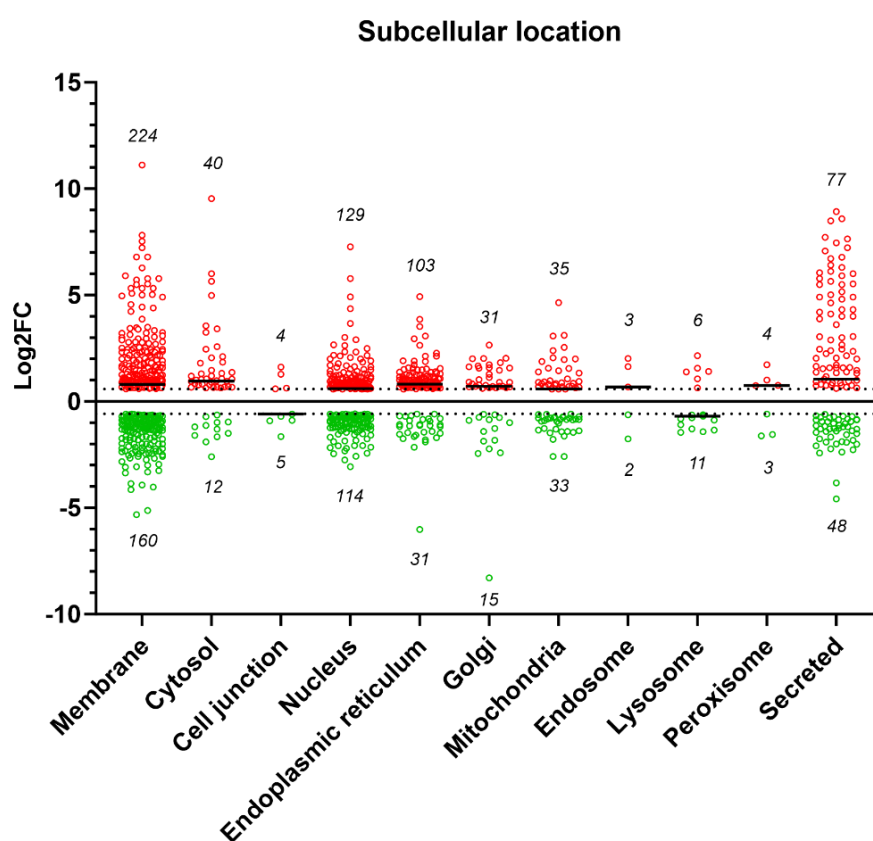


Figure 3.6. Subcellular location of detected proteins.

Membrane proteins and nuclear proteins are the most abundant among the differentially expressed genes, 384 and 243 genes in total, respectively, while endosome and peroxisome proteins are the least abundant, 5 and 7 genes, respectively. The numbers indicate the count of genes associated with each subcellular location. The dotted line represents the cutoff, $\text{Log}_2\text{FC} \pm 0.58$. Graph was generated using GraphPad Prism.

lysosome and cell junction, most subcellular locations showed more upregulated genes than downregulated genes. In the case of the endoplasmic reticulum and cytosol, the number of upregulated genes was more than three times higher, and in the Golgi apparatus, it was double. For the other locations, the number of upregulated and downregulated genes was approximately equal. Surprisingly, 68 differentially expressed genes were associated with the mitochondria. Given that *C. rodentium* is known to target and disrupt this organelle, we expected these genes to be primarily downregulated, rather than showing both up- and downregulation.

3.3.5 Pathway alterations during *C. rodentium* infection.

The next step was to investigate which pathways are associated with the differentially expressed genes during *C. rodentium* infection. Cytoscape plug-in ClueGO and IPA were used to identify altered pathways. Then, the genes within these altered pathways were individually analysed to determine their expression changes during infection.

Alterations included pathways associated with the regulation of defence responses, such as leukocyte migration, cytokine production and apoptosis, which are common in infectious diseases (**Figure 3.7**). Pathways involved in actin cytoskeleton reorganization were altered, reflecting changes in cell structure during *C. rodentium* infection, a known effect of attaching and effacing pathogens. Protein alterations included proteolysis and protein glycosylation, and, additionally, metabolic pathways, such as the pentose-phosphate shunt, prostaglandin metabolic process, lipid metabolism and cholesterol biosynthetic process, were also affected. While changes in lipid and cholesterol metabolism were expected during infection (Berger et al. 2017), the alteration in the prostaglandin metabolic pathway was a new finding. This pathway will be studied and discussed further in Chapter 5 of this thesis.

Most pathway changes corresponded with upregulated genes, with over 50% of the genes identified exhibiting upregulation across all pathways (**Figure 3.7**). The pentose phosphate shunt pathway had the highest representation, with 57% of its associated genes identified, 87% of which were upregulated. Similarly, the cholesterol biosynthetic and prostaglandin metabolic pathways showed a high percentage of genes identified (30% and 33%, respectively), with 94% of the genes in the cholesterol biosynthetic pathway being upregulated.

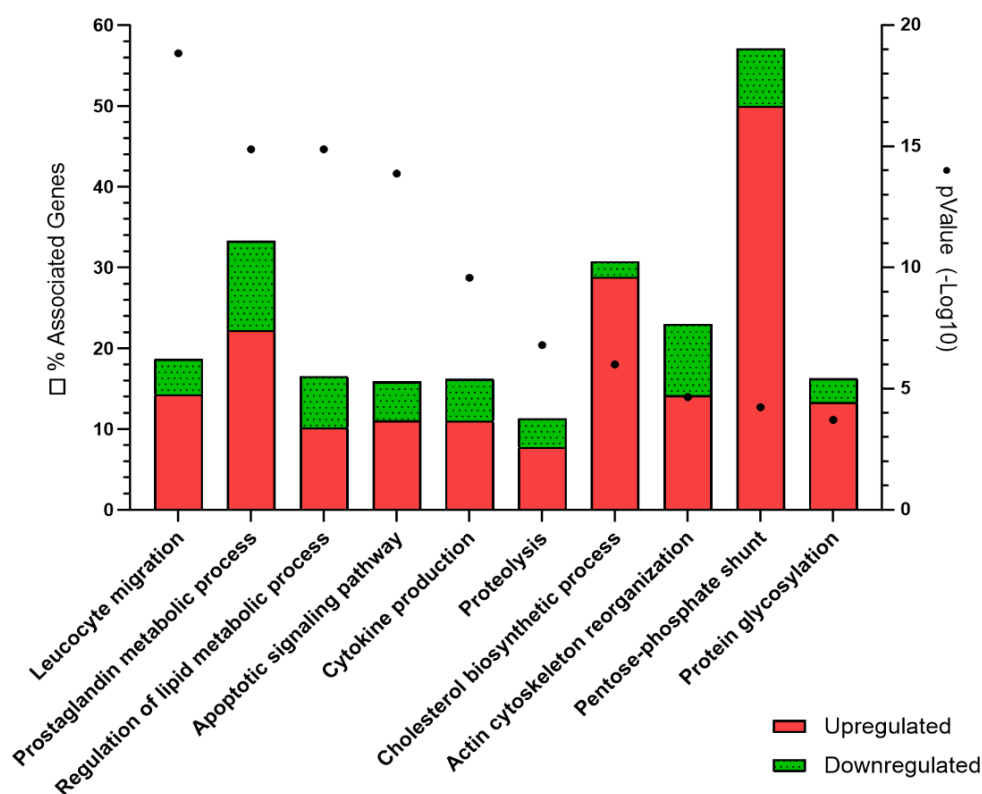


Figure 3.7. Percentage of associated genes per pathway affected during *C. rodentium* infection. The graph shows the percentage of associated genes identified per pathway and the differential regulation. The pentose-phosphate shunt is the pathway with a higher percentage of associated genes (57%), followed by the prostaglandin metabolic process (33%), and the cholesterol biosynthetic process (30%). $-\log_{10} p \text{ value} > 1.30$ was considered significant. The graph was generated with GraphPad Prism.

Furthermore, **Figure 3.8** illustrates how these pathways are connected, with the innate immune response positioned centrally. It is connected to responses to bacterium, granulocyte chemotaxis, cytokine production, and protein metabolic processes. This suggests that the immune response triggered by *C. rodentium* infection plays a pivotal role in regulating cellular responses during infection.

The investigation of the pentose phosphate pathway (PPP) revealed a clear upregulation of key enzymes (**Figure 3.9**). H6pd, which metabolises glucose-6-phosphate, exhibited a 4.4-fold increase ($p= 4.0E^{-14}$). Enzymes Pgd, Rpia and Rpe, involved in regulating the production of ribulose, ribose and xylulose 5 phosphate, respectively, were upregulated by 2.1 ($p= 2.8E^{-19}$), 1.5 ($p= 2.3E^{-02}$), and 1.7 times ($p= 4.7E^{-03}$). Additionally, Tkt, a transketolase mediating the production of fructose-6-phosphate, a sugar that can be incorporated into the glycolysis pathway to generate cellular energy, showed a 1.7-fold increase ($p= 1.9E^{-05}$). This suggests that during infection, the upregulation of the PPP provides an alternative mechanism for cellular energy production.

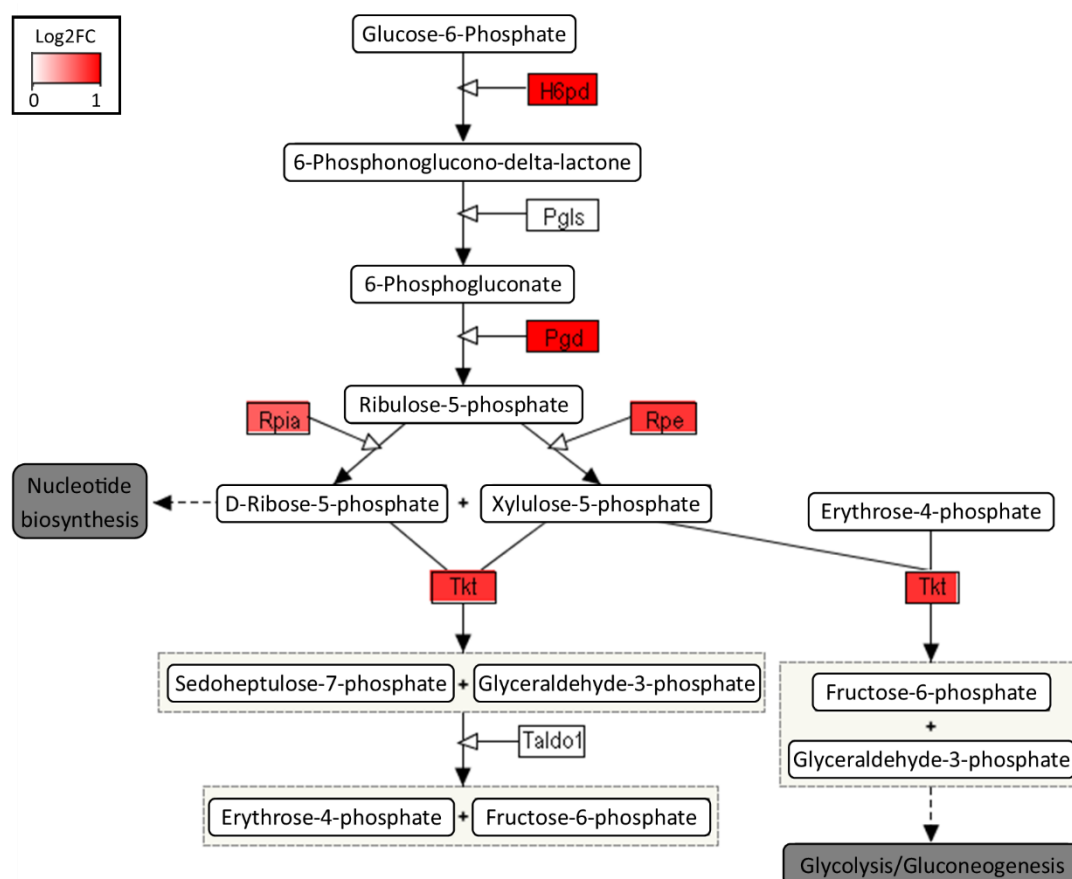


Figure 3.9. Upregulation of the pentose phosphate pathway during infection.

Enzymes involved in the pentose phosphate pathway (PPP) showed significant upregulation ($\log_2FC > 0.58$, indicated in red), including H6pd, Pgd, Rpia, Rpe, and Tkt. Diagram generated with PathVisio.

Transcriptomic analysis revealed the upregulation of genes belonging to the proteasome system (**Figure 3.10**, **Figure 3.11A** and **B**). The proteasome 26S is the main protein-degrading machine in eukaryotic cells, responsible for breaking down proteins marked with ubiquitin (Bard et al. 2018). This upregulation suggests an increase in the availability of proteasomes for protein degradation during *C. rodentium* infection.

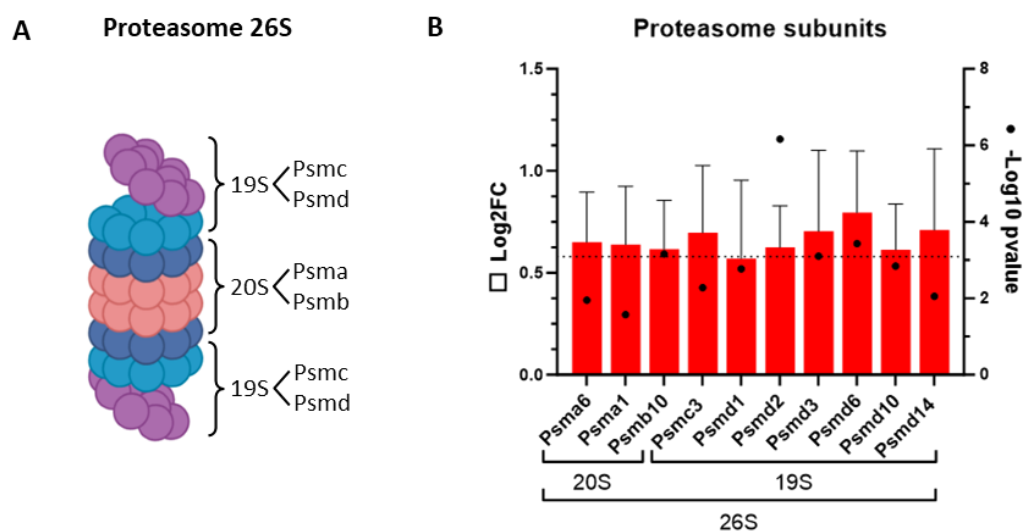


Figure 3.10. Proteasome subunits structure and expression during infection. Proteasome subunits from the 19S and 20S components (A) showed upregulation during *C. rodentium* infection (B). The dotted line represents the cutoff, $\text{Log}_2\text{FC} > 0.58$. Graph was made using GraphPad Prism. Diagram was made using BioRender.

Since the ubiquitin and proteasome systems are linked, we studied the ubiquitin enzymes, including the ubiquitin-activating enzyme (E1), ubiquitin-conjugating enzyme (E2), and ubiquitin ligases (E3) (**Figure 3.11A**). Uba1, Ube2h, Ube2d2b, E1 and E2 enzymes, showed clear upregulation during infection (by 1.6, 1.7 and 3.2 times) (**Figure 3.11B**). However, the E3 enzymes exhibited a diverse pattern, with both upregulated and downregulated genes. Notably, Trim27 and Rnf183, associated with pro-inflammatory responses in colitis (Zou et al. 2021), were upregulated in the transcriptome (by 1.9 times and 4.4 times, respectively). Conversely, Trim62 and Rnf8, linked to anti-inflammatory responses, were downregulated (2.5 and 1.8 times, respectively).

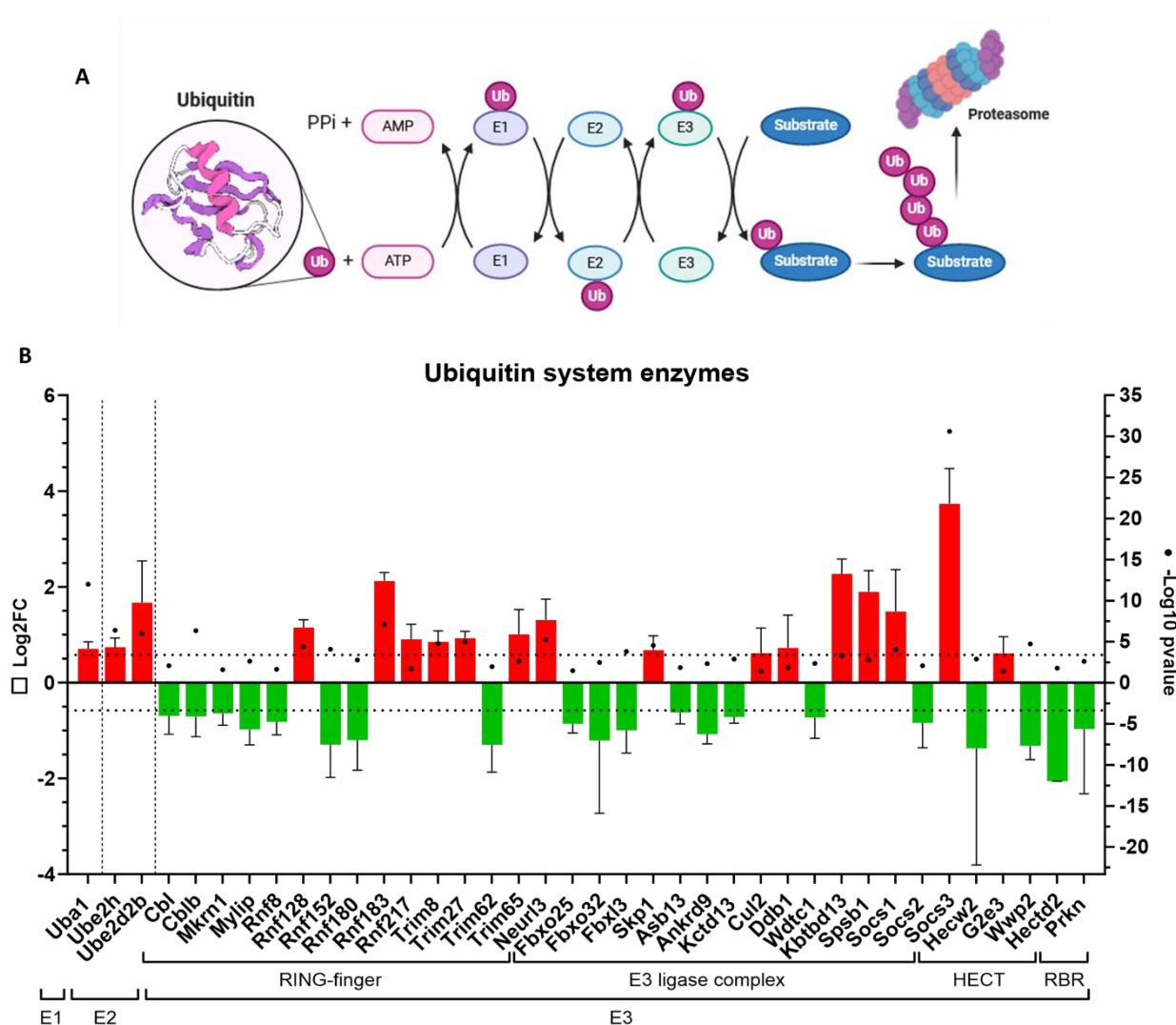


Figure 3.11. Ubiquitin-proteasome system and *C. rodentium* infection.

(A) Diagram showing how ubiquitin-proteasome enzymes add ubiquitin molecules to substrate protein. (B) Ubiquitin system enzymes regulation. The dotted line represents the cutoff, $\text{Log}_2\text{FC} \pm 0.58$. The graph was made using GraphPad Prism. The diagram was made with BioRender.com.

These findings suggest that while the activation and conjugation steps of the ubiquitin-proteasome pathway are increased, the ligation of ubiquitin to substrate proteins might be selectively regulated. This selective regulation could affect the overall protein degradation process and contribute to the inflammatory response during infection.

3.4 Discussion.

While proteomic and metabolomic methods have typically been employed to study the effects of *C. rodentium* infection in the host, this study utilised a transcriptomic approach to investigate the in vivo effects of *C. rodentium* infection. The objective was to explore the dynamics of bacteria-host interactions by characterising the transcriptome profile of *C. rodentium*-infected intestinal epithelial cells.

Our findings demonstrate the effectiveness of transcriptomics in elucidating changes within host cells during bacterial infection. We discovered that the majority of pathways altered during infection are associated with immune response, inflammation, or metabolism (**Figure 3.7**), which are well-known pathways affected during infection. Additionally, we identified some novel pathways such as the prostaglandin metabolic process, proteolysis, and the pentose phosphate shunt.

3.4.1 [Transcriptome of *C. rodentium*-infected intestinal epithelial cells.](#)

Analysis of the transcriptome of *C. rodentium*-infected intestinal epithelial cells began with an assessment of RNA quality, which identified impurities and DNA contamination, necessitating a secondary DNase treatment that resulted in RNA degradation and reduced concentrations. Despite these challenges, sequencing proceeded with the best-quality RNA samples available.

The RNA sequencing analysis identified 11836 unique mouse genes, representing approximately 53.75% of the protein-coding genes in the mouse genome (Breschi et al. 2017). Of these, 1738 (14.7%) demonstrated differential regulation. The majority of the remaining genes showed no significant change (69.9%) or presented inconsistent alterations (15.4%), possibly due to variations in RNA expression patterns among the mice.

Considerable variations in gene expression profiles were observed within infected and non-infected mice, with consistent changes observed in a majority of samples but reversed trends in some individuals (NI1.1 and NI2.2 for the no-infected group, and I1.3 and I2.2 for the infected group) (**Figure 3.4B**). These variations impacted the overall expression pattern of some of these genes, leading to their classification as non-differentially expressed. These differences could potentially be attributed to individual differences in immune responses or

genetic backgrounds. However, considering the consistent genetic profile of the mice provided by Charles River, the primary factor contributing to these variations likely stems from the suboptimal RNA quality in the samples. Degraded RNA could complicate alignment and mapping processes during sequencing, potentially resulting in the underrepresentation or omission of RNA fragments.

Despite these variations, the transcriptome analysis successfully identified differentially expressed genes during *C. rodentium* infection. This underlines the dynamic nature of the host response and emphasises the importance of maintaining high RNA quality to ensure accurate gene expression profiling.

3.4.2 [Pathway analysis and novel findings during *C. rodentium* infection.](#)

The transcriptome analysis focused on the distribution of differentially expressed genes, revealing a complex network with diverse connections between multiple pathways (**Figure 3.7**). A total of 383 pathways were identified, with only 10 selected for further investigation, leaving 373 pathways unstudied. This limitation highlights the need for further investigation, as only a small fraction of the identified pathways were investigated.

Among these pathways are those known to undergo alterations during *C. rodentium* infection, including cytokine production, cholesterol metabolism, and granulocyte migration, as well as the prostaglandin metabolic process, the pentose phosphate shunt, and proteolysis, novel identified pathways. These findings are consistent with previous studies that have documented the activation of inflammation, immune response, and alterations in lipid metabolism pathways during *C. rodentium* infection (Collins et al. 2014b; Berger et al. 2017; Mullineaux-Sanders et al. 2019).

Our transcriptomic analysis reaffirms these established observations and identifies additional pathways altered during *C. rodentium* infection that need further exploration. These include the prostaglandin metabolic process (Chapter 5), the pentose phosphate shunt, and proteolysis with a focus on the ubiquitin-proteasome system.

3.4.3 [Identification of secreted proteins in response to infection.](#)

In a comprehensive examination of the differentially regulated genes, it was observed that 125 genes encoded secreted proteins (**Figure 3.6**), which was noteworthy. Secreted proteins

can be challenging to detect with other traditional proteomic techniques, highlighting the advantage of using transcriptomic analysis in this case.

These secreted proteins are released into the lumen or the lamina propria of intestinal epithelial cells and could play pivotal roles in intercellular communication, immune responses, and various physiological processes. A deeper analysis revealed that most of the upregulated secreted proteins during *C. rodentium* infection have antimicrobial functions. Interestingly, these are also grouped into the top 20 upregulated genes of the transcriptome, highlighting their critical role in the response to bacterial infection. Antimicrobial proteins are known to be upregulated during infectious diseases, including infection with *C. rodentium* (Rodrigues et al. 2012; Mullineaux-Sanders et al. 2019; Xiao et al. 2019; Lee and Kim 2022; Melchior et al. 2024), so the detection of these genes in the transcriptome of infected epithelial cells was expected.

Examples include the metal-sequestering antimicrobial proteins calgranulin A and B (S100a8 and S100a9), Lipocalin 2 (Lcn2), the lectins Reg3b and Reg3g (though not in the top 20), and the matrix metalloprotease 9 (MMP9). MMP9 is a metalloprotease that digests extracellular matrix and opens tight junctions, characteristic of colitis. Notably, our analysis revealed changes in metalloprotease inhibitors, including an increase in *Timp1* and reductions in *Timp3*, *Adamts18*, and the probable metalloprotease inhibitors *Gasp1* and *Gasp2*. This regulation suggests a dynamic balance that may favour MMP9 activity during infection, potentially contributing to tissue remodelling and inflammation, both hallmarks of colitis pathology and *C. rodentium* infection (Rodrigues et al. 2012).

Remarkably, interleukin-15 (IL-15), is a secreted protein that was downregulated during infection (4.8 times, $p = 4.8E^{-04}$). This molecule is known for its protective immune response to microbes and proinflammatory role, and its activation typically regulates the destruction of infected cells by cytotoxic T lymphocytes (Jabri and Abadie 2015). Such findings contradict previous research suggesting its upregulation during viral and bacterial infections and inflammatory diseases (Jabri and Abadie 2015; Vitale et al. 2016). The downregulation of IL-15 during *C. rodentium* infection could be interpreted as a bacterial strategy to evade the host's immune response, which could potentially facilitate bacterial persistence within the host.

The simultaneous upregulation and downregulation of proinflammatory molecules indicate that *C. rodentium* triggers an immune response in the host while maintaining a balance between these molecules. This allows the bacterium to avoid being destroyed by an uncontrolled immune response, enabling it to survive attached to the intestinal epithelial cells and multiply, thereby maintaining and prolonging the infection.

3.4.4 *C. rodentium* induces metabolic changes in intestinal epithelial cells.

Pathway analysis revealed that the pentose phosphate pathway (PPP) is upregulated during infection (**Figure 3.9**). The PPP, operating parallel to glycolysis, converts glucose-6-phosphate (G-6-P) from glycolysis into ribose-5-phosphate (R-5-P) while generating NADPH (nicotinamide adenine dinucleotide phosphate) (Teslaa et al. 2023). The upregulation of this pathway during infection suggests increased production of R-5-P and NADPH, aligning with observed metabolic shifts in the intestinal epithelial cells during *C. rodentium* infection, as outlined by Berger et al. (2017).

The Warburg effect, which involves the transition from OXPHOS to glycolysis, is a hallmark of proliferating cells, including cancer cells and those infected by AE pathogens (Vander Heiden et al. 2009; Cho et al. 2018; Escoll and Buchrieser 2018). Despite glycolysis yielding less energy compared to OXPHOS (2 ATP molecules versus 36 ATP molecules per glucose molecule, respectively), it supports the rapid proliferation demands of these cells by providing the building blocks for amino acids, fatty acids, and nucleotides necessary for cells proliferation (Vander Heiden et al. 2009).

The PPP is closely associated with the Warburg effect, branching from glycolysis at the first step of G-6-P conversion. The upregulation of the PPP further facilitates this metabolic shift by supplying metabolic intermediates crucial for cell proliferation and adaptation to proliferative states. The production of R-5-P is crucial for nucleotide synthesis, as nucleotides serve as the building blocks of DNA and are essential for cell proliferation and DNA repair. Given that *C. rodentium* infection causes the induction of cell proliferation and crypt hyperplasia, it is expected that the intestinal epithelial cells adapt to infection by undergoing metabolic changes to meet their altered demands. Upregulating the PPP to increase R-5-P production during infection ensures that the cells have the necessary nucleotides to support the synthesis of new cells.

Additionally, PPP also produces NADPH, which is a biosynthetic precursor for macromolecules such as fatty acids and cholesterol (Escoll and Buchrieser 2018). During infection with *C. rodentium*, there is an increase in the cholesterol biosynthesis pathway, as seen in **Figure 3.7** and demonstrated by Berger et al. (2017). Cholesterol is crucial for maintaining cell membrane integrity, so it could be hypothesised that the enterocytes need the upregulation of the PPP to meet the cholesterol needs of proliferating cells during infection. Moreover, fatty acids like arachidonic acid need NADPH for their synthesis. Prostaglandins, derived from arachidonic acid, are pro-inflammatory molecules whose biosynthesis pathway shows upregulation during infection (**Figure 3.7**). Since NADPH is necessary for the synthesis of its precursor, the increased PPP activity and the NADPH production could be linked to the upregulation of the prostaglandin biosynthesis pathway.

In summary, the upregulation of the PPP during *C. rodentium* infection highlights its critical role in meeting the biosynthetic demands of host cells. Future research should focus on elucidating the precise regulatory mechanisms governing PPP activity and its interaction with other metabolic pathways during infection.

3.4.5 Ubiquitin-Proteasome system and *C. rodentium*.

C. rodentium infection promotes the induction of colonic crypt hyperplasia in the intestine. Interestingly, this infection shares similarities with colorectal cancer (CRC), where there is uncontrolled proliferation of cells. Notably, in CRC, the ubiquitin-proteasome system (UPS) is often dysregulated (Liu et al. 2018; Zou et al. 2021; Sun et al. 2023), leading to the stabilisation of oncogenic proteins and the degradation of tumour suppressor proteins. Similarly, during *C. rodentium* infection, we observed alterations in the expression of UPS-related genes, with both upregulated and downregulated enzymes and increased expression of proteasome subunits (**Figure 3.10** and **Figure 3.11**).

For instance, the E1 and E2 enzymes Uba1, Ube2h, Ube2d2b, and the E3 ligase Socs1 are all upregulated in CRC (Tobelaim et al. 2015; Sobah et al. 2021; Huang et al. 2022) and showed upregulation in the transcriptome of *C. rodentium*-infected cells. Conversely, the E3 ligase Socs2, which is normally downregulated in CRC (Letellier et al. 2014), also showed downregulation in the transcriptome. Additionally, the downregulation of the *Cbl* gene in

CRC promotes tumour growth (Lyle et al. 2019), and could explain why its expression is reduced in *C. rodentium*-infected enterocytes.

Cbl is an E3 ligase protein that can be classified into Cbl, Cbl-b and Cbl-c. Ryu et al. (2021) demonstrated that Cbl-c ubiquitinates the EPEC and *C. rodentium* translocated protein Tir, promoting its degradation by the proteasome. Tir is essential for the attachment of the bacteria to the enterocyte, so its degradation induces the detachment of EPEC and enhances host defence. They further showed that using a proteasome inhibitor in vivo increases the *C. rodentium* load, highlighting the importance of this E3 ligase in host defence against the bacterium.

In our study, we observed the downregulation of two of these ligases, Cbl and Cbl-b. However, *Cbl-c*, which encodes the E3 ligase that targets Tir for degradation, showed no alteration in expression. Simultaneously, the upregulation of proteasome subunits suggests an increased availability of proteasomes for Tir degradation. This suggests a potential compensatory mechanism where the increased availability of proteasomes, along with the maintained expression of *Cbl-c*, ensures effective degradation of Tir and detachment of the bacteria.

Taken together, these findings suggest that *C. rodentium* might target the UPS of the enterocyte host to promote cell proliferation and support the pathogen. While the expression of *Cbl* and *Cbl-b* is reduced, potentially promoting cell growth, the stability of *Cbl-c* and enhanced proteasome presence are important for maintaining host defence mechanisms against *C. rodentium* infection. This balance emphasises the complex regulatory dynamics of the ubiquitin-proteasome system, where the up and downregulation of certain ligases may facilitate cell proliferation, yet the unchanged expression of *Cbl-c* and the increased proteasome expression might play a crucial role in effective pathogen defence.

Moreover, some of the T3SS effector proteins of *C. rodentium*, EPEC and EHEC are also E3 ligases (Kim et al. 2014;). For example, the NleL (non-LEE-encoded ligase) effector protein has E3 ubiquitin ligase activity and modulates Tir-mediated pedestal formation in EHEC infection and contributes to *C. rodentium* virulence (Piscatelli et al. 2011). Additionally, NleG acts as an E3 ligase, and it is important in the virulence of *C. rodentium* infection. The

deletion of *NleG1*, *NleG7* and *NleG8* reduced diarrhoeal symptoms, negatively impacted colonisation, and increased the survival rate of infected mice, respectively (Popov et al. 2023). These bacterial E3 ligases can manipulate the host cell's UPS to facilitate infection, highlighting a complex interplay between bacterial and host E3 ligases in regulating infection dynamics. Future studies could explore the specific mechanisms by which these bacterial E3 ligases modulate host pathways, potentially revealing novel therapeutic targets to mitigate bacterial virulence and enhance host defence against enteric pathogens.

3.5 Conclusions.

The main conclusions following the investigation of the transcriptome profile of *C. rodentium*-infected enterocytes in mice were as follows:

- Transcriptome analysis allowed us to gather key information about the response of the host to *C. rodentium* infection, providing significant insights into the genetic response to infection through a transcriptomic approach. It offered a distinct advantage over traditional proteomic techniques by identifying genes encoding secreted proteins.
- The analysis allowed the identification of specific genes and pathways that undergo differential regulation during infection, enhancing our understanding of the host's immune and metabolic responses to *C. rodentium*.
- *C. rodentium* infection induces metabolic changes in the host, particularly through upregulation of the Pentose Phosphate Pathway, which likely enhances ribulose-5-phosphate production. This metabolic shift supports nucleotide synthesis and provides essential biosynthetic resources for proliferating cells.
- Infection also induces alterations in the ubiquitin-proteasome system of host cells, potentially facilitating cell proliferation and contributing to inflammatory responses.

These findings emphasise the complex molecular mechanisms at play in the interaction between host and pathogen during *C. rodentium* infection, highlighting the importance of transcriptomic approaches in discovering these dynamics. Furthermore, they provide potential targets for further research and could contribute to the development of therapeutic interventions.

CHAPTER 4: Comparative analysis -
Understanding transcriptome and proteome of
C. rodentium-infected intestinal epithelial cells

4 CHAPTER 4: Comparative analysis - Understanding transcriptome and proteome of *C. rodentium*-infected intestinal epithelial cells.

4.1 Introduction.

Understanding host-pathogen interactions at the molecular level is essential for determining the complex dynamics of infection and the immune response. Two key techniques for such analysis are proteomics and transcriptomics. Proteomic analysis focuses on identifying and quantifying the entire set of proteins (proteome) expressed by a cell, tissue or organism under specific conditions (Aslam et al. 2017; Dupree et al. 2020). This approach directly identifies the functional molecules that perform cell processes, providing insights into protein modifications, interactions, and cellular localisation.

Conversely, transcriptomics investigates the RNA transcripts (transcriptome) produced under specific conditions. By analysing RNA levels, transcriptomics provides information about gene expression, identifying which genes are upregulated or downregulated in response to stimuli such as infection (Mutz et al. 2013; de Jong et al. 2019). This technique provides valuable information on the regulatory mechanisms responsible for cellular responses.

While these techniques are invaluable tools, each has its limitations. Common issues with proteomics include protein extraction, detection sensitivity, and accurate quantification, particularly for low-abundance proteins. Additionally, post-translational modifications (PTMs), such as phosphorylation, glycosylation, and ubiquitination, require specialised techniques for detailed analysis (Goshe and Smith 2003). Transcriptomics, on the other hand, does not necessarily correlate directly with protein levels. The relationship between mRNA and protein abundance is influenced by factors, including translation efficiency, protein degradation, and PTMs (Vogel and Marcotte 2012).

Given these limitations, incorporating data from both proteomics and transcriptomics provides a more comprehensive understanding of biological processes. While transcriptomics reveals potential changes in gene expression, proteomics confirms whether these changes lead to corresponding alterations at the protein level, validating and extending transcriptomic findings. This integrative approach offers a more complete and

dynamic view of the biological processes and regulatory mechanisms activated during infection.

By integrating data from both approaches, critical molecules and pathways involved in the host's response to infection can be identified more effectively. This chapter presents a comparative analysis of transcriptomic and proteomic profiles of mice infected with *C. rodentium*, highlighting the importance of multi-omics approaches in studying complex biological processes and providing a deeper understanding of pathogenesis.

4.2 Aims and Objectives.

This chapter aimed to investigate the molecular responses of mice to *C. rodentium* infection through comprehensive transcriptomic and proteomic analyses. To achieve this goal, the specific objectives were:

- Analyse the gene expression and protein patterns in intestinal epithelial cells during *C. rodentium* infection.
- Investigate the correlation between transcriptome and proteome of known altered pathways during *C. rodentium* infection in mice.
- Examine the effects of *C. rodentium* infection on mitochondria.

4.3 Results.

4.3.1 Transcriptome and proteome of *C. rodentium*-infected enterocytes.

The combined transcriptome and proteome analysis of infected enterocytes revealed distinct and overlapping gene and protein identifications. The transcriptome identified 11836 unique mouse genes, which is 2839 more than the 8997 proteins identified in the proteome. Notably, 3981 unique entries were unique to the transcriptome, while 1142 were unique to the proteome. Among these, 632 genes were differentially expressed in the transcriptome, and 415 proteins were differentially expressed in the proteome. Additionally, 7855 entries were common to both datasets, with 380 differentially expressed in both, 1219 differentially expressed only in the proteome, and 576 only in the transcriptome (**Figure 4.1**).

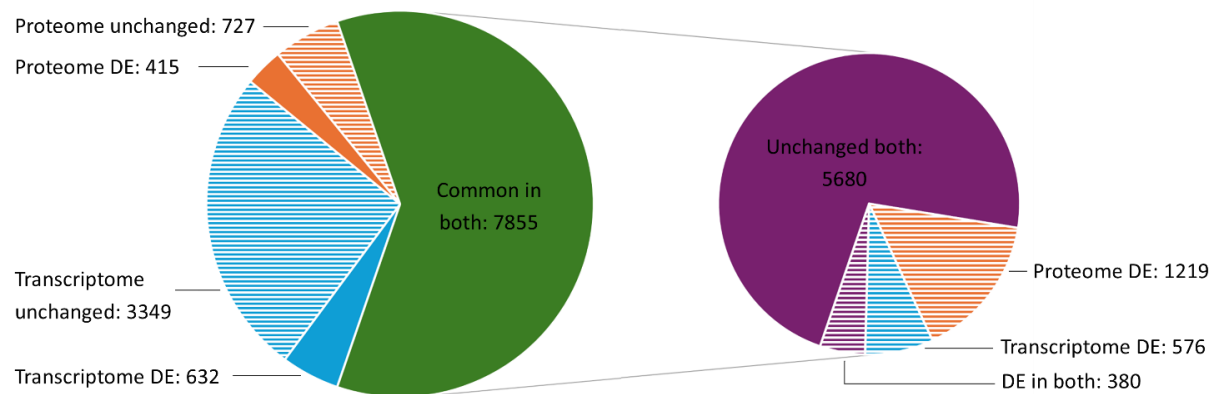


Figure 4.1. Transcriptome and proteome of *C. rodentium*-infected enterocytes.

The pie charts illustrate the overlap and unique entries between the transcriptome and proteome datasets. The left chart shows 11836 genes identified in the transcriptome and 8997 proteins in the proteome, with 7855 entries common to both. Unique entries include 3981 exclusive to the transcriptome and 1142 exclusive to the proteome, with 632 differentially expressed (DE) entries in the transcriptome and 415 in the proteome. The right chart focuses on the common entries, showing 5680 unchanged, 1219 DE only in the proteome, 576 DE only in the transcriptome, and 380 DE in both.

The 3981 genes exclusively identified in the transcriptome include several that play pivotal roles in critical pathways. Notable examples include genes involved in prostaglandin metabolism, such as *mPGES-1* and *Cox2*, which are crucial for inflammatory responses, the proliferation marker *Ki67*, and cyclins involved in the cell cycle. Additionally, key genes in

the Wnt signalling pathway, which is pivotal in maintaining intestinal stem cell fate and promoting progenitor cell proliferation, were identified.

In the proteome, the 1142 unique proteins included a notable presence of ribosomal proteins, which, while also detected in the transcriptome, were more abundantly represented in the proteome. Histones were also prominently identified in the proteome, complementing those detected in the transcriptome.

Further analysis of the 7855 common entries revealed that only 380 were differentially expressed across both datasets, indicating both upregulated and downregulated genes and proteins (**Figure 4.1**). In addition, 7475 entries exhibited altered expression patterns across either the transcriptome or proteome. Among these, 576 were differentially expressed in the transcriptome, 1219 in the proteome, while 5680 showed fluctuations in expression levels that did not meet the criteria for differential expression (**Figure 4.1**).

These findings suggest that while many genes and proteins displayed variability in their expression, only a small fraction exhibited significant and consistent changes across both datasets. This highlights the complexity of the regulatory mechanisms involved in response to infection.

Next, we investigated whether the 380 genes and proteins exhibited similar alteration patterns, such as uniform upregulation or downregulation, or if their changes differed between the transcriptome and proteome. Furthermore, we explored which cellular processes or pathways were affected by these alterations.

As shown in **Figure 4.2**, out of the 380 common entries, 345 exhibited consistent patterns: 187 were upregulated in both datasets, and 158 were downregulated in both. The upregulated entries were predominantly involved in antimicrobial response, immune response and cholesterol metabolism. In contrast, the downregulated entries were predominantly involved in lipid and amino acid metabolism, as well as protein modification processes.

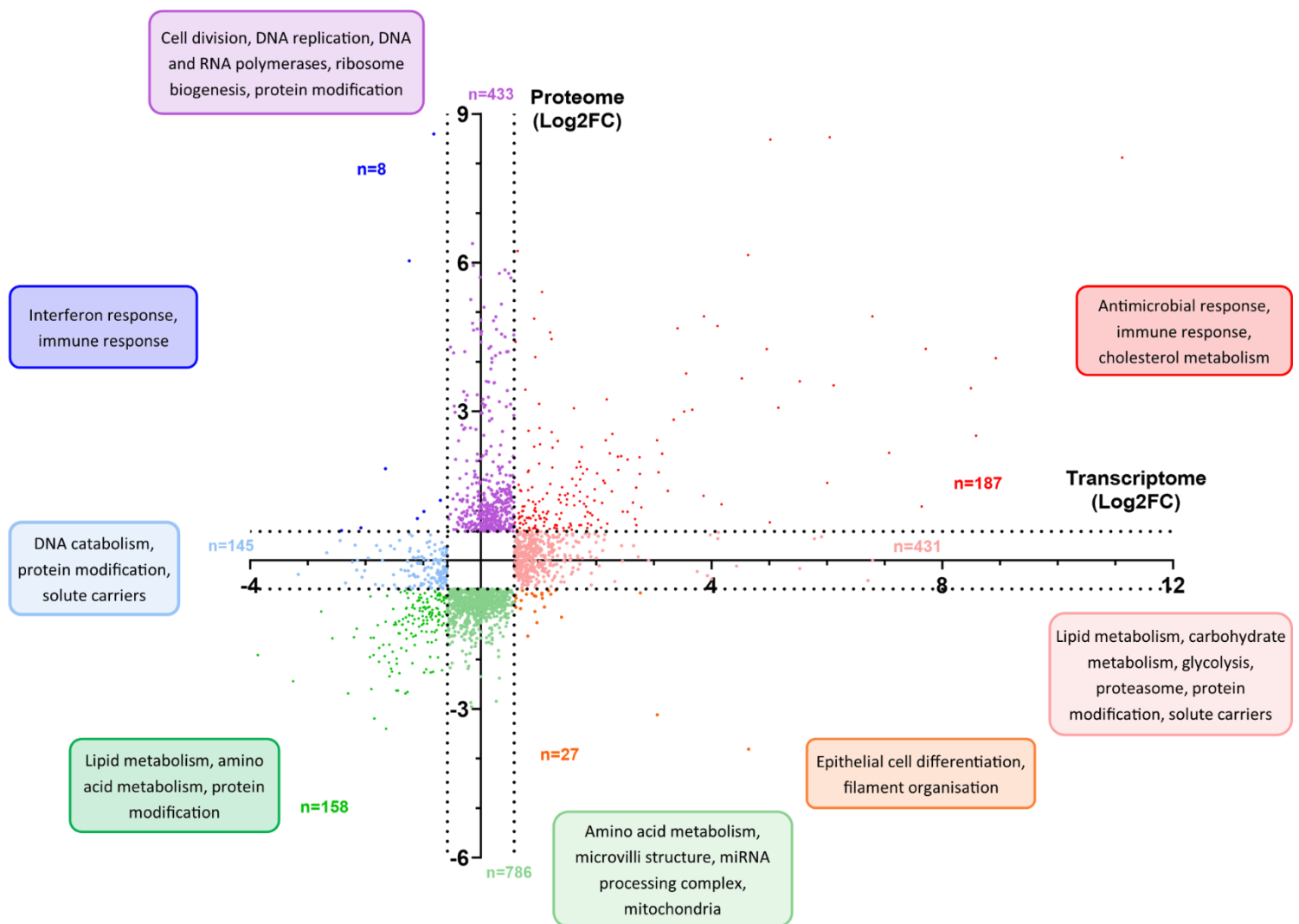


Figure 4.2. Comparison of gene expression and protein abundance changes in *C. rodentium*-infected enterocytes.

The scatter plot displays differential gene expression and protein abundance. It shows 187 upregulated (red) and 158 downregulated (green) data points. Additionally, 27 entries are upregulated in the transcriptome but downregulated in the proteome (orange), and 8 are upregulated in the proteome but downregulated in the transcriptome (blue). Some proteins show changes in one dataset but not the other. Values were plotted considering a p -value < 0.05 . Figure created with GraphPad Prism.

However, 35 entries displayed opposite changes between the transcriptome and proteome: 8 entries showed increased abundance in the proteome but decreased expression in the transcriptome, while 27 entries showed decreased abundance in the proteome but increased expression in the transcriptome. The entries with increased abundance in the proteome but decreased expression in the transcriptome were primarily linked to immune responses and interferon responses. Conversely, the entries with decreased abundance in

the proteome but increased expression in the transcriptome were involved in pathways related to epithelial cell differentiation and filament organisation.

Additionally, 1219 entries were altered in the proteome but remained unaltered in the transcriptome. Of these, 433 entries showed increased abundance in the proteome, involving pathways related to cell division, DNA replication, and ribosome biogenesis, among others. In contrast, 786 entries showed decreased abundance, predominantly associated with microvilli structure, miRNA processing complex, and mitochondria.

Furthermore, 576 entries showed changes in the transcriptome but not in the proteome. Among these, 431 were upregulated in the transcriptome, involving pathways related to lipid and carbohydrate metabolism, glycolysis, and proteasome. Conversely, 145 entries were downregulated, affecting processes such as DNA catabolism and protein modification pathways.

These discrepancies between transcriptome and proteome data highlight the complex regulatory mechanisms during infection. RNA and protein stability can be influenced during infection by miRNA activity, altered post-translational processes, and differential mRNA stability, which could explain the difference observed between transcript and protein levels. Understanding these mechanisms is crucial for interpreting how cellular processes adapt to infection. Therefore, the next step focused on investigating the gene expression and protein abundance of molecules involved in some of these regulatory processes.

4.3.2 [Antimicrobial response of intestinal epithelial cells during *C. rodentium* infection.](#)

The analysis showed that levels of proteins and genes involved in the antimicrobial response were upregulated during infection. This alteration was expected, as *C. rodentium* infection triggers an immune response in the host, stimulating immune cells to secrete interleukin 22 (IL-22), a cytokine involved in inflammation processes (Collins et al. 2014b; Silberger et al. 2017; Mullineaux-Sanders et al. 2019; Stockinger 2021). Since IL-22 is not expressed by enterocytes, the impact of this cytokine on intestinal epithelial cells was investigated by analysing the molecules that are regulated in response to IL-22.

The results showed strong correlations between gene expression and protein abundance (**Figure 4.3**). This included molecules involved in nutritional immunity, such as lipocalin 2

(encoded by *Lcn2*), lactotransferrin (encoded by *Ltf*), calgranulin A (encoded by *S100a8*) and calgranulin B (encoded by *S100a9*), all of which showed similar upregulation in both the transcriptome and proteome. Similarly, bactericidal proteins such as regenerating islet-derived 3-beta and gamma (encoded by *Reg3b* and *Reg3g*) showed significant increases: *Reg3b* was increased 200-fold (p-value $1.4E^{-07}$) and *Reg3g* by 69-fold (p-value $1.8E^{-10}$) in the transcriptome, compared to 2-fold and 12-fold increases in the proteome, respectively. Other antimicrobial genes that showed increased expression were *Hmox1* (encoding Heme oxygenase 1), *Hp* (Haptoglobin), *Ido1* (Indoleamine 2,3-dioxygenase 1), *Mmp9* (Matrix metalloproteinase 9), and *Nos2* (Inducible nitric oxide synthase).

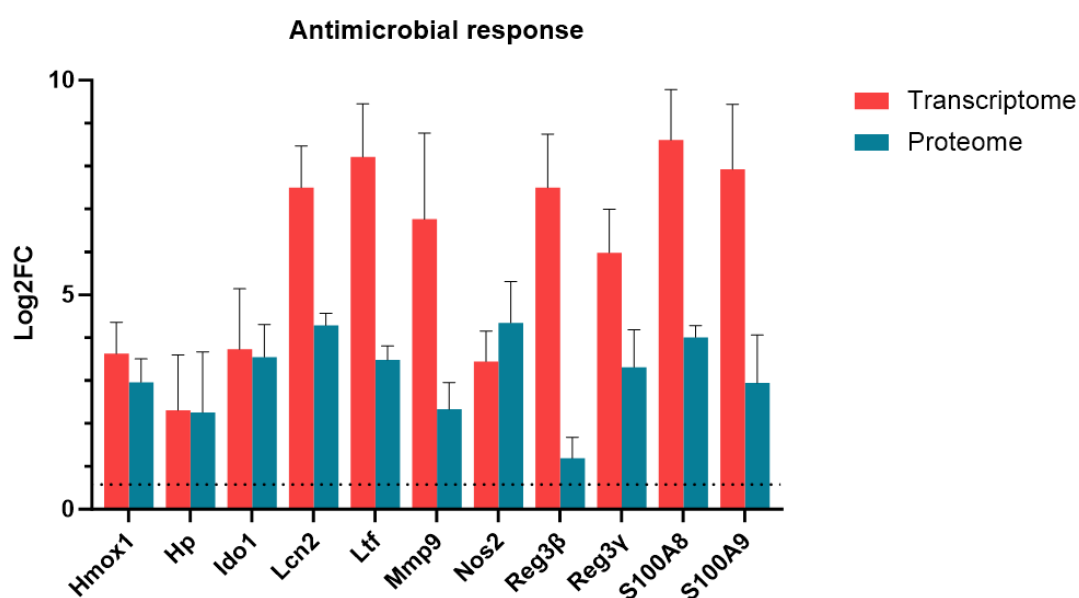


Figure 4.3. Infection with *C. rodentium* triggers antimicrobial gene expression and antimicrobial protein production.

Antimicrobial genes and protein abundance showed an upregulation in response to infection with *C. rodentium*. The result shows that both gene expression and protein abundance are altered in the same manner. The dotted line represents the cutoff, $\log_2FC=0.58$. Data from 6 mice were used for the transcriptome, and data from 4 mice were used for the proteome. Figure created with GraphPad Prism.

4.3.3 Cholesterol metabolism of intestinal epithelial cells during *C. rodentium* infection.

The cholesterol metabolism pathway was detected as one upregulated pathway in both transcriptome and proteome (**Figure 4.2**). This change aligns with findings by Berger et al. (2017), who demonstrated an elevated abundance of the cholesterol efflux and biosynthesis pathway during *C. rodentium* infection.

The diagram in **Figure 4.4A** summarises the cholesterol biosynthesis pathway, revealing increased gene expression and elevated protein abundance during infection. This analysis demonstrated a direct correlation between transcriptome and proteome levels, with only three exceptions in the proteome showing no significant change in abundance (shown in white).

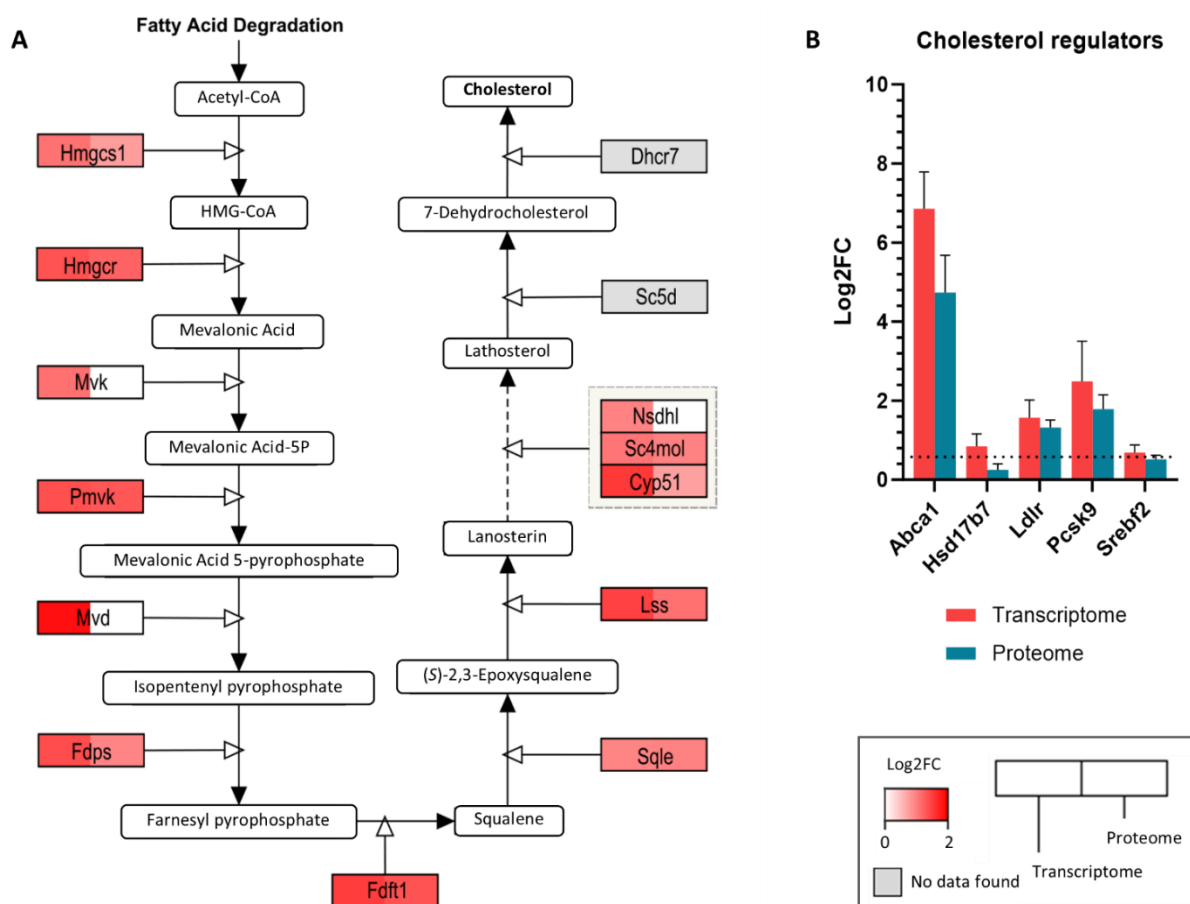


Figure 4.4. *C. rodentium* induces upregulation of cholesterol metabolism.

(A) Diagram showing the cholesterol synthesis pathway, with gene expression on the left and protein abundance on the right. Both transcriptome and proteome show similar alterations. Diagram generated with PathVisio. (B) The transcriptomic and proteomic results demonstrate upregulated expression of genes involved in cholesterol metabolism and increased protein abundance. The dotted line represents the cutoff, $\log_2FC = 0.58$. Data from 6 mice were used for the transcriptome, and data from 4 mice were used for the proteome. Graph generated with GraphPad Prism.

The initial enzymes of the pathway, Hydroxymethylglutaryl-CoA synthase (encoded by *Hmgcs1*) and HMG-CoA reductase (encoded by *Hmgcr*), showed significant upregulation in both the transcriptome and proteome, with increases of 2.1-fold (p-value $5.4E^{-07}$) and 2.6-fold (p-value $1.5E^{-08}$) in the transcriptome, respectively, and 1.7 times and 2.3 times in the proteome. Notably, Mevalonate kinase (encoded by *Mvk*), mevalonate-

(diphospho)decarboxylase (encoded by *Mvd*), and Sterol-4-alpha-carboxylate 3-dehydrogenase (encoded by *Nsdhl*) showed upregulation in the transcriptome, while their protein abundance did not show significant changes (**Figure 4.4A**).

The ATP-binding cassette protein 1 (encoded by *Abca1*), essential in cholesterol transport, showed significantly increased gene expression (by 110.7-fold, p-value $3.5E^{-68}$) and increased protein levels during infection (by 30.2-fold) (**Figure 4.4B**). Additionally, the LDL receptor (encoded by *Ldlr*) and the proprotein convertase 9 (encoded by *Pcsk9*), a protein involved in cholesterol uptake and receptor recycling, demonstrated upregulation and increased abundance. These results align with the findings showing increased RNA levels of the transcription factor *Srebf2* (by 1.6-fold, p-value $3.2E^{-06}$), which regulates the expression of genes involved in the cholesterol biosynthesis pathway, although its protein levels remained just below the significance threshold for change. The findings confirm that *C. rodentium* infection leads to an increase in cholesterol biosynthesis in IEC.

4.3.4 [Impact of *C. rodentium* infection on microvilli of intestinal epithelial cells.](#)

The intestinal epithelium is formed by enterocytes, which aid with digestion and nutrient absorption. The apical surface of these cells is lined with microvilli, cellular projections that significantly increase the surface area for absorption (Markovic and Brubaker 2019). AE pathogens, such as *C. rodentium*, induce an intimate attachment to the host cell and the effacement of the cell microvilli during infection. It has been demonstrated that *C. rodentium* leads to the erasement of the host cell microvilli, resulting in reduced protein abundance (Berger et al. 2018). In this study, we investigated whether disruption of microvilli results from bacterial protein targeting or modulation of gene expression.

Microvilli are supported by an actin core and several structural proteins, including Espin, Plastin, and Villin, which help maintain the structure (Markovic and Brubaker 2019). **Figure 4.5** illustrates a discrepancy between transcriptome and proteome data, with most genes showing unchanged expression while protein levels are reduced. Specifically, *Espin* and *Villin* show no change at the RNA level but a decrease in protein abundance by 2.1-fold and 1.5-fold, respectively. Importantly, Ezrin and Nherf1, which link membrane proteins to the actin cytoskeleton (Donowitz et al. 2010; Delacour et al. 2016), showed unchanged gene levels but decreased in abundance (1.8 and 1.9 times, respectively). Plastin-1 and Plastin-3

decreased 1.6 and 2.1, respectively, while the gene expression was only reduced for *Plastin-3* (1.8 times, p-value $3.9E^{-02}$) and remained unchanged for *Plastin-1*. Moreover, *Cobl* displayed reduced gene expression (2-fold, p-value $2.2E^{-04}$) and protein abundance (1.9-fold). Notably, although *Myo7b* and *Espin* showed downregulated gene expression, the results do not achieve statistical significance (p-value > 0.05). Similarly, *Spectrin*'s gene expression and protein levels are reduced during infection, but no significant changes are observed in either transcriptome or proteome (shown in white in **Figure 4.5**).

As anticipated, the results showed that protein abundance of the microvilli structural proteins was reduced during infection. RNA expression analysis indicated that the genes encoding these proteins remain largely unchanged, suggesting that the destruction of the microvilli is an active process occurring post-transcription rather than at the transcription stage.

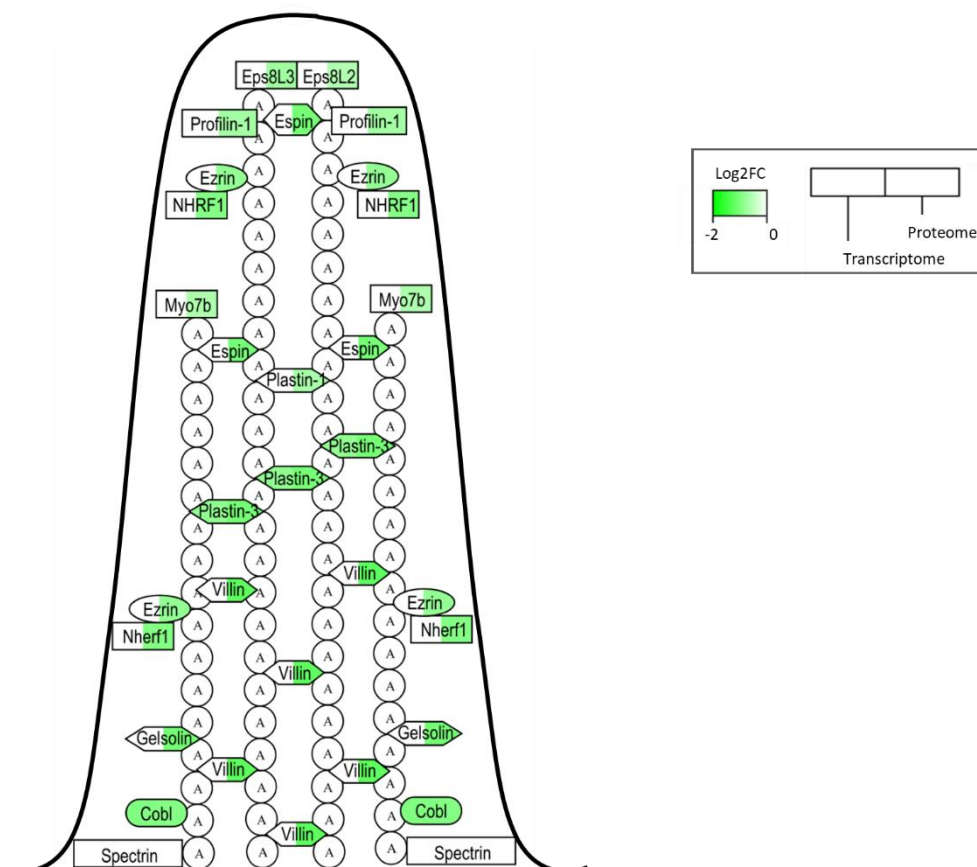


Figure 4.5. Microvilli structure of intestinal epithelial cells during *C. rodentium* infection. The diagram illustrates the microvilli structure of intestinal epithelial cells. It shows unchanged gene expression (left side) alongside reduced protein abundance during infection (right side). Data from 6 mice were used for the transcriptome, and data from 4 mice were used for the proteome. Diagram generated with PathVisio.

4.3.5 Effects of *C. rodentium* on the mitochondria of intestinal epithelial cells.

Mitochondria play a crucial role in cellular health and energy production via the tricarboxylic acid (TCA) cycle and oxidative phosphorylation (OXPHOS) at the mitochondrial membrane (Pfanner et al. 2019). During *C. rodentium* infection, host mitochondria are targeted, leading to degradation and reduced protein abundance of components within the OXPHOS pathway (Berger et al. 2017).

In this study, we investigated whether mitochondrial disruption results from bacterial protein targeting or modulation of gene expression by examining the expression of genes encoding mitochondrial proteins. The accompanying diagram of the mitochondria highlights the location of these proteins (**Figure 4.6**).

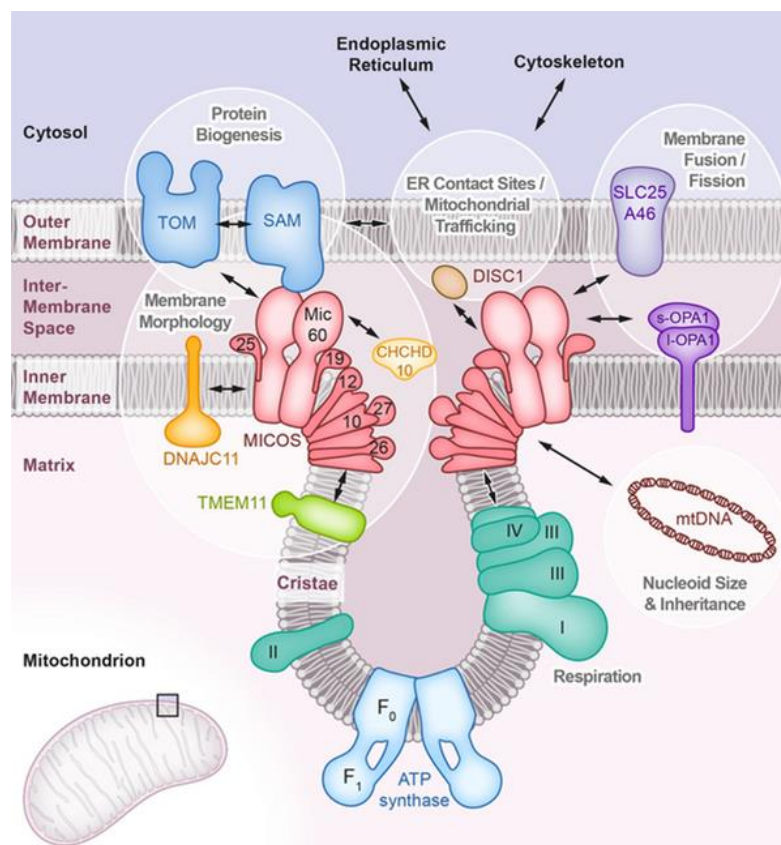


Figure 4.6. Key components of mitochondrial structure.

This figure illustrates the mitochondrial structure, highlighting key components involved in its function. It features the TOM and SAM complexes for protein import, which are essential for protein import, the MICOS complex for cristae organisation, and Opa1 for mitochondrial fusion and dynamics. The figure also shows the respiratory chain complexes (I-IV) and ATP synthase (complex V), alongside mt-DNA encoded genes, structural proteins, and solute carrier genes, all of which are critical for maintaining mitochondrial function. Image adapted from Prof. Dr. Nikolaus Pfanner, CIBSS - Centre for Integrative Biological Signalling Studies, University of Freiburg.

Tomm20, a component of the Tom Complex (Translocase of the Outer Membrane) involved in mitochondrial protein import (Pfanner et al. 2019), remains stable at both the transcript and protein levels during infection (**Figure 4.7**), which suggests that mitochondrial protein import is not directly affected by *C. rodentium*.

In contrast, Samm50, part of the SAM Complex (Sorting and Assembly Machinery), along with Mic60 and Mic13 from the MICOS (Mitochondrial Contact Site and Cristae Organizing System) complex, show a reduction in protein levels despite unchanged mRNA levels.

Similarly, Opa1, involved in mitochondrial fusion and dynamics, exhibits decreased protein levels while its transcript levels remain stable. This consistent pattern of reduced protein levels with stable transcript levels suggests that the infection leads to post-transcriptional modifications or protein degradation within these complexes.

Moreover, mitochondrial DNA-encoded genes such as *Mtco1*, *Mt-Cyb*, *Mtnd3*, *Mtnd4*, and *Mtnd5* also demonstrate stable transcript levels but decreased protein abundance. This

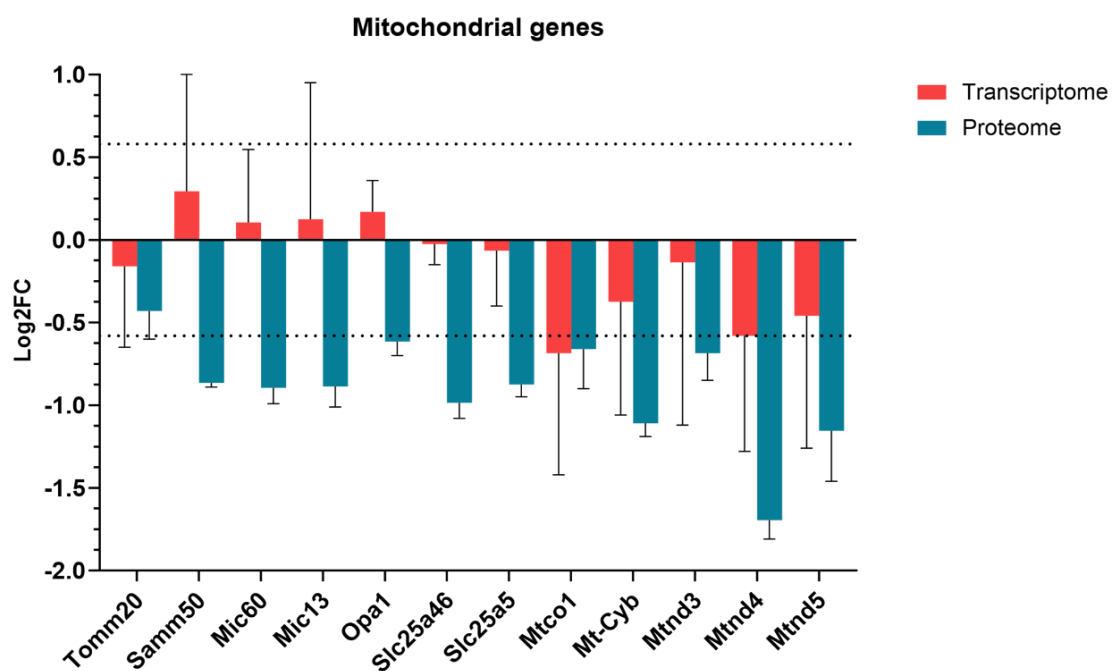


Figure 4.7. Mitochondrial gene expression and protein abundance.

The figure shows that Tomm20 remains unchanged at both the transcript and proteome levels. Samm50 and proteins of the MICOS complex exhibit decreased abundance despite stable RNA levels. Similarly, Opa1, solute carriers Slc25a46 and Slc25a5, and mt-DNA encoded genes (*Mtco1*, *Mt-Cyb*, *Mtnd3*, *Mtnd4*, *Mtnd5*), display reduced protein levels with stable RNA expression. Data from 6 mice were used for the transcriptome, and data from 4 mice were used for the proteome. Figure generated with GraphPad Prism.

further reinforces the conclusion that the observed mitochondrial dysfunction is primarily due to post-translational processes, rather than alterations in gene expression.

Following these results, we continued our analysis by studying the OXPHOS complex.

OXPHOS comprises five protein complexes integrated into the inner mitochondrial membrane: complex I, II, III, IV and V (Nolfi-Donagan et al. 2020). **Figure 4.8** illustrates that all Complex II proteins were identified; Complexes I and III had the most proteins (36 and 8, respectively), and Complexes IV and V had fewer (9 and 14, respectively).

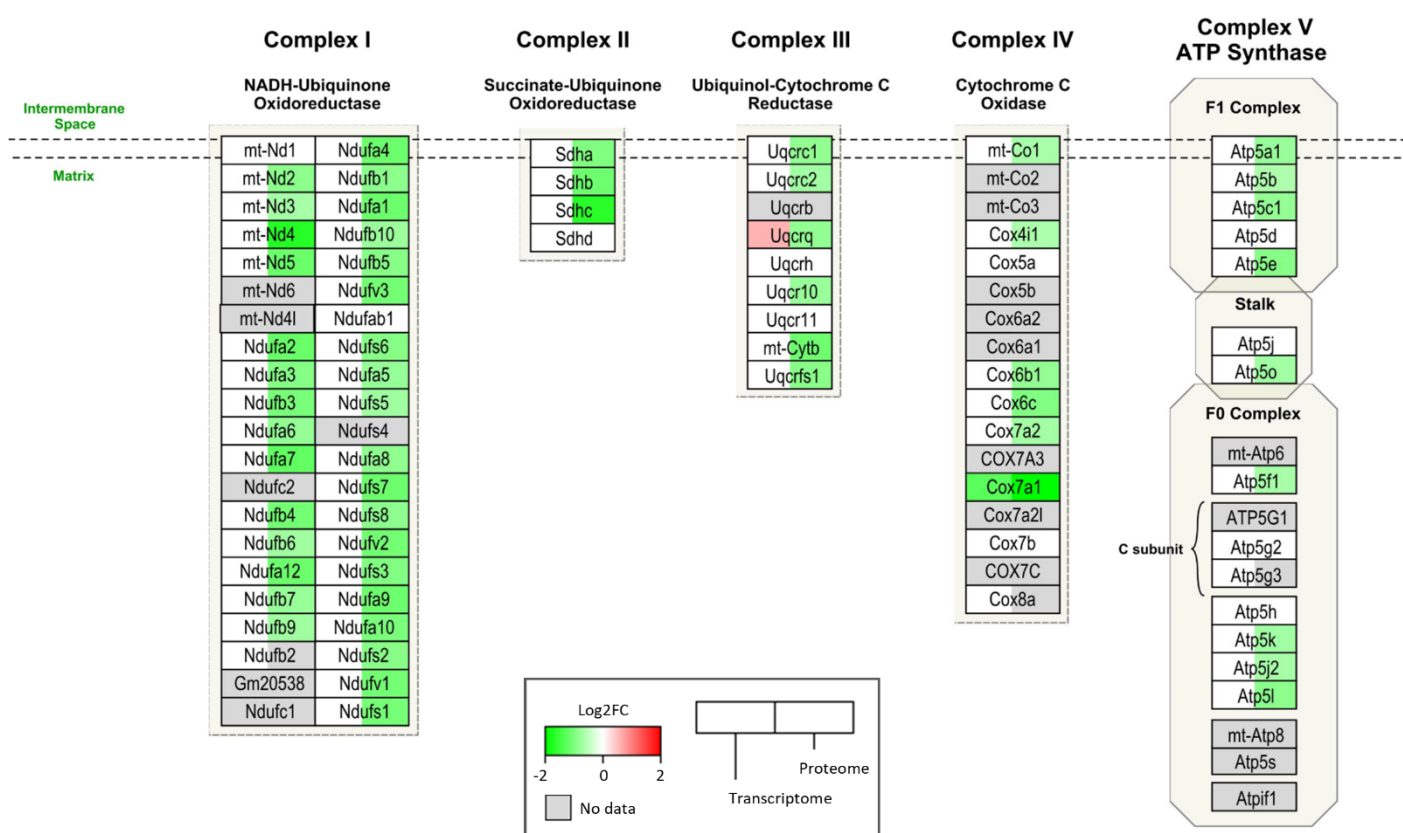


Figure 4.8. Effects of *C. rodentium* infection on mitochondrial OXPHOS proteins.

The figure illustrates the changes in mitochondrial protein levels associated with oxidative phosphorylation complexes I to V during *C. rodentium* infection. A reduction in protein abundance is represented by green, while white indicates proteins with no significant change. The proteomic analysis reveals a notable decrease in protein levels, whereas the transcriptomic data show no significant changes. Transcriptome data were obtained from 6 mice, and proteome data from 4 mice. Diagram generated with PathVisio.

Interestingly, gene expression for these proteins remained unchanged across all complexes despite decreased protein abundance. The only exceptions were the cytochrome C oxidase subunit 7A1 (encoded by *Cox7a1*), which showed reduced levels in both transcriptome (by 2.4 fold) and proteome (by 6.3 fold), and the ubiquinol-cytochrome C reductase complex III subunit VII (encoded by *Uqcrcq*), which showed increased gene expression (1.5 times, $4.8E^{-02}$) and reduced levels at the proteome (1.8 times). Additionally, the transcriptome showed better coverage than the proteome, as it identified three more entries than the proteome alone: NADH-ubiquinone oxidoreductase subunit B2 (encoded by *Ndufb2*), cytochrome C oxidase subunit 8A (encoded by *Cox8a*), and ATP synthase membrane subunit C locus 3 (encoded by *Atp5g3*).

The transcriptome and proteome data analysis reveals that while mitochondrial proteins decrease during infection, RNA levels remain consistent, which suggests that *C. rodentium* actively targets enterocyte mitochondria.

To further investigate the effects of infection on mitochondria, CMT93 cells (mouse colon cells) were infected for 9 hours with *C. rodentium*, and the mitochondria were examined for morphological changes. Since the mitochondrial protein Tomm20 remained unaltered at both RNA and protein levels during infection (**Figure 4.7**), an antibody against this molecule was used for immunostaining. Moreover, carbonyl cyanide m-chlorophenyl hydrazone (CCCP), an uncoupling agent of oxidative phosphorylation that inhibits mitochondrial function, was used as a positive control.

The results show that mitochondria of non-infected cells have a long, structured shape. In contrast, cells treated with CCCP and those infected with *C. rodentium* display disorganised, fragmented and smaller mitochondria (**Figure 4.9**). This observation is consistent with the study by Ma et al. (2006), which also reported smaller, distorted mitochondria in *C. rodentium*-infected colonic epithelial cells.

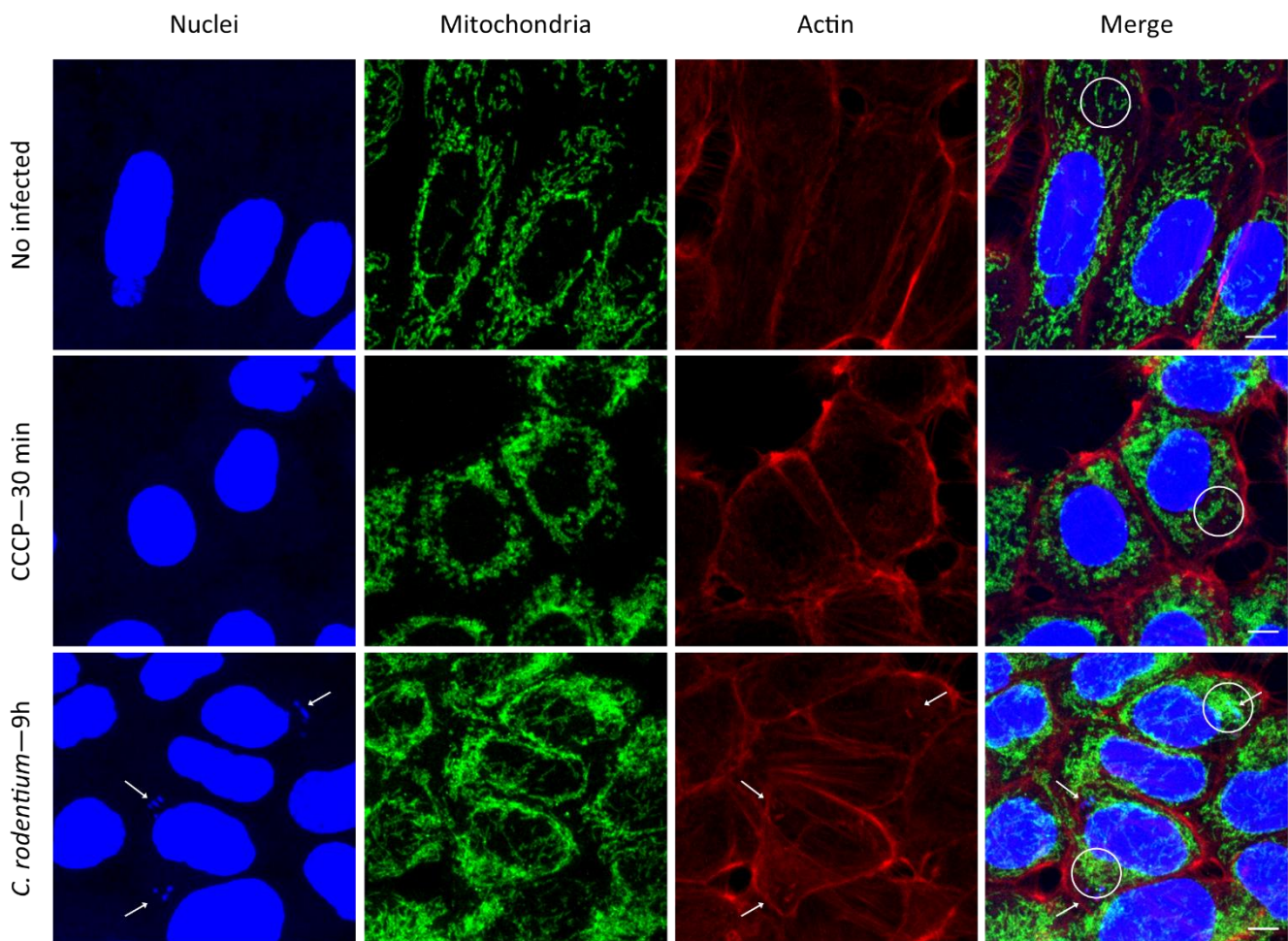


Figure 4.9. Effects of *Citrobacter rodentium* infection on mitochondrial morphology. Confocal microscopy images illustrating the impact of *C. rodentium* infection on mitochondrial morphology. Non-infected cells exhibit long, structured mitochondria, whereas infected cells show disorganised, fragmented, and smaller mitochondria. Arrows indicate pedestal formation by *C. rodentium* attachment to host cells. Circles highlight the mitochondria in different conditions.

These observations suggest that *C. rodentium* actively targets and disrupts mitochondrial integrity and function, inducing fragmentation of mitochondria. Furthermore, the transcriptome and proteome data reveal decreased mitochondrial protein levels despite unchanged RNA levels, suggesting that *C. rodentium* targets mitochondrial function and structure through post-transcriptional mechanisms.

4.4 Discussion.

4.4.1 Integrative analysis of transcriptome and proteome of *C. rodentium*-infected enterocytes.

Transcriptomics and proteomics are widely used for studying biological processes and diseases (Breschi et al. 2017; Casamassimi et al. 2017; Greco and Cristea 2017; Al-Amrani et al. 2021; Kolobkov et al. 2022). While it is generally assumed that mRNA levels correspond to protein abundance, studies have shown that the correlation between mRNA and protein can be low under both normal physiological conditions and disease (Ghazalpour et al. 2011; Schwanhäusser et al. 2011; Haider and Pal 2013).

Our study of the transcriptome and proteome of *C. rodentium*-infected enterocytes revealed some unexpected findings. We found a notably low correlation between the two in infected enterocytes: our combined analysis revealed that only 380 entries were differentially expressed in both datasets (**Figure 4.2**). Additionally, most entries showed changes in the transcriptome without corresponding alterations in the proteome and vice versa. Gene expression is regulated by transcription, translation, mRNA degradation, and protein degradation, so modifications in these processes could explain the different regulation between gene expression and protein abundance observed in this study.

Our study also shed light on the role of post-translational regulation in response to *C. rodentium* infection. Notably, molecules related to the proteasome complex and associated with protein modification processes showed changes in the transcriptome but remained unchanged in the proteome (**Figure 4.2**). The proteasome, a key player in protein degradation and post-translational regulation in eukaryotic cells demonstrated increased gene expression without corresponding changes in protein abundance. This suggests that increased expression of genes associated with the proteasome complex may not necessarily correlate with increased proteasome numbers. Furthermore, protein modification processes, such as ubiquitination, were not exclusive to the upregulated transcriptome with unchanged proteome. These processes displayed multiple patterns, indicating the significant role of post-translational regulation in regulating protein degradation in the host in response to *C. rodentium* infection.

Additionally, molecules belonging to the miRNA processing complex were identified within those showing proteome changes (decreased protein) but no transcriptome alteration. miRNA are small non-coding RNA essential in regulating gene expression. Since they regulate gene expression by inducing mRNA degradation and translational repression, this could explain the poor correlation between the transcriptome and proteome of *C. rodentium*-infected enterocytes. Notably, Wen et al. (2019) demonstrated that the miRNome of *C. rodentium*-infected enterocytes in mice is altered during infection, with various miRNAs being either upregulated or downregulated, highlighting the importance of this pathway in regulating host-pathogen interactions. This pathway will be studied further in Chapter 6.

Moreover, our findings indicate that a transcriptomic approach identifies a greater number of molecules compared to proteomics (**Figure 4.1**). This observation is significant because relying solely on proteomics would result in missing crucial information about molecular changes during infection. It emphasises the importance of incorporating transcriptomics in such studies. Nevertheless, unique proteins identified in the proteome also highlight the necessity of integrating both omics approaches for a comprehensive understanding. Notably, the prostaglandin metabolism pathway was predominantly identified through transcriptomic analysis. Prostaglandins are molecules involved in inflammation, immune response, and cell proliferation (Ricciotti and Fitzgerald 2011; Aoki and Narumiya 2012; Allaj et al. 2013), all processes induced by *C. rodentium* infection. To elucidate its specific role in the infection process, this pathway will be studied further in Chapter 5.

Integrating transcriptomic and proteomic data provides a comprehensive understanding of the molecular responses during *C. rodentium* infection. This highlights the complexity of gene regulation and the importance of considering multiple levels of gene expression analysis in infectious disease research.

4.4.2 *C. rodentium* infection induces changes in the host enterocyte.

C. rodentium infection induced various well-documented changes in host enterocytes, including alterations in cholesterol metabolism, antimicrobial peptide production, microvilli structure, and mitochondrial function.

Among the pathways with a strong correlation between transcriptome and proteome were cholesterol metabolism and antimicrobial peptide production, both showing increased gene expression and protein abundance (**Figure 4.3** and **Figure 4.4**). These pathways are well-documented to be stimulated during *C. rodentium* infection in enterocytes (Berger et al. 2017; Hopkins et al. 2019; Mullineaux-Sanders et al. 2019; Carson et al. 2020; Melchior et al. 2024). Therefore, increased gene expression and protein levels were expected and unsurprising. Transcriptomics allowed us to corroborate and validate these findings, reinforcing the proposal of using transcriptomics and proteomics together.

Furthermore, we observed changes in the proteome (reduced protein abundance) of microvilli and mitochondria without corresponding alterations at the gene expression level (unchanged gene expression) (**Figure 4.5**, **Figure 4.7** and **Figure 4.8**). It is known that *C. rodentium* targets the microvilli of enterocytes and host mitochondria, resulting in a decrease in protein abundance during infection (Ma et al. 2006; Papatheodorou et al. 2006; Berger et al. 2018; Ramachandran et al. 2020). Our findings confirm that the reduced protein levels in microvilli and mitochondria are a result of the bacteria's direct disruption of these structures, rather than changes in RNA expression.

Several studies have shown that T3SS effector proteins target various structures and organelles in the host cell during infection. *C. rodentium* induces the effacement of the enterocyte microvilli upon infection, and T3SS effectors play a crucial role in this process. For example, the T3SS effector protein EspB, which forms part of the translocated pore and is secreted into the host cell, binds to myosin, inhibiting its interaction with actin filaments and thus inducing microvilli effacement (Iizumi et al. 2007). Tir (the translocated intimin receptor) also coordinates with EspF, intimin and Map to cause microvilli effacement (Dean et al. 2006). This complex interaction between effectors leads to the destruction of the microvilli, which matches our results showing reduced microvilli proteins during infection (**Figure 4.5**).

Mitochondria, which play a crucial role in cellular health and energy production, are also targeted by an array of T3SS effectors during *C. rodentium* infection. These include Map (mitochondrial-associated protein), EspZ, and EspF, all localising to the host mitochondria upon infection (Nougayrede and Donnenberg 2004; Nagai et al. 2005; Ma et al. 2006;

Shames et al. 2011; Hua et al. 2018). While Map impairs mitochondrial function and induces disruption of the morphology (Ma et al. 2006), EspZ reduces mitochondrial membrane potential and causes cell death (Nagai et al. 2005). These match our findings, which show reduced mitochondrial proteins involved in OXPHOS, TOM, SAM, and MICOS complexes, and structural changes in the mitochondria of infected CMT93 cells (**Figure 4.7**, **Figure 4.8** and **Figure 4.9**).

By examining the gene expression of microvilli and mitochondria, we demonstrate that the bacteria-induced changes are due to physical disruption rather than alterations in gene expression. Literature indicates that T3SS effectors such as EspB, Tir, Map, EspF and EspZ target the enterocyte microvilli and mitochondria. Our results suggest that these effectors cause damage not by altering RNA expression but likely by promoting protein degradation. These findings highlight the complex mechanisms used by *C. rodentium* to disrupt host cellular structures and emphasise the importance of integrating both transcriptomic and proteomic data to fully understand the pathogen's impact.

4.4.3 Cell proliferation and DNA replication molecules are enhanced during *C. rodentium* infection.

During infection with *C. rodentium*, there is an increase in cell proliferation, leading to colonic crypt hyperplasia (CCH), primarily driven by increased stimulation of transit-amplifying (TA) intestinal cells (Collins et al. 2014b). TA cells are intermediate cells that originate from the proliferation and partial differentiation of stem cells in the lower half of the crypt. There, they rapidly divide multiple times before differentiating into mature intestinal cell types (Barker et al. 2008). The proliferation of these cells increases during *C. rodentium* infection, resulting in CCH.

Our integrated transcriptome and proteome data analysis identified key molecules involved in cell cycle regulation and DNA replication. These showed increased protein abundance without changes in the gene expression (**Figure 4.2**). Haus2, a subunit of the HAUS augmin-like complex crucial for microtubule-dependent amplification during cell division (Lawo et al. 2009), showed a significant 21.2-fold increase in the proteome. Although Haus6 was not detected in the transcriptome or proteome of infected enterocytes in our study, its

documented role in enhancing cell proliferation in colorectal cancer suggests a potential role for Haus proteins in modulating cellular responses during *C. rodentium* infection (Shen et al. 2022).

Furthermore, the proliferating cell nuclear antigen (*Pcna*), important for cell cycle regulation and DNA replication (Strzalka and Ziemienowicz 2011), showed a 2-fold increase in the proteome during infection, indicating heightened DNA replication activity. Similarly, *Orc1*, a component of the Origin Recognition Complex (ORC) crucial for DNA replication initiation, and *Mcm3*, a component of the MCM2-7 complex essential for DNA replication elongation, both exhibited a 2.3-fold increase in the proteome. These complexes are essential for ensuring accurate DNA replication initiation and elongation (Li and Stillman 2012), reflecting the increased replicative demand induced by *C. rodentium* infection.

Interestingly, despite the significant increase in protein levels, we did not observe corresponding changes in the RNA levels of *Pcna*, *Orc1* and *Mcm3*. This discrepancy supports the idea that *C. rodentium* may influence post-translational processes, such as protein stabilisation or reduced degradation, rather than altering gene expression directly. These post-translational modifications could lead to increased protein levels and support enhanced cell proliferation during infection. Previous reports indicated increased cell cycle and DNA replication at the protein level during *C. rodentium* infection (Hopkins et al. 2019; Carson et al. 2020), aligning with our findings and reinforcing the need to integrate both transcriptomic and proteomic analyses for a comprehensive understanding of the pathogen's impact.

4.5 Conclusions.

The main conclusions following a comparative analysis of the transcriptome and proteome of *C. rodentium*-infected enterocytes were as follows:

- The transcriptome and proteome of *C. rodentium*-infected enterocytes showed no strong correlation between gene expression and protein level changes, suggesting that post-transcriptional and post-translational processes are at play during infection.
- Transcriptome analysis identified more genes than proteomics alone, demonstrating better coverage and highlighting the importance of using both approaches together.
- Transcriptome analysis identified unique altered pathways, such as the upregulation of the prostaglandin metabolism pathway, which proteomics could not confirm.
- The investigation of well-documented pathways altered during *C. rodentium* infection indicated that mitochondrial and microvilli disruption is likely due to the active degradation of proteins rather than a modulation of gene expression.
- The joint analysis revealed a poor correlation between the gene expression and protein level of molecules involved in DNA replication and cell cycle, suggesting that post-translational processes modulate these to promote cell proliferation during infection.

These findings highlight the complexity of host-pathogen interactions and emphasise the need for integrated multi-omics approaches to understand the molecular mechanisms underlying *C. rodentium* infection.

CHAPTER 5: Prostaglandin biosynthesis
regulation during *Citrobacter rodentium* infection

5 CHAPTER 5: Prostaglandin biosynthesis regulation during *Citrobacter rodentium* infection.

5.1 Introduction.

My previous pathway analysis suggested that the prostaglandin biosynthesis could be altered during *C. rodentium* infection. As a result, the connection between infection and prostaglandin regulation will be explored further.

Prostaglandins are lipid molecules derived from arachidonic acid, playing crucial roles in various physiological processes such as reproduction, gastrointestinal fluid secretion, cell proliferation, immune response, and inflammation. Under normal conditions, prostaglandin levels are relatively low. However, their levels significantly increase in response to inflammation, bacterial or viral infections, and other pathological conditions, such as cancer (Eckmann et al. 1997; Na et al. 2011; Agard et al. 2013; Mccarthy et al. 2013; Dennis and Norris 2015; Sander et al. 2017; Wang et al. 2021).

Prostaglandins are synthesised from membrane phospholipids and, although some have a dual role, can be broadly categorised into pro-inflammatory (e.g., PGE₂, PGF_{2α}) and anti-inflammatory (e.g., PGD₂, PGI₂) prostaglandins (Dorris and Peebles 2012; Murata and Maehara 2016; Sander et al. 2017; Wautier and Wautier 2023). Of particular interest is PGE₂, a pro-inflammatory molecule synthesised by various cell types, including immune cells, that is known to mediate cell proliferation (Agard et al. 2013; Fan et al. 2015; Mo et al. 2015). Similarly, PGF_{2α}, another pro-inflammatory prostaglandin, modulates cell growth (Horsley and Pavlath 2003).

PGE₂ is critical in regulating immune responses during viral and bacterial pathogenesis caused by Gram-negative and Gram-positive bacteria, including *Salmonella*, *E. coli*, and *Mycobacterium tuberculosis*. PGE₂'s effects on these infections vary, with studies showing that it can have inhibitory, stimulatory, or dual roles in viral replication cycles and can also inhibit pro-inflammatory immune responses during bacterial infections (Agard et al. 2013; Sander et al. 2017).

Based on the evidence, we hypothesise that *C. rodentium* infection also alters the prostaglandin metabolism pathway of infected enterocytes.

5.2 Aims and Objectives.

This chapter aimed to examine the effects of prostaglandin metabolism on *C. rodentium* infection in mice. To accomplish this aim, the following specific objectives were outlined:

- Analyse the gene expression and protein patterns of key enzymes implicated in prostaglandin metabolism.
- Investigate the function of prostaglandins in infected mice.

5.3 Results.

5.3.1 The prostaglandin biosynthesis pathway is altered during *Citrobacter rodentium* infection.

Pathway analysis revealed significant alterations in prostaglandin metabolism during infection with *C. rodentium* (p -value $1.3E^{-15}$), identifying 18 molecules involved in this pathway. Molecules identified in the analysis and related ones were individually examined to determine changes in gene expression.

37 genes involved in prostaglandin metabolism were identified, including those for prostaglandin biosynthesis, modulators, and degradation. Among these genes, 46% were upregulated (17 genes), 38% were either unchanged or not reproducible (14 genes), and 16% were downregulated (6 genes) (**Figure 5.1**).

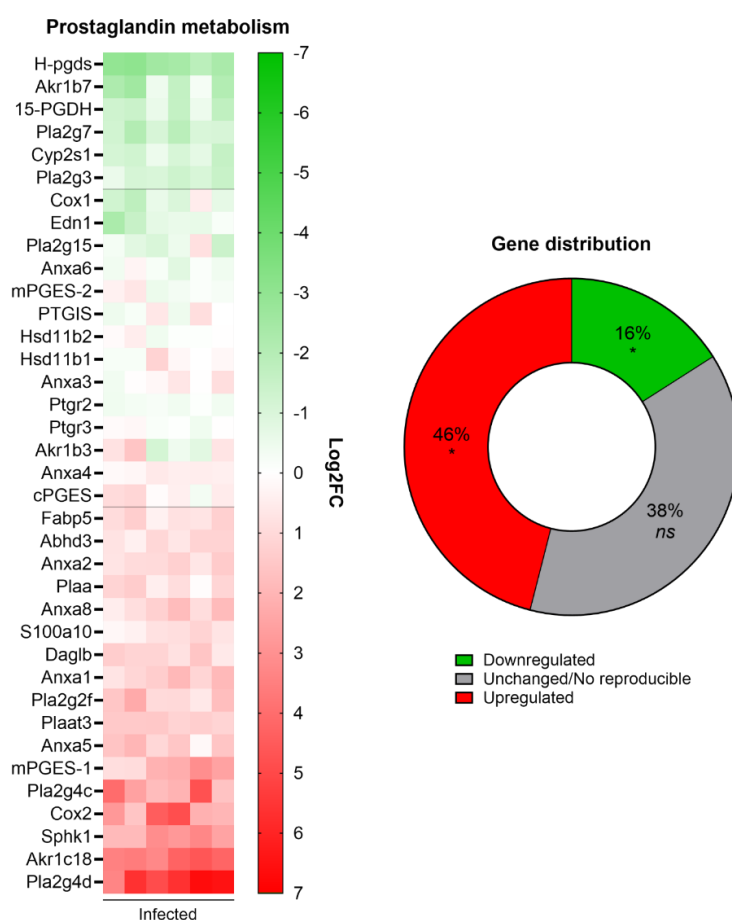


Figure 5.1. Prostaglandin metabolism regulation in *C. rodentium* infection.

The heat map illustrates the regulation of genes associated with prostaglandin metabolism during *C. rodentium* infection, presented as the Log₂FC (Log₂ fold change) of individual genes. Each column represents one mouse. The pie chart illustrates the gene distribution. *, p Value < 0.05; ns, non-significant. Graphs created with GraphPad Prism.

To determine if the changes in gene expression correlate with protein abundance, proteome data from previous experiences (Berger et al. 2017) were compared. Interestingly, 8 of the genes identified in the prostaglandin biosynthesis in the transcriptome were not found in the proteome, and, in some cases, there was no correlation between gene expression and protein levels (**Figure 5.2**). This highlights the complexity of gene-protein relationships and the importance of dual “omic” analysis.

Membrane phospholipids are directly metabolised by phospholipase A₂ (PLA₂) into arachidonic acid (Burke and Dennis 2009; Khan and Ilies 2023). Whereas secretory phospholipase (Group IIF, III and Group VII) were generally downregulated (*Pla2g2f* increased 2.5 times, and *Pla2g3* and *Pla2g7* decreased 2.2 times and 2.3 times, respectively), cytoplasmic PLA₂ (Group IVC, IVD) and proteins with phospholipase activity (*Plaat3* and *Abhd3*) were upregulated significantly (5.1, 50, 2.7 and 2.1 fold change respectively), suggesting increased arachidonic acid production (**Figure 5.2A** and **Figure 5.3**). *Plaat3* was also increased in the proteome (2.8-fold). Interestingly, the regulator Phospholipase A₂ Activating Protein (*Plaa*), which positively regulates cytosolic PLA₂, is upregulated (2.1 fold), and *Anxa1*, which negatively regulates cytosolic PLA₂, also showed increased expression (2.4 fold) (**Figure 5.2A**, **Figure 5.2C**, and **Figure 5.3**). These changes indicate a shift towards increased arachidonic acid availability during infection.

Arachidonic acid is then further metabolised by Cyclooxygenase 1 (encoded by *Ptgs1* or *Cox1*) and Cyclooxygenase 2 (encoded by *Ptgs2* or *Cox2*) to produce prostaglandin H₂. While the gene expression of *Cox1* showed downregulation, the results were not reproducible (p-value > 0.05); hence, they are shown in white in **Figure 5.3**. Whereas *Cox1* is constitutively expressed, *Cox2* expression is upregulated during inflammation (O'Neill and Ford-Hutchinson 1993). Accordingly, *Cox2* expression increased 5.7-fold during infection with *C. rodentium* (p-value 2.9E⁻⁶) (**Figure 5.2A** and **Figure 5.3**), suggesting a predominant role of *Cox2* in the inflammatory response during infection.

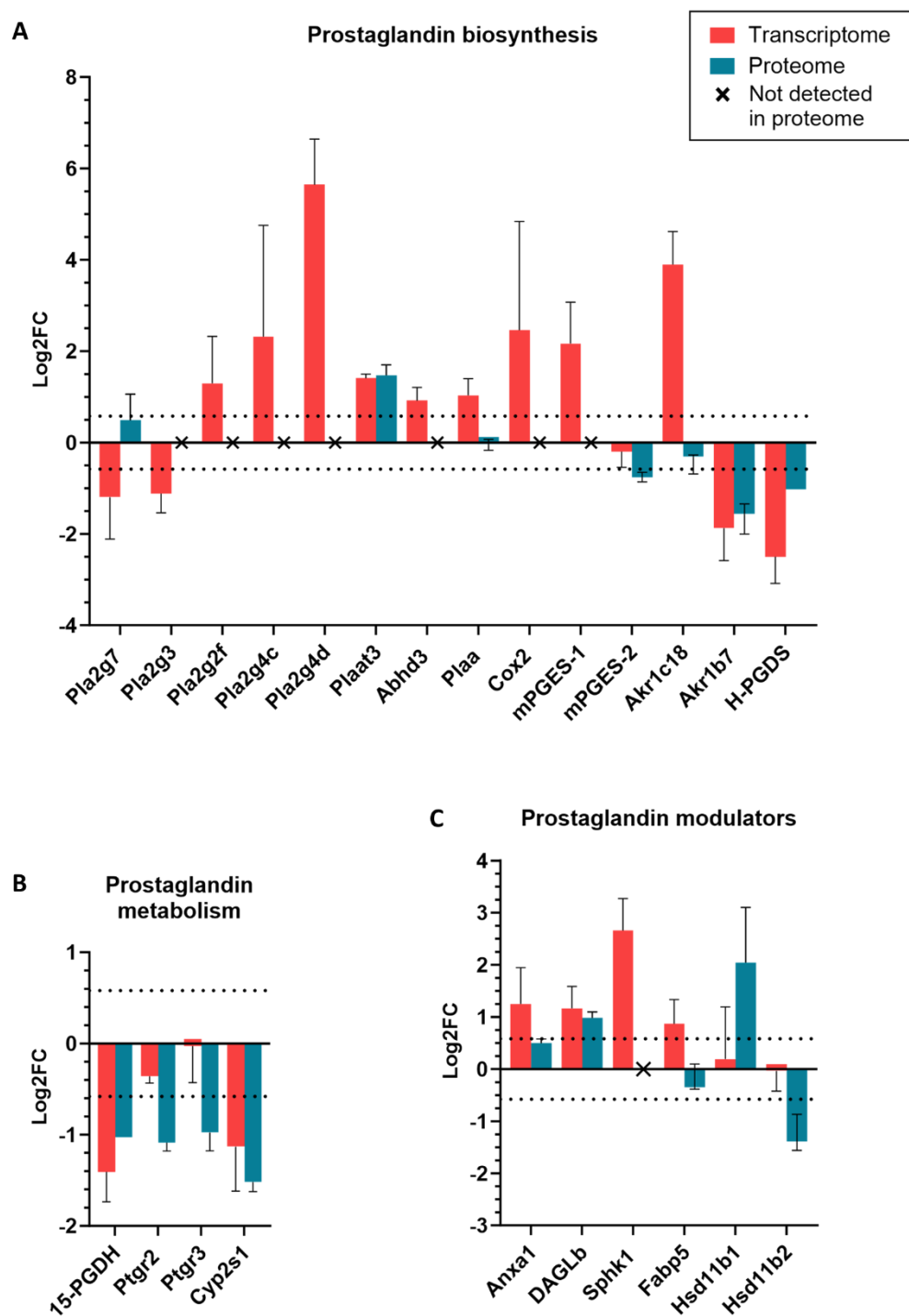


Figure 5.2. Modulation of prostaglandin biosynthesis in *C. rodentium* infection: integration of transcriptome and proteome data.

(A) General upregulation of genes involved in the prostaglandin biosynthesis, contrasting with proteomic data that shows most proteins are undetected, unchanged, or decreased during *C. rodentium* infection. (B) Downregulation of genes involved in prostaglandin metabolism during infection. (C) Changes in prostaglandin modulators during infection. Transcriptome data were obtained from 6 mice, and proteome data from 4 mice. Graphs were generated using GraphPad Prism.

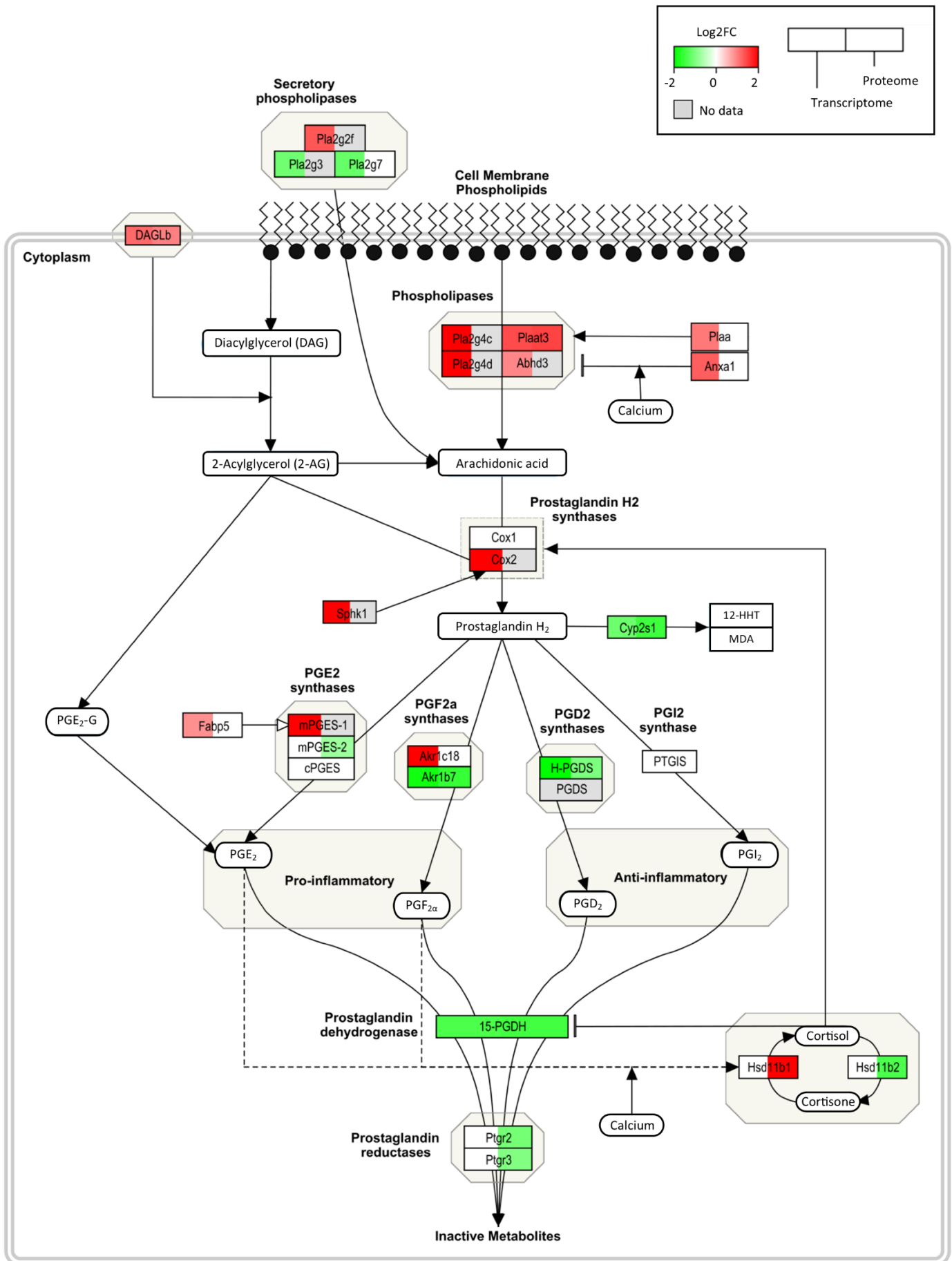


Figure 5.3. Regulation of prostaglandins biosynthesis in *C. rodentium* infection.

Schematic representation of the prostaglandin biosynthesis pathway showing the regulation of genes involved in producing pro-inflammatory prostaglandins (PGE_2 and $\text{PGF}_{2\alpha}$) and anti-inflammatory prostaglandins (PGD_2 and PGI_2). The diagram highlights the effect of some modulators on the pathway and the metabolism of prostaglandins. Transcriptome data were obtained from 6 mice, and proteome data from 4 mice. Image was generated using PathVisio.

Figure on page 95.

Following the production of prostaglandin H_2 , it is converted by prostaglandin synthases to PGE_2 , $\text{PGF}_{2\alpha}$, PGD_2 and PGI_2 . Microsomal prostaglandin E synthase-1 (encoded by *mPGES1*), which is typically induced in inflamed tissues (Jiang et al. 2021), showed significant upregulation during infection (4.5 times), similar to its positive regulator *Fabp5* (Fatty acid-binding protein 5) (increased 1.8-fold) (Bogdan et al. 2018) (**Figure 5.2A** and **C**, and **Figure 5.3**).

The prostaglandin $\text{F}_{2\alpha}$ synthases *Akr1c18* and *Akr1b7* showed opposite changes; while the former was increased 15.2 times, the latter was reduced 3.6-fold (**Figure 5.2A** and **Figure 5.3**). The prostaglandin D_2 synthase (encoded by *H-PGDS*) showed a good correlation between transcriptome and proteome, as gene expression decreased 5.7 times and protein abundance 2 times. These results highlight the dynamic regulation of prostaglandin synthases in response to infection.

Different enzymes mediate the metabolism of prostaglandins. 15-hydroxyprostaglandin dehydrogenase (encoded by *15-PGDH*) showed decreased gene expression and protein abundance during infection (2.7 times and 2.8 times, respectively) (**Figure 5.2B** and **Figure 5.3**). Similarly, prostaglandin reductases *Ptgr2* and *Ptgr3*, which metabolise prostaglandins to inactive compounds, showed decreased protein abundance (2 times each) and unchanged gene expression. Additionally, the Cytochrome P450 2S1 (encoded by *Cyp2s1*), which inactivates prostaglandins by metabolising prostaglandin H_2 to 12-HHT and MDA, showed decreased gene expression and protein abundance during infection (2.2 times and 2.9 times, respectively). These results indicate a reduced capacity for prostaglandin metabolism during infection.

An additional reaction by *Cox2* is the metabolism of 2-Acylglycerol (2-AG) to PGE_2 -glycerol ester ($\text{PGE}_2\text{-G}$), an inflammatory metabolite that can be further metabolised to PGE_2 (Hu et

al. 2008; Brüser et al. 2017; Kingsley et al. 2019). The enzyme diacylglycerol lipase beta (DAGLb), which produces 2-AG (Hsu et al. 2012), was upregulated in the transcriptome (2.2-fold) and the proteome (2-fold). Notably, the gene expression of *Sphk1*, which activates Cox2 (Pettus et al. 2003), was upregulated 6.3 times (**Figure 5.2C** and **Figure 5.3**). These findings suggest a pathway shift favouring the production of PGE₂ and its derivatives during infection.

Cortisol is another Cox2 modulator. While there were no changes in the transcriptome, the enzyme Hsd11b1, involved in cortisol production, was increased in the proteome (4.1-fold), and the enzyme involved in its metabolism, Hsd11b2, was decreased (2.6 times). Moreover, cortisol negatively regulates 15-PGDH, which is responsible for the metabolism of prostaglandins. Thus, the regulation of Cox2 and prostaglandin metabolism may be significantly influenced by cortisol dynamics during infection.

5.3.2 Effect of prostaglandin metabolism pathway on *C. rodentium* infection.

To study the impact of the prostaglandin biosynthesis pathway on *C. rodentium* infection, mice were treated with acetylsalicylic acid (Aspirin or ASA), an anti-inflammatory drug which inhibits Cox production, and infected with *C. rodentium*. Over the course of the infection (8 days), water consumption was measured, mice were weighed, and stool samples were collected. At the peak of infection (day 8), mice were humanly sacrificed, and colonic tissue was collected for histology.

Aspirin was incorporated into the drinking water, and a fresh solution was provided every other day. The results show that mice consumed between 26 mg/kg and 29.9 mg/kg aspirin daily, which was expected, as the recommended aspirin dosage was 25 mg/kg mouse (**Table 5.1**).

	Daily Water consumption	Daily ASA consumption
	Volume (mL)/mouse	ASA (mg/kg)/mouse
Aspirin + <i>C. rodentium</i>	4.8	29.9
Aspirin + No infected	4.2	26

Table 5.1. Daily water and aspirin consumption across experimental groups.

Stool samples were used to assess *C. rodentium* colonisation in mice. The results reveal no difference in CFU/g stool between mice treated with aspirin and those without treatment, demonstrating no distinctive colonisation at day 7 post-infection (see **Figure 5.4A**). These findings demonstrate that using a Cox inhibitor does not impact the ability of the bacteria to colonise the host, indicating that any observed changes are unlikely to be attributed to variations in the bacterial counts.

Individual weight loss was tracked as an indicator of animal health. The results revealed that mice treated with aspirin experienced weight loss on day 8 post-infection compared to infected mice without aspirin treatment (**Figure 5.4B**).

C. rodentium infection induces the enlargement of the intestinal crypt, leading to colonic CCH. Since prostaglandins play a role in inducing cell proliferation, treating *C. rodentium*-infected mice with aspirin could potentially reverse the effects of *C. rodentium* on the

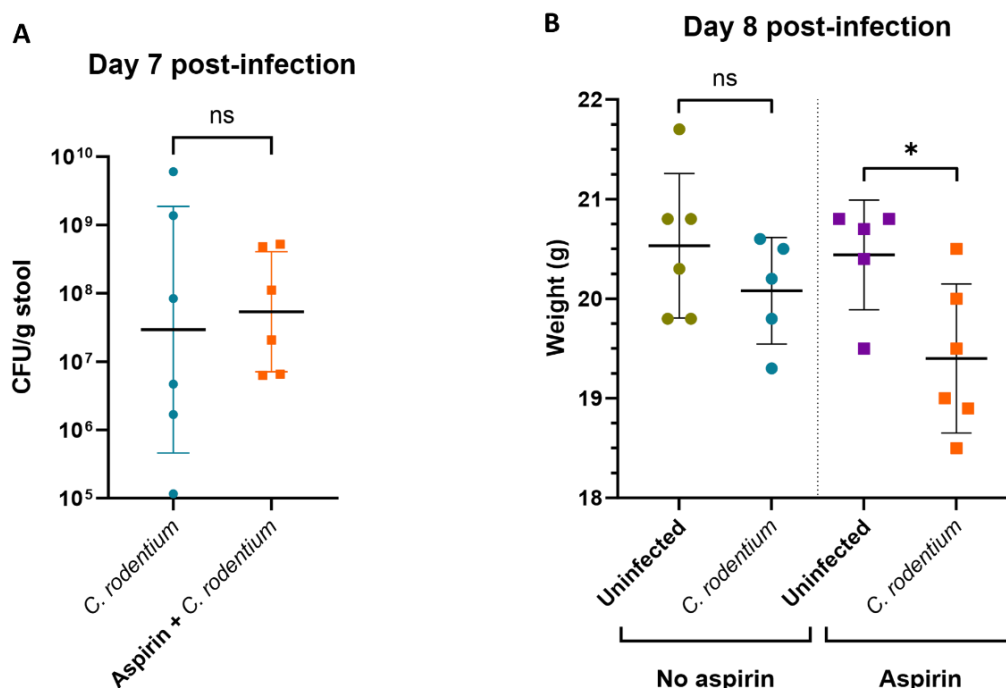


Figure 5.4. *C. rodentium* colonisation and mice weight at day 7 and day 8 post-infection. (A) Stool samples cultured on agar plates at day 7 post-infection showed no significant change in CFU/g stool between aspirin-treated and non-treated mice. Each dot represents the median for individual mice; each sample was prepared in triplicates. (B) Weight fluctuations monitored over time showed mice under aspirin treatment and *C. rodentium* infection decreased weight at 8 days post-infection compared to the non-treated group. Graphs and statistical analysis were performed using GraphPad Prism; Mann-Whitney test, two-tailed *p*-Value. ns: non-significant; *: *p*Value<0.05.

intestinal crypt. The next step was to determine if the induction of colonic crypt hyperplasia was changed with aspirin treatment. Histology samples from all groups were collected, and crypt length was measured. The results show the development of colonic crypt hyperplasia in both *C. rodentium*-infected groups, either non-treated or treated with aspirin, suggesting that the effects of aspirin treatment do not influence the progression of colonic crypt hyperplasia (**Figure 5.5**).

Mice stools were collected over the length of the experiment to determine lipocalin 2 (Lcn 2) levels. Lcn 2 is an acute-phase molecule that rapidly increases expression during inflammation and is used as an inflammatory marker. Since aspirin is a non-steroidal anti-inflammatory drug that inhibits Cox enzymes, it is expected that the use of aspirin reduces Lcn 2 production. The collected stools were weighed, dissolved in PBS, and analysed for Lcn 2 production by ELISA.

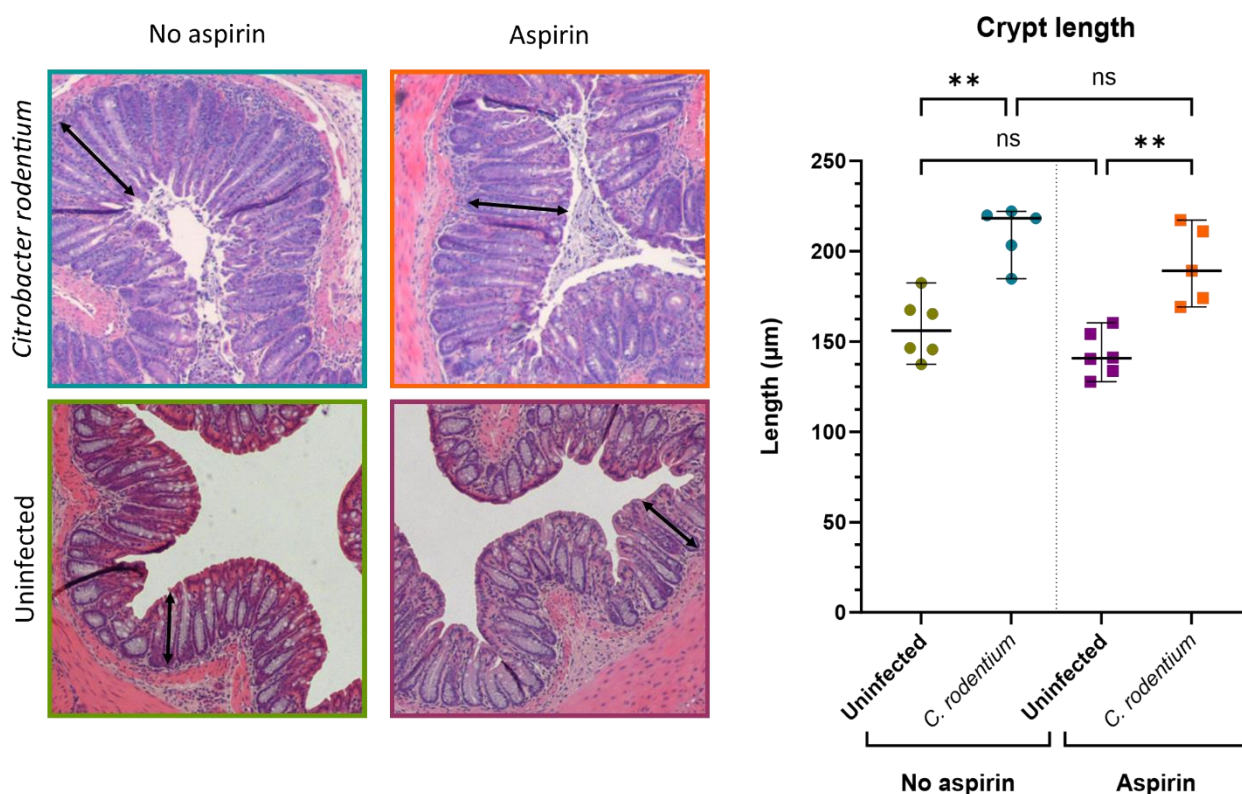


Figure 5.5. Impact of aspirin treatment on colonic crypt hyperplasia development.

Colonic crypt hyperplasia development in both *C. rodentium*-infected groups. Aspirin treatment does not influence hyperplasia development. Crypt length was measured (arrows) with Image J for all animals and all conditions. Each point represents the median from an individual mouse. Graph and statistical analysis were performed using GraphPad Prism. Two-way ANOVA was performed. Ns: no significant; **: p Value < 0.05.

The results showed that Lcn 2 production is stimulated during *C. rodentium* infection at days 5 and 8 post-infection (**Figure 5.6**). However, there is no distinction in Lcn 2 production between aspirin-treated and non-aspirin-treated mice, suggesting that the aspirin dose was insufficient to reduce inflammation during *C. rodentium* infection.

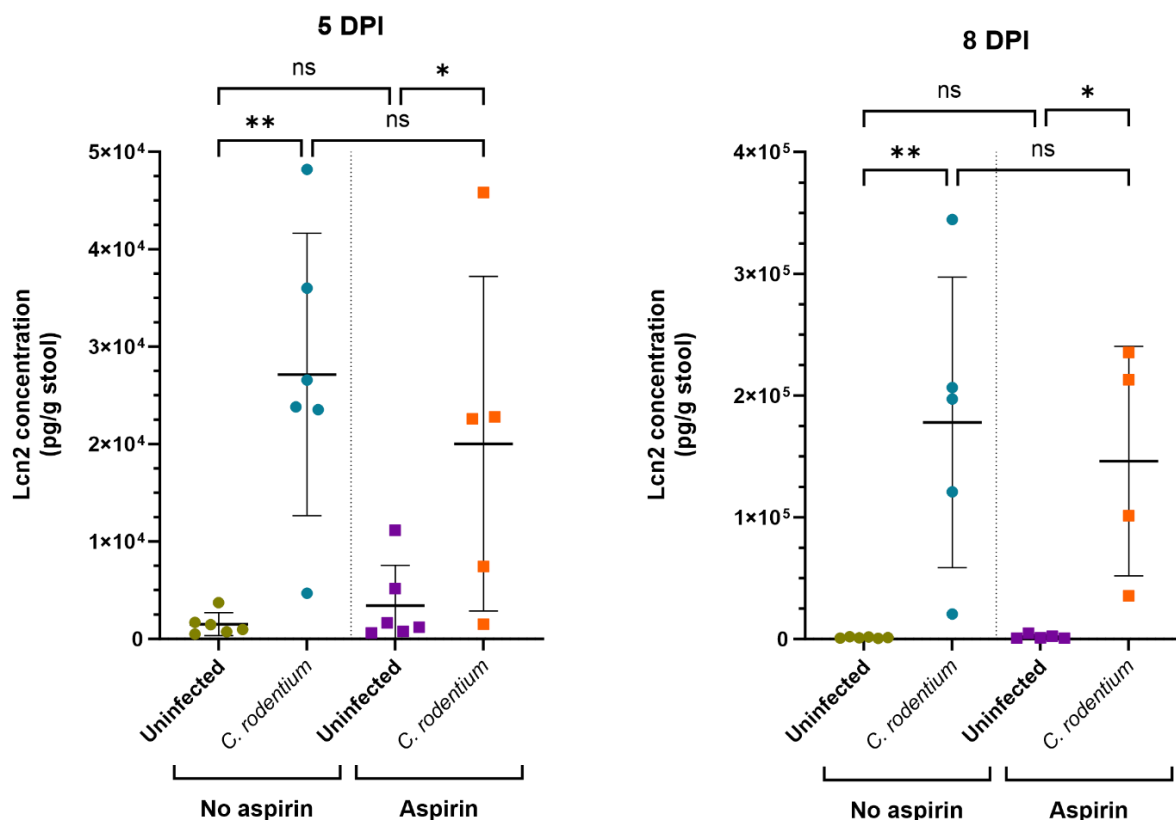


Figure 5.6. Lipocalin-2 levels during *C. rodentium* infection at 5 and 8 days post-infection.

ELISA results indicate increased Lcn 2 production at 5 and 8 DPI for both groups during *C. rodentium* infection. Importantly, aspirin treatment does not modify Lcn 2 production for any of the groups on both days post-infection. Each point represents the mean from an individual mouse; samples were measured in duplicate. Graphs and statistical analysis were performed using Graph Prism. Two-way ANOVA was performed. Ns: no significant; * or **: pValue<0.05.

The results presented in this section demonstrate that aspirin does not alter the Lcn 2 production or the crypt length of infected enterocytes, as they were similar in infected mice treated with aspirin to those infected mice non-treated with aspirin. The only difference between treatment groups was that aspirin-treated mice experienced weight loss during infection. These results suggest that this experiment's selected aspirin dose does not significantly impact the effects of *C. rodentium* infection in mice colon.

5.4 Discussion.

In this chapter, we investigated the prostaglandin metabolism pathway during *C. rodentium* infection. Our approach combined transcriptomic and proteomic analyses of infected IECs and evaluated the impact of aspirin treatment on infected mice, aiming to elucidate the role of prostaglandins during infection.

5.4.1 Prostaglandin profile of *C. rodentium*-infected enterocytes.

Prostaglandins play pivotal roles in maintaining physiological homeostasis and are dynamically regulated during inflammatory responses (Ricciotti and Fitzgerald 2011). Our study demonstrates an increase in the induction of Prostaglandin E₂ (PGE₂), a potent pro-inflammatory mediator, during *C. rodentium* infection (**Figure 5.2A** and **Figure 5.3**). This increase is accompanied by changes in gene expression that illustrate the induction of the prostaglandin biosynthesis pathway during infection.

The increased expression of genes encoding phospholipases and Cyclooxygenase-2 (Cox2), crucial for arachidonic acid and Prostaglandin H₂ synthesis, further supports the activation of prostaglandin biosynthesis pathways in response to infection. Cox2 is notably overexpressed during bacterial infections and it is implicated in various cancers, including colorectal cancer, highlighting its role in infection-associated inflammation (Agard et al. 2013; Allaj et al. 2013; Sander et al. 2017; Oyesola and Tait Wojno 2021). Additionally, Raymond et al. (2011) showed that the T3SS effector protein EspT triggers Cox2 expression and PGE₂ secretion in a human macrophage model. These findings highlight the importance of the T3SS effectors in pathogen-host interactions and suggest that the T3SS may play an important role in regulating pro-inflammatory prostaglandin production observed during infection with *C. rodentium*.

In addition to the increased expression of Cox2, we observed further modulation of prostaglandin pathways during *C. rodentium* infection, with a significant upregulation of microsomal Prostaglandin E synthase-1 (mPGES-1) in infected cells, and increased expression of *Fabp5*, a regulator of mPGES-1. This supports the idea that PGE₂ production is increased during *C. rodentium* infection. Interestingly, mPGES-1 was not detected at the proteomic level, and *Fabp5* showed no corresponding changes in protein abundance. This

discrepancy suggests that the upregulation of mPGES-1 may be a direct consequence of the infection, and is not dependent on the levels of its regulator Fabp5.

Given PGE₂'s role in promoting tumorigenesis and cell proliferation in conditions such as colorectal cancer (Wang and Dubois 2010; Iwanaga et al. 2014; Dennis and Norris 2015), its increased biosynthesis during *C. rodentium* infection aligns with pathological changes observed in infected mice. Moreover, our results suggest that the synthesis of the inflammatory PGE₂-glycerol ester (PGE₂-G) is also upregulated during *C. rodentium* infection, further implicating enhanced pro-inflammatory responses during infection (**Figure 5.3**).

Furthermore, the downregulation of H-PGDS, responsible for synthesising the anti-inflammatory PGD₂, suggests a decrease in the production of the anti-inflammatory prostaglandin during *C. rodentium* infection. Given that PGD₂ protects against uncontrolled cell growth and its deficiency exacerbates colitis and tumour formation in colitis-associated cancer (Iwanaga et al. 2014), this shift potentially contributes to enhanced colonic crypt hyperplasia observed during *C. rodentium* infection.

Overall, the results from this study demonstrate that there is a shift towards a pro-inflammatory prostaglandin profile during infection, evidenced by the upregulation of genes involved in the synthesis of prostaglandin precursors and PGE₂, alongside a reduction in the expression of genes involved in PGD₂ synthesis.

5.4.2 [Annexin A1 effects on *C. rodentium* infection.](#)

Phospholipase A2 initiates the release of arachidonic acid from cell membranes, a crucial step in prostaglandin biosynthesis. Our study revealed a general upregulation of PLA2 genes during *C. rodentium* infection, although specific downregulation was observed in *Pla2g3* and *Pla2g7* (**Figure 5.2A**).

Annexin A1 (*Anxa1*) exerts anti-inflammatory effects by inhibiting PLA2 and subsequent eicosanoid synthesis, including prostaglandins. Despite an increase in *Anxa1* gene expression during infection, protein levels remained unchanged (**Figure 5.3**). This discrepancy suggests that while the host may initiate protective responses via *Anxa1*, *C. rodentium* might counteract these effects by degrading the protein, potentially undermining host defences. Interestingly, Wen et al. (2019) observed that during *C. rodentium* infection,

the mouse miRNA mmu-miR-7a-2-3p, predicted to target Anxa1, was upregulated, further supporting this hypothesis.

Anxa1 exerts its protective effect by binding to N-Formyl peptide receptor 2 (Fpr2), triggering anti-inflammatory cascades (Yang et al. 2013). Fpr2-deficient mice display increased susceptibility to *C. rodentium* colonisation and severe colitis, with decreased mucus production in the colon, highlighting Anxa1's significance in mucosal immunity (Sharba et al. 2019). Additionally, Anxa1 has therapeutic potential in colitis treatment, promoting gastric wound healing and tissue recovery in inflammatory bowel diseases (Babbin et al. 2008; Leoni et al. 2013). Recent studies by Broering et al. (2022) further highlight Anxa1's efficacy in reducing colitis symptoms and improving tissue recovery, emphasising Anxa1 as a potential therapeutic agent against *C. rodentium* infection.

5.4.3 Prostaglandin metabolism is reduced during *C. rodentium* infection.

In addition to increased prostaglandin production, our results indicate reduced metabolism during *C. rodentium* infection (**Figure 5.2A** and **Figure 5.3**), reflecting an alteration in the balance of prostaglandin synthesis and degradation during infection.

Prostaglandin metabolism occurs via the action of 15-hydroxyprostaglandin dehydrogenase (15-PGDH), which inactivates prostaglandins and antagonises Cox2 activity (Yan et al. 2004; Na et al. 2011). We observed downregulation of 15-PGDH expression and reduced protein abundance (2.7 and 2.8 times) in *C. rodentium*-infected enterocytes of mice. This downregulation suggests that *C. rodentium* may activate mechanisms to stabilise prostaglandins in infected tissues, enhancing inflammation and cell growth.

Emerging evidence highlights the critical role of 15-PGDH in regulating inflammatory processes and carcinogenesis. Downregulation of 15-PGDH is implicated in colorectal cancer and other malignancies, facilitating PGE₂ accumulation and supporting tumour progression (Yan et al. 2004; Backlund et al. 2005; Myung et al. 2006; Vainio et al. 2011). Thus, the downregulation of 15-PGDH during *C. rodentium* infection likely contributes to the inflammatory and proliferative environment observed.

Furthermore, cortisol induction during *C. rodentium* infection (**Figure 5.3**) links stress responses to prostaglandin dysregulation. Cortisol enhances PGE₂ and PGF_{2α} production

while inhibiting 15-PGDH activity, potentially exacerbating the observed reduction in prostaglandin metabolism (Patel and Challis 2002; Wang et al. 2020). The cortisol induction might be responsible for the reduced prostaglandin metabolism observed in this study, indicating that *C. rodentium* may be using this strategy to modulate the host's inflammatory response. Importantly, using the proteomic approach allowed us to detect this regulation, as protein abundance significantly changed during infection (**Figure 5.2C**). Transcriptomic analysis alone would not have identified this process, as there were no changes at the gene expression level, highlighting the importance of using both approaches together.

Our study highlights the complex interplay between prostaglandin metabolism, immune responses, and pathogen virulence during *C. rodentium* infection. The downregulation of 15-PGDH and the altered prostaglandin profile contribute to an inflammatory and proliferative environment. These findings underscore the therapeutic potential of targeting the prostaglandin pathway in managing infectious and inflammatory diseases, highlighting 15-PGDH and Anxa1 as promising candidates for future research and therapeutic development. Furthermore, the combined use of transcriptomic and proteomic approaches proved essential in discovering these regulatory mechanisms, emphasising the importance of comprehensive analysis for a thorough understanding of host-pathogen interactions.

5.4.4 Aspirin effects on *C. rodentium* infection.

To study the impact of the prostaglandin biosynthesis pathway on *C. rodentium* infection, mice were treated with aspirin, an anti-inflammatory drug which inhibits Cox1 and Cox2 production, and infected with *C. rodentium*. Since prostaglandins are linked with cell proliferation in malignant processes such as cancers, the hypothesis was that these molecules were responsible for inducing inflammation and colonic crypt hyperplasia during *C. rodentium* infection in mice. Therefore, aspirin was expected to inhibit prostaglandin synthesis, potentially repressing colitis associated with *C. rodentium*.

Interestingly, our results showed no beneficial effects of treating *C. rodentium*-infected mice with aspirin. There were no significant differences in the colonisation of mice, colonic crypt hyperplasia development, or lipocalin-2 production: CFU/g of stool, crypt length, and lipocalin-2 levels were similar in infected mice treated with aspirin than in those non-treated with aspirin (**Figure 5.4A**, **Figure 5.5**, **Figure 5.6**). The only difference between the groups

was that mice infected with *C. rodentium* and receiving an oral dose of aspirin experienced weight loss by day 8 post-infection (**Figure 5.4B**).

Multiple factors could explain weight loss during treatment with aspirin. Aspirin-associated side effects, such as gastrointestinal irritation and pain (Li et al. 2020), can decrease appetite and food intake tolerance. Additionally, treatment with NSAIDs (Non-Steroidal Anti-Inflammatory Drugs) like aspirin can disrupt the microbiota, which is important for nutrient absorption and gut health, potentially leading to malabsorption of nutrients and weight loss.

Maseda et al. (2019) studied the effects of co-treatment with indomethacin, a Cox inhibitor, and *Clostridium difficile* (*C. diff*) infection, a bacterium that is the leading cause of antibiotic-associated colitis. While it promoted a change in the microbiota, disrupted the tight junctions, increased tissue damage, and induced severe colitis, it did not significantly change the weight loss associated with *C. diff* infection. This discrepancy could be due to differences in the pathogenic mechanisms of *C. diff* and *C. rodentium* and the specific effects of the NSAIDs used. While it can be speculated that similar changes in the microbiota could occur during aspirin treatment and *C. rodentium* infection, promoting loss of appetite and weight loss, the combined effects of aspirin and *C. rodentium* might lead to more pronounced gastrointestinal symptoms and subsequent weight loss than observed with *C. diff*.

Interestingly, Dejeni et al. (2018) reported that mice infected with *C. rodentium* and treated intraperitoneally with indometacin did not experience weight loss, contrary to our experiment with aspirin. This difference could be attributed to the route of administration, as using an intraperitoneal route could reduce the gastrointestinal side effects of aspirin and reduce weight loss.

Dejeni et al. (2018) also studied the effects of indomethacin on prostaglandin production and found that PGE₂ was reduced in infected mice treated with the Cox inhibitor.

Unfortunately, the colonic tissue we collected for ex vivo explants and PGE₂ ELISA detection did not work, so these results cannot be compared to our experiment. Nevertheless, their study lacked infection controls: they did not evaluate the colonisation of mice in the different treatment groups or check for colonic crypt hyperplasia. If indomethacin treatment reduces *C. rodentium* colonisation and the infection is less virulent, this could

explain the decreased PGE₂ levels. Therefore, attributing the reduction in PGE₂ solely to indomethacin treatment could be biased.

Our study focused on day 8 post-infection based on our previous transcriptome data showing changes at that time. Although we did not see any changes in the pathogenicity at 8 days post-infection, extending the study to 21 days, when mice infected with *C. rodentium* clear the bacteria, might reveal prolonged infection clearance kinetics typical for *C. rodentium*. Observing the mice beyond 8 days post-infection could provide insights into the long-term effects of aspirin treatment on weight and infection clearance.

The absence of alterations in pathogenicity observed during aspirin treatment implies that the administered dose might not effectively inhibit Cox2 or that prostaglandins may not contribute significantly to crypt hyperplasia or Lcn 2 production in *C. rodentium* infection. Further investigation through an extended study and higher dose is required to establish the link between prostaglandin biosynthesis and *C. rodentium* infection. Moreover, an alternative approach to increasing aspirin dosage could involve early intervention by inhibiting the prostaglandin biosynthesis pathway through phospholipase inhibition.

5.5 Conclusions.

The main conclusions following the investigation of the prostaglandin metabolism effects on *C. rodentium* infection in mice were as follows:

- The majority of the genes involved in prostaglandin metabolism identified by transcriptomics showed upregulation during *C. rodentium* infection. We observed an increase in the pro-inflammatory PGE₂ synthesis and a decrease in the anti-inflammatory PGD₂ synthesis, suggesting a shift towards a pro-inflammatory environment that may contribute to the observed colonic crypt hyperplasia.
- There was a lack of correlation between the proteome and transcriptomic of infected enterocytes, highlighting the importance of using more than one technique to investigate the effects of these molecules on *C. rodentium* infection in mice.
- Cortisol synthesis is induced during *C. rodentium* infection, potentially promoting the synthesis of prostaglandin precursors by increasing *Cox2* expression and inhibiting the prostaglandin metabolism by inhibiting the expression of 15-PGDH.
- Treatment of mice with a low dose of aspirin and infecting them with *C. rodentium* does not change the pathogenicity of the infection, suggesting that the dose was insufficient to inhibit the pathway or that prostaglandins are not responsible for *C. rodentium* inflammation pathogenesis.
- Aspirin treatment combined with *C. rodentium* infection promotes weight loss in mice by 8 days post-infection, likely due to gastrointestinal irritation and microbiota disruption, both potential side effects of aspirin.

Future work should include metabolomic analysis of *C. rodentium*-infected enterocytes and alternative prostaglandin inhibitors to further elucidate the connection between the prostaglandin biosynthesis pathway and *C. rodentium* infection. This will help decipher the link between the prostaglandin biosynthesis pathway and *C. rodentium* infection, providing a clearer understanding of the molecular mechanisms and potential therapeutic targets.

CHAPTER 6: Establish how the RNA-induced Silencing Complex (RISC) is regulated during *C. rodentium* infection

6 CHAPTER 6: Establish how the RNA-induced Silencing Complex (RISC) is regulated during *C. rodentium* infection.

6.1 Introduction.

Analysis of the transcriptome and proteome of IEC from mice infected with *C. rodentium* revealed a lack of correlation between gene expression and protein abundance. This discrepancy suggests that bacteria may modulate protein stability or degradation through post-transcriptional and post-translational processes (**Figure 6.1**). Post-transcriptional processes are often regulated by microRNAs (miRNAs), which are non-coding RNA that regulate protein expression by inhibiting translation, targeting ribosomes, or targeting mRNA for degradation (Eulalio et al. 2008; Huntzinger and Izaurralde 2011; Saliminejad et al. 2019). miRNAs exert their regulatory effects by incorporating into a protein complex known as the RNA-induced silencing complex (RISC), which includes Argonaute (Ago) proteins 1 and 2.

During bacterial infections, it is well-established that pathogens can manipulate host miRNA to their advantage. Examples of these include the intestinal pathogens *Helicobacter pylori*, *Salmonella*, and *Listeria* (Das et al. 2016; Zhou et al. 2018; Tong et al. 2023). For example, *H. pylori* can induce changes in miRNA expression in the host to promote intracellular

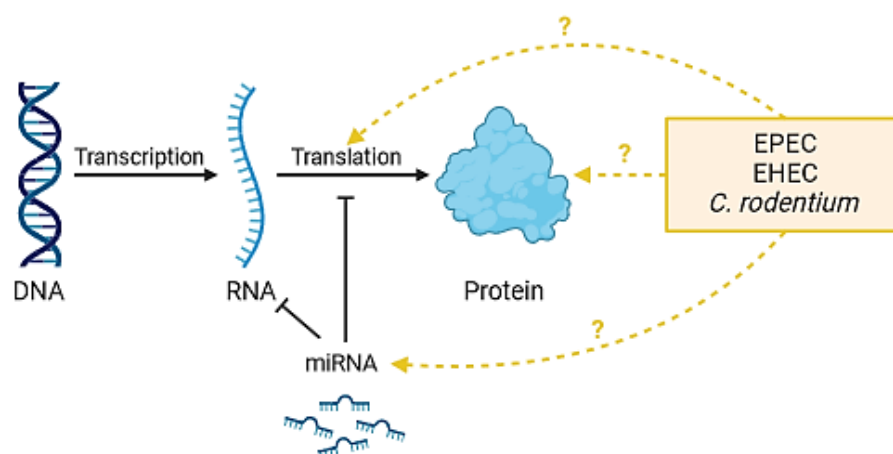


Figure 6.1. Post-transcriptional regulation: impact of microRNAs and pathogenic bacteria. The figure illustrates the processes of transcription (DNA to RNA) and translation (RNA to protein), highlighting the regulatory effects of microRNAs (miRNAs) in RNA stability and translation. Additionally, it illustrates the potential regulatory effects exerted by pathogenic bacteria, such as *C. rodentium*, EHEC and EPEC, on these processes. Figure created with BioRender.com.

survival (Tang et al. 2012). *Salmonella* infection has been shown to alter miRNA profiles to contribute to disease pathogenesis (Zhou et al. 2018). Similarly, it has been proposed that *Listeria* can hijack the host's miRNA machinery to evade immune detection (Maudet et al. 2014). Interestingly, *C. rodentium* infection also leads to changes in the expression of host miRNAs (Wen et al. 2019). However, little is known about how the bacteria manipulate the miRNAs.

To understand the host-pathogen interaction and the role of miRNA regulation during *C. rodentium* infection, this chapter focuses on investigating the RNA-induced silencing complex and its components.

6.2 Aims and Objectives.

This chapter aimed to examine the effects of *C. rodentium* infection on post-transcriptional regulation mediated by miRNAs. To accomplish this aim, the following objectives were established:

- Investigate the RNA and protein levels of miRNA targets during infection.
- Examine the effects of *C. rodentium* on the RNA-induced silencing complex.
- Analyse the impact of *C. rodentium*'s type three secretion system on argonaute proteins.

6.3 Results.

6.3.1 Changes in miRNA during *C. rodentium* infection.

To investigate how the miRNAs alter protein expression during *C. rodentium* infection, we analysed the miRNome published by Wen et al. (2019). We selected two miRNAs from this dataset for further investigation: the upregulated mmu-miR-92a and the downregulated mmu-miR-361 (**Figure 6.2**).

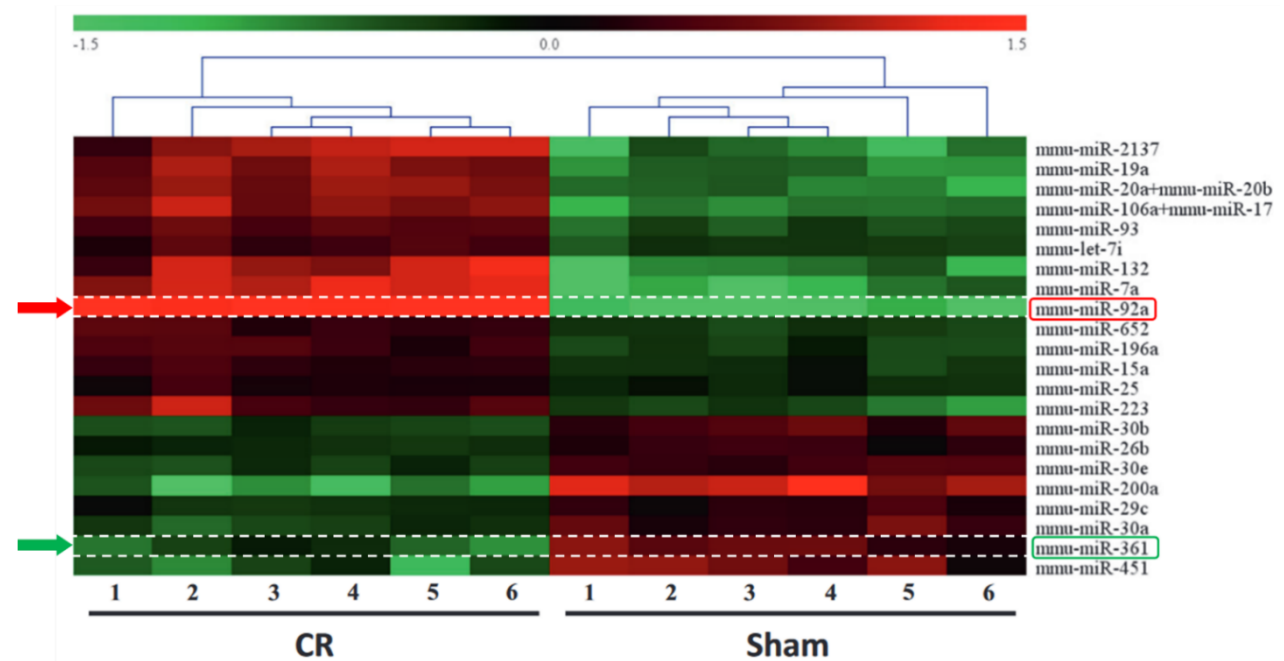


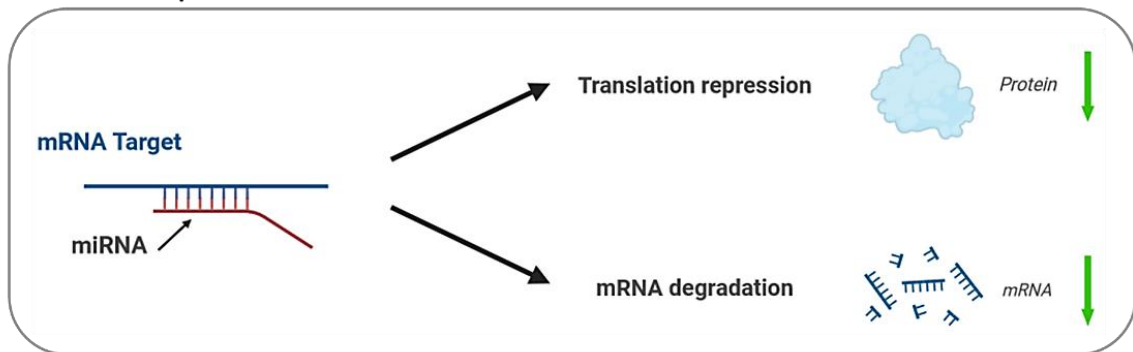
Figure 6.2. miRNAs and *C. rodentium* infection.

The heat map illustrates alterations in miRNA expression within intestinal epithelial cells during infection. Arrows highlight the miRNAs selected for analysis in this study, mmu-miR-92a and mmu-miR-361. Figure adapted from Wen et al (2018).

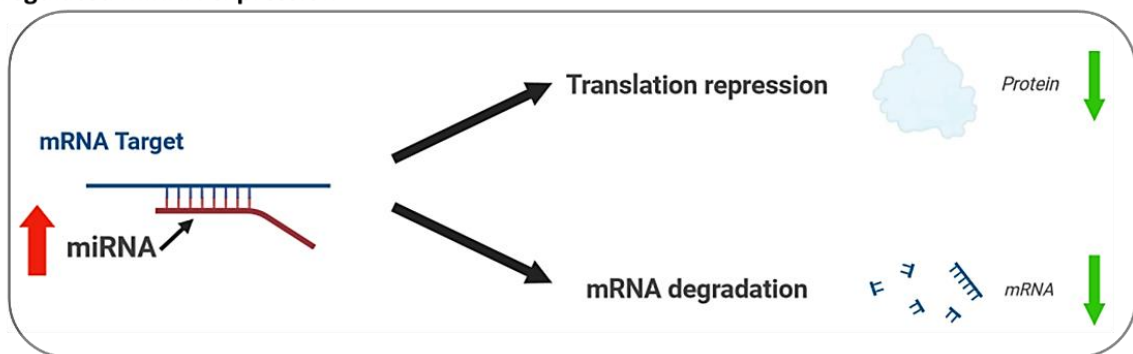
The selection process involved several steps. Initially, we studied the comprehensive miRNome provided by Wen et al. (2019) and reviewed studies that demonstrated the effects of these miRNAs on specific targets. Research indicated that mmu-miR-92a could downregulate *Foxo1* (encoding Forkhead box protein O1) (Fujiwara et al. 2022), involved in the regulation of immune responses, apoptosis, cell proliferation, and mucus secretion (Chen et al. 2021). Additionally, mmu-miR-361 was shown to downregulate *Sh2b1* (encoding SH2B adapter protein 1) (Chen et al. 2016), involved in insulin signalling, inflammation, and cell proliferation (Chen et al. 2016; Cheng et al. 2020). Then, we examined the transcriptome and proteome data for these targets.

Since miRNAs are molecules that regulate gene expression by repressing translation or degrading mRNA (Figure 6.3A), it is expected that for upregulated miRNA, its targets decrease (Figure 6.3B), and for downregulated miRNA, its targets increase (Figure 6.3C).

A. Normal miRNA expression



B. Upregulated miRNA expression



C. Downregulated miRNA expression

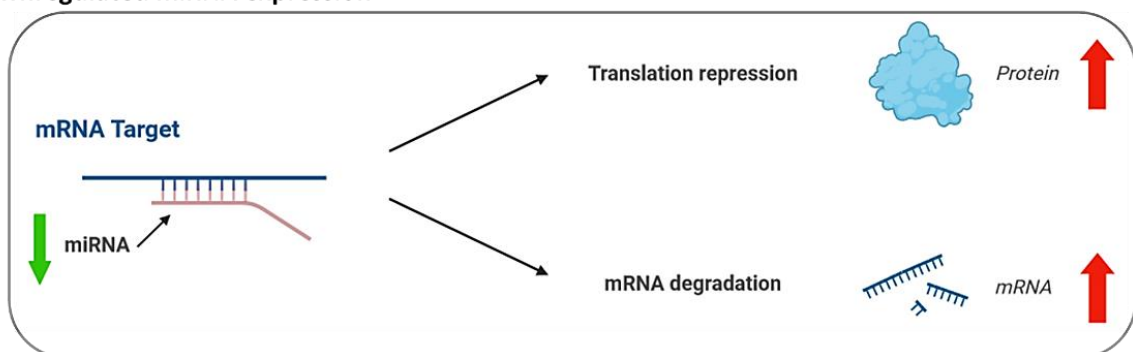


Figure 6.3. Diagram showing the effect of miRNAs on mRNA and protein abundance. Normal miRNA levels (A) lead to decreased mRNA and protein, by translation repression and mRNA degradation. The upregulation of miRNAs (B) (red arrow) leads to increased translation repression and mRNA degradation, and, consequently, decreased protein abundance and mRNA levels (green arrows). The downregulation of miRNAs (C) (green arrows) leads to reduced translation repression and mRNA degradation, and, consequently, increased protein and mRNA levels (red arrows). Figure created with BioRender.com.

C. rodentium induces an upregulation of mmu-miR-92a and a downregulation of mmu-miR-361. However, the effects of infection on these miRNA targets, *Foxo1* and *Sh2b1*, respectively, are unknown (Figure 6.4A). For the upregulated mmu-miR-92a-2-5p, we observed no change in the gene expression of *Foxo1* (Figure 6.4B). Interestingly, the protein abundance increased, which is opposite to what was expected. Similarly, the expression of *Sh2b1* was unaltered during infection. However, the protein level decreased despite the miRNA being downregulated (Figure 6.4B), suggesting that the expression of mRNA, miRNA targets, and protein abundance do not correlate.

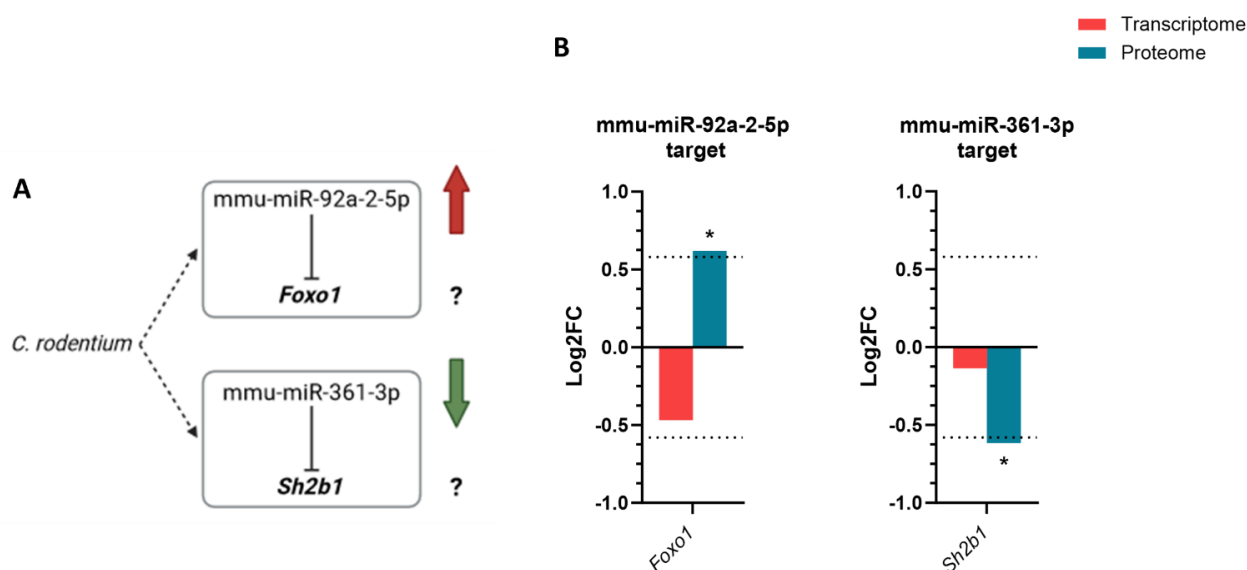


Figure 6.4. *C. rodentium* and miRNA targets.

(A) *C. rodentium* induces an upregulation (red arrow) of mmu-miR-92a and a downregulation of mmu-miR-361 (green arrow). However, the effects on these miRNA targets, *Foxo1* and *Sh2b1*, respectively, are unknown. Created with BioRender.com. (B) RNA levels for both targets remain unchanged during infection. Interestingly, *Foxo1* abundance is increased, and *Sh2b1* abundance is decreased during infection. **p*value < 0.05. Graph created with GraphPad Prism.

Next, we examined the predicted targets of these miRNAs using the bioinformatics tool miRDB (Chen and Wang 2020), identifying a range of potential target genes for both mmu-miR-92a-5p and mmu-miR-361-3p. A target score >80 was used to select the miRNA targets. For mmu-miR-92a-2-5p, we identified 211 predicted targets, with 143 present in the transcriptome and 88 in the proteome (Table 6.1). Interestingly, while 12 targets showed upregulation in the transcriptome, only 8 were upregulated in the proteome. Similarly, 9 targets showed decreased RNA levels, whereas 17 showed downregulation in the proteome. For mmu-miR-361-3p, 72 predicted targets were identified, with 45 present in the

transcriptome and 29 in the proteome (**Table 6.1**). Although 5 were upregulated in the transcriptome, only 1 showed upregulation at the proteome. Equally, 2 targets demonstrated downregulated RNA, while 3 showed downregulation in the proteome.

		mmu-miR-92a-2-5p	mmu-miR-361-3p
Total predicted targets		211	72
Targets in transcriptome		143	45
Targets in proteome		88	29
Transcriptome	Up	12	5
	Down	9	2
	Unchanged	122	38
Proteome	Up	8	1
	Down	17	3
	Unchanged	63	25

Table 6.1. Number of predicted targets for mmu-miR-92a-2-5p and mmu-miR-361-3p in transcriptome and proteome.

These disparities between the transcriptome and proteome highlight the complexity of miRNA-mediated regulation and emphasise the need for a comprehensive analysis of the expression patterns in both datasets.

For the upregulated miRNA mmu-miR-92a-2-5p, the anticipated results were decreased RNA and protein levels. However, among the differentially expressed genes identified in the transcriptome, 5 showed increased expression, opposite to what was expected, and their encoded proteins remained unchanged (Ptgfrn, Mlec, Mknk2, Hgf and Spry4) (**Figure 6.5A**). Similarly, 7 proteins showed increased abundance despite unchanged RNA levels (Spry4 was upregulated in both the transcriptome and proteome) (**Figure 6.5A**).

Regarding mmu-miR-361-3p, downregulated miRNA, the expected results were increased RNA and protein levels. Nevertheless, one differentially expressed gene identified in the transcriptome (*Scamp1*) exhibited reduced expression with unaltered protein abundance, contradicting expectations (**Figure 6.5B**). Conversely, out of the differentially expressed proteins also present in the transcriptome, 3 showed decreased abundance despite unchanged RNA levels (Vipr, Rbbp9 and Bcl113).

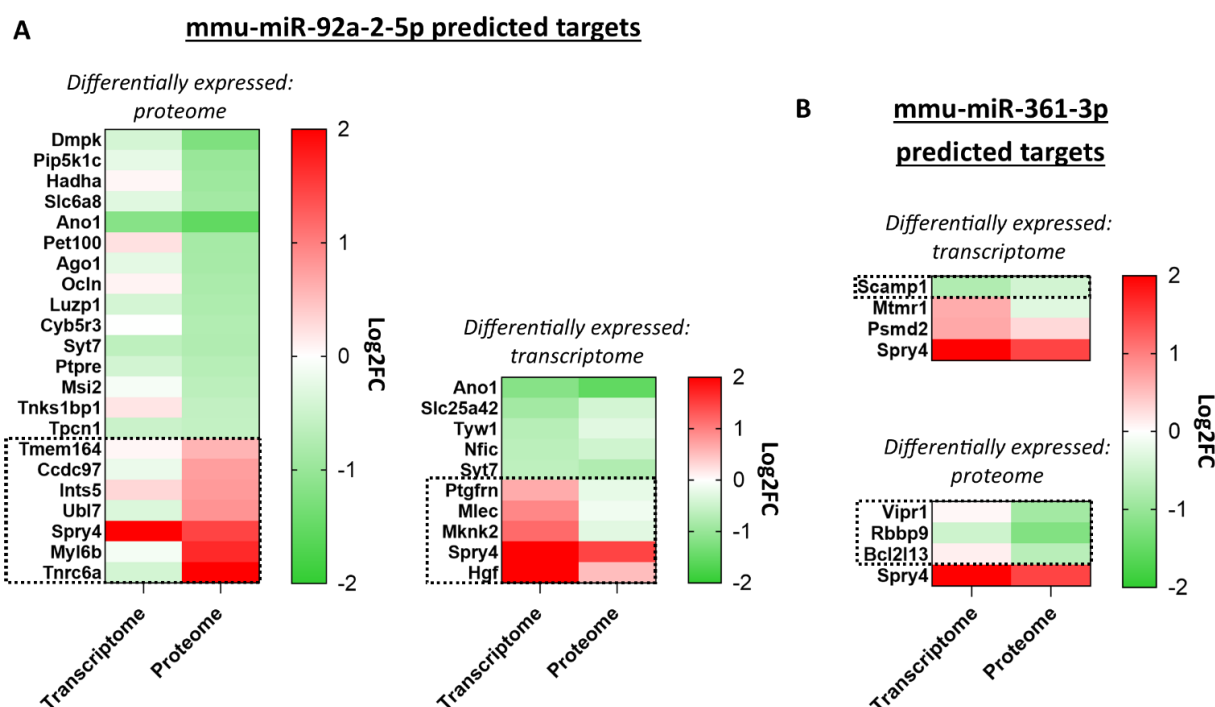


Figure 6.5. Integrated transcriptome and proteome heatmaps of predicted targets of mmu-miR-92a-2-5p and mmu-miR-361-3p.

(A) Heatmap shows that, despite increased miRNA levels, some target genes exhibit unchanged RNA levels with increased protein abundance (dashed boxes), while others show upregulated expression and unaltered protein abundance. (B) Conversely, despite decreased miRNA levels, certain target genes display downregulation expression with unaltered protein levels, while others show unchanged RNA levels despite decreased protein abundance (dashed boxes). Genes/proteins with a \log_2FC cutoff of ± 0.58 are considered changing. Heat maps generated with GraphPad Prism.

Our study revealed a disconnection between miRNA expression, gene expression and protein abundance during *C. rodentium* infection, emphasising the importance of integrating transcriptomic and proteomic data to understand gene regulation mechanisms. We next focus on studying the RISC, essential for miRNA-mediated gene silencing, during *C. rodentium* infection.

6.3.2 *C. rodentium* and the RNA-induced Silencing Complex (RISC).

We investigated the gene expression and protein abundance of key components involved in miRNA synthesis and the RNA-induced silencing complex (RISC) (Figure 6.6). The RISC is crucial for miRNA function, as it incorporates mature miRNAs and guides them to their target mRNAs, resulting in mRNA degradation or translational repression.

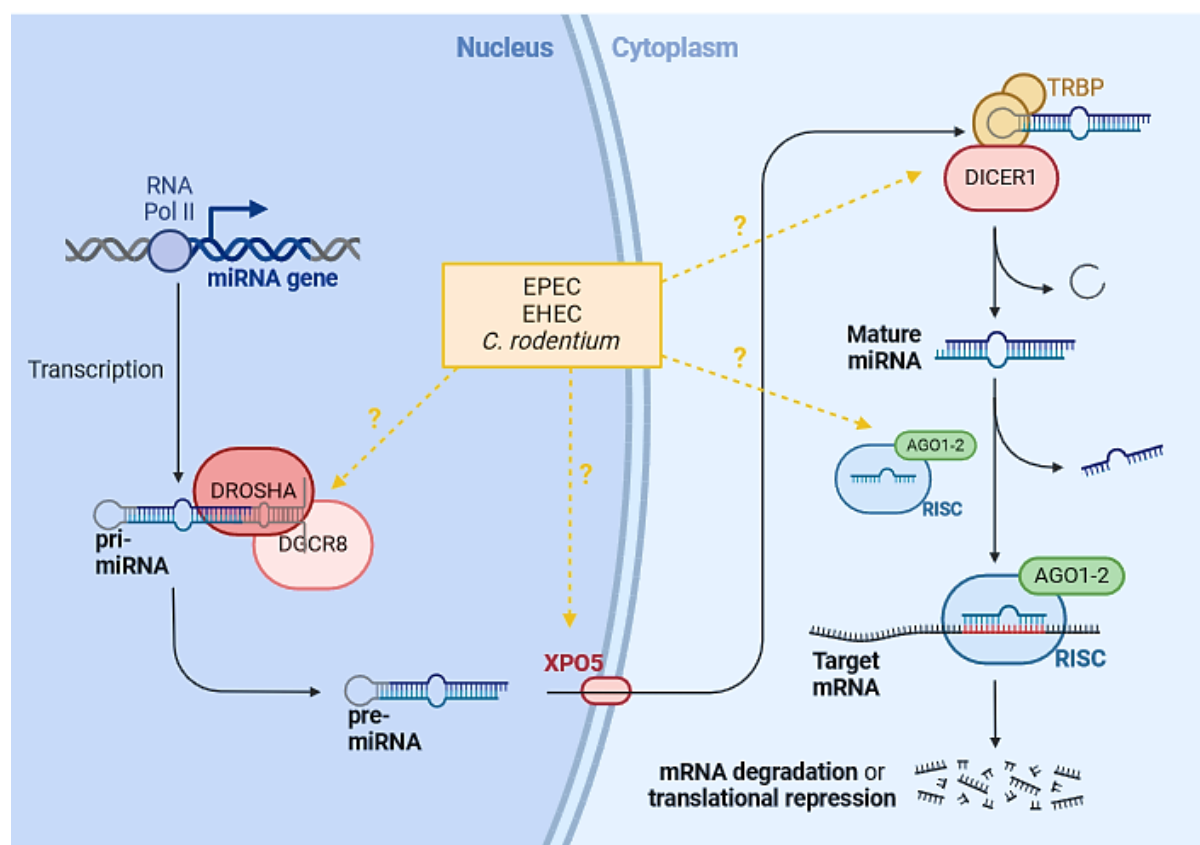


Figure 6.6. Overview of miRNA synthesis process.

miRNA synthesis begins in the nucleus with the transcription of pri-miRNA, which is processed into pre-miRNA by Drosha and Dgcr8 enzymes, and exported to the cytoplasm via exportin Xpo5. Once here, it is processed by Dicer and Trbp enzymes to the mature miRNA. The mature miRNA comprises two strains, the targeting strain, responsible for recognising the target mRNA and promoting protein repression, and the passenger strain. For its action, mature miRNA must be loaded into the RISC, composed of Argonaute proteins (Ago) 1 and 2. Once formed, the RISC binds to the target mRNA, leading to mRNA degradation or translation repression. Figure was created using BioRender.com.

Our analysis revealed that the RISC proteins Ago1 and Ago2 were significantly decreased in abundance (1.8 and 1.6, respectively) despite RNA levels remaining unchanged (**Figure 6.7**). Interestingly, the RNA expression and protein abundance of the proteins involved in miRNA synthesis (Drosha, Dgcr8, Xpo5, Tarbp2, Dicer1) did not vary during infection. These results suggest that the bacteria might target the RISC complex to modulate miRNA effects, potentially disrupting gene regulation and aiding in its pathogenicity.

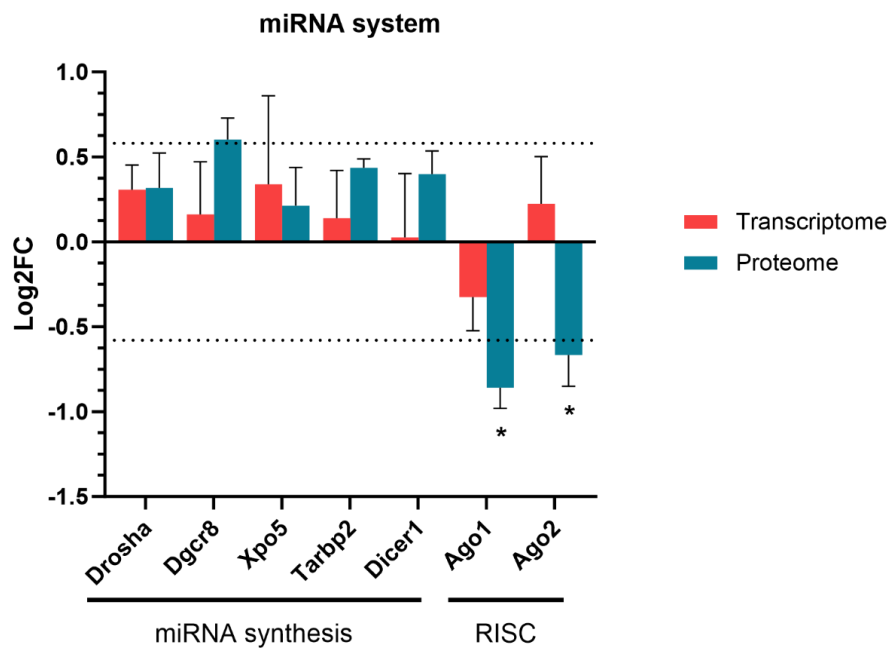


Figure 6.7. Gene expression and protein abundance of miRNA system proteins.

The graph shows the gene expression and the protein abundance of key proteins involved in the miRNA synthesis and RNA-induced silencing complex (RISC). The results show a decrease in the abundance of Ago1 and Ago2 proteins during infection, while the RNA level remains unaltered. The dotted lines represent the log2FC cutoff, ± 0.58 . * p -value < 0.05. Graph generated with GraphPad Prism.

6.3.3 *C. rodentium* and the Ago1 and Ago2 proteins.

The following section investigated the modulation of Ago1 and Ago2 by *C. rodentium* in vitro using two cell lines: HeLa cells (derived from human cervical tissue) and CMT93 cells (derived from mouse colon tissue). Western Blot analysis aimed to detect Ago1 and Ago2 expression in these cells. However, specific antibodies did not show conclusive results. Subsequently, permanent cell lines expressing Ago proteins with an HA tag (a tag added to the target protein to facilitate detection and purification) were developed.

To achieve this, plasmids expressing HA-Ago proteins (HA-Ago1 and HA-Ago2) were designed and expressed in HeLa cells and CMT93 cells. First, to confirm that protein expression and detection were successful, plasmids were transfected into the cells. Then, a viral transduction protocol, which allows for the integration of genes of interest into the genome of a target cell through a pseudoviral infection, was used to generate the permanent cell lines. Given the conservation of Ago1 and Ago2 sequences between humans and mice, the same plasmids were employed for both cell lines.

Western Blot analysis utilising antibodies against the HA tag confirmed the successful expression of these proteins in both cell types (**Figure 6.8A** and **B**). Results demonstrated the detection of Ago1 and Ago2 proteins at their expected molecular weight (approximately 97 kDa). Notably, a higher molecular weight band was observed for CMT93-HA-Ago1 (**Figure 6.8B**), approximately 120 kDa. This discrepancy could be attributed to the plasmid design, which includes an expressed puromycin-auto slice protein-HA-Ago1 construct. The delayed processing by the auto-slice protein may lead to the detection of HA linked to both puromycin and argonaute proteins, thereby increasing the band size by approximately 25 kDa.

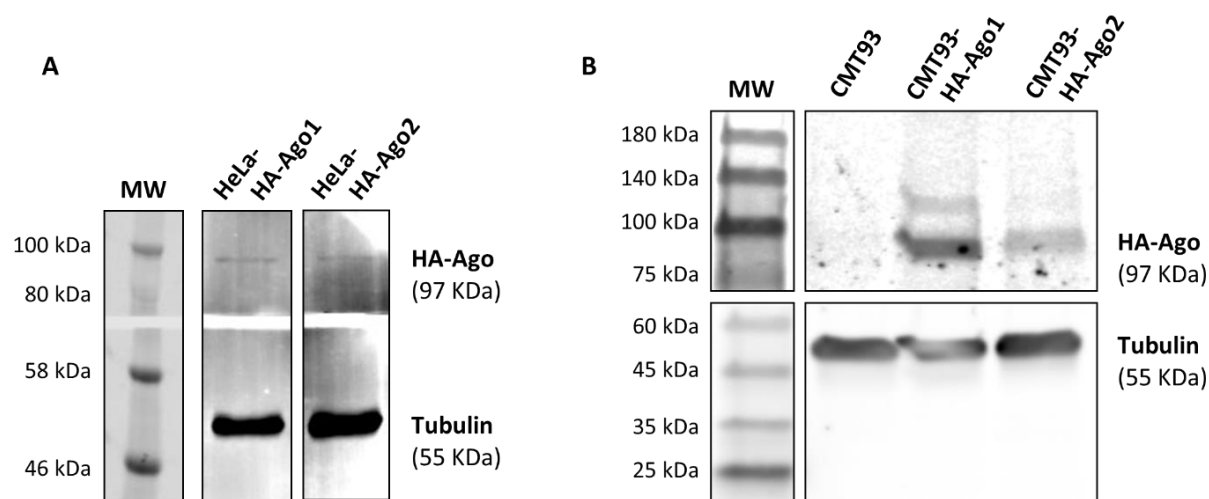


Figure 6.8. Western Blot result shows HA-Ago 1 and HA-Ago2 expression in HeLa and CMT93 cells. HeLa cells and CMT93 cells were cultured, lysed, and analysed by Western Blot. Results show that HA-Ago1 and HA-Ago2 are expressed in (A) HeLa cells and (B) CMT93 cells.

Since the bands detected in HeLa cells appeared less clear and lighter than those expressed in the CMT93 cells, we focused our investigation only on the latter. The next steps involved infecting cells with *C. rodentium* to investigate any changes in the abundance of the HA-Ago proteins. To determine the optimal infection time, preliminary tests were conducted where CMT93 cells were infected with *C. rodentium* for various durations: 1 hour and at 1-hour intervals up to 9 hours (i.e., 1 hour, 2 hours, 3 hours, etcetera). The samples were processed by immunostaining against actin to detect pedestal formation, which helped identify the optimal infection duration. Cells that demonstrated pedestal formation indicate that they have been successfully infected by *C. rodentium*. Based on these preliminary tests, a 6-hour infection period was chosen for subsequent experiments.

The following steps involved infecting cells with *C. rodentium* for 6 hours with two strains: *C. rodentium* wild type (CR WT) and a mutant lacking the EspA filament protein (CR Δ EspA). Without the filament, the bacteria's T3SS becomes non-functional, preventing the injection of effector proteins into the host cell. The rationale behind using this bacterial strain is to investigate whether the T3SS effector proteins are responsible for the observed changes in Ago1 and Ago2 abundance in vivo.

The results indicate that HA-Ago1 abundance decreases during infection with *C. rodentium* WT and returns to normal levels when cells are infected with *C. rodentium* Δ EspA (Figure 6.9A and B). In contrast, the results show no significant change in the abundance of

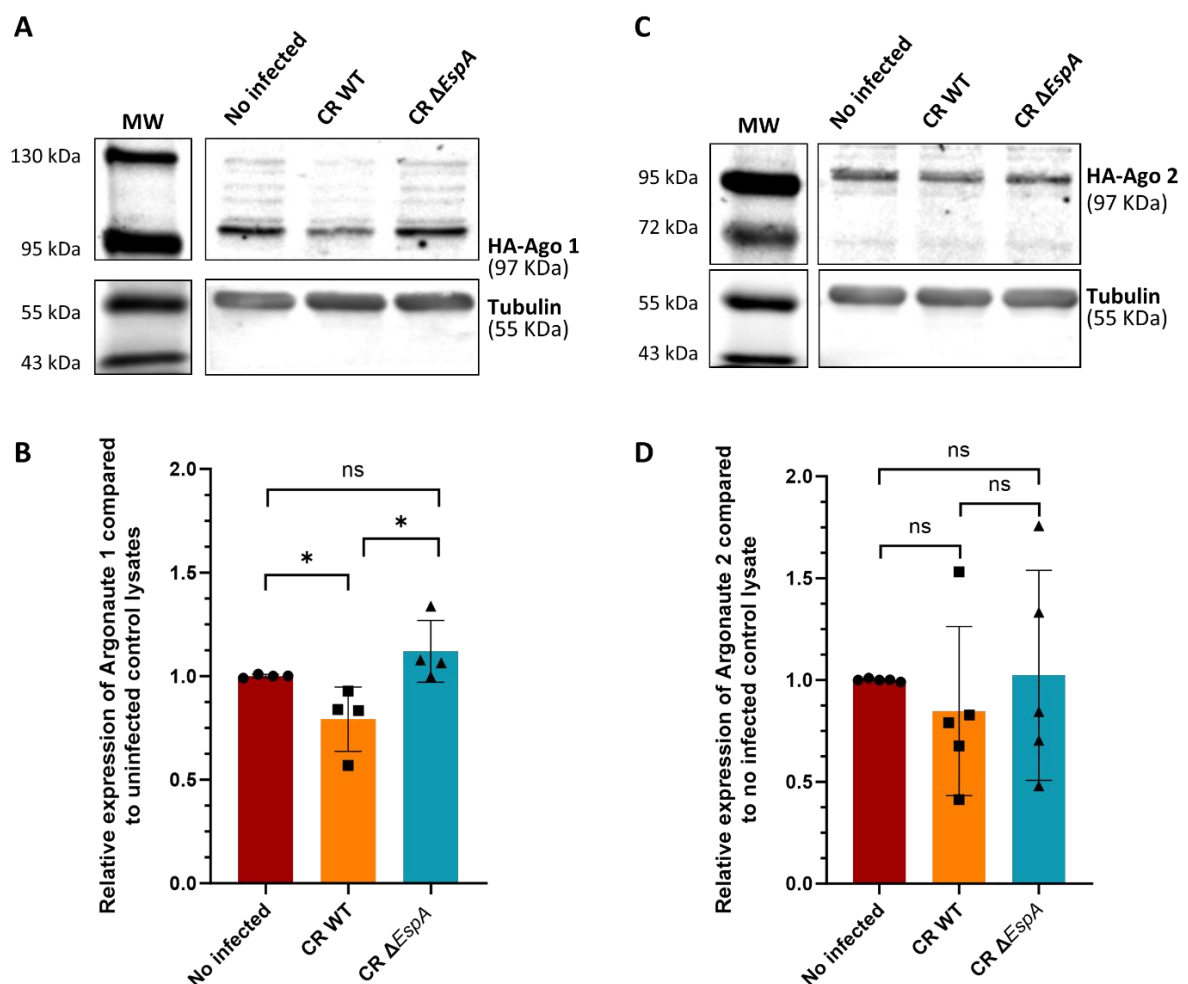


Figure 6.9. Western Blot analysis of HA-Ago1/Ago2 levels in CMT93 cells after 6h infection. (A-B) HA-Ago1 levels decrease during CR WT infection and return to baseline with CR Δ EspA infection. (C-D) HA-Ago2 levels remain unchanged during CR WT and CR Δ EspA infections. Representative images are shown. Data represent mean \pm SD from 4-5 independent experiments. * $p < 0.05$; ns = non-significant (Mann-Whitney test, unpaired, non-parametric, two-tailed p Value). Graphs generated with GraphPad Prism.

HA-Ago2 during infection with either bacterial strain (**Figure 6.9C** and D). This observation suggests that when there is a functional T3SS, the effector proteins might target the Ago1 protein but not Ago2.

Immunostaining of infected cells was also conducted by a colleague to determine the cellular localisation of Ago proteins and to assess any potential changes in their localisation during infection. However, the results were inconclusive and did not confirm the expected localisation patterns.

In conclusion, these findings suggest that the T3SS of *C. rodentium* may play a role in modulating the abundance of Ago1 protein, but not Ago2, during infection. Further investigation into the specific mechanisms underlying this mechanism is needed to elucidate the precise interaction between *C. rodentium* and host cell regulatory pathways.

6.4 Discussion.

This chapter investigated the effects of *C. rodentium* infection on the host miRNA system, particularly focusing on how the infection impacts miRNA targets and the overall regulatory system by analysing both transcriptome and proteome data. Our study revealed a disconnect between miRNA expression, gene expression and protein abundance of miRNA targets during *C. rodentium* infection (see **Figure 6.4** and **Figure 6.5**). This highlights the complexity of gene regulation and emphasises the importance of integrating transcriptomic and proteomic data to understand gene regulation mechanisms.

6.4.1 [miRNA system and *C. rodentium*](#).

Our study revealed that changes in miRNA levels do not always correlate with alterations in their target mRNA or protein levels. For instance, as illustrated in **Figure 6.4**, despite the upregulation of mmu-miR-92a-2-5p, the expected downregulation of its target Foxo1 did not occur. Instead, Foxo1 protein levels increased during infection, despite unchanged RNA levels. Foxo1 regulates mucus secretion by goblet cells in the intestinal epithelium, and its loss can compromise intestinal barrier integrity by reducing the mucus layer, enhancing susceptibility to gut inflammation and infection (Bergstrom et al. 2010; Chen et al. 2021). During *C. rodentium* infection, goblet cells decrease and the mucus layer is adversely affected (Chan et al. 2013; Silberger et al. 2017). The increased abundance of Foxo1 protein observed could reflect a compensatory response by colonic cells to counteract this effect and restore mucus production as a defensive measure to maintain intestinal barrier integrity and combat the infection.

Additionally, the role of miR-155 is notable, as miR-155 deficient mice are more susceptible to *C. rodentium* infection (Clare et al. 2013). This miRNA is crucial for regulating immune responses, and its deficiency highlights the importance of miRNAs in host defences against the pathogen. *C. rodentium* might exploit these miRNA disruptions to manipulate host immune responses and enhance its survival. By modulating the expression and activity of host miRNAs, *C. rodentium* might create a more beneficial environment, potentially by affecting key immune pathways and cellular processes crucial for its pathogenicity.

Furthermore, the upregulation of the miR-17-92 cluster, which is linked to colorectal cancer, is observed during *C. rodentium* infection (**Figure 6.2**). This cluster includes miR-17, miR-18a,

miR-19a, miR-19b, miR-20a, and miR-92a (Al-Nakhle 2024). Specifically, miR-19 enhances cell proliferation by stimulating EGFR (epidermal growth factor receptor) (Michas et al. 2023; Al-Nakhle 2024), which shows a 2-fold increase at the transcript level and a 1.5-fold increase at the protein level during infection. This suggests that EGFR may contribute to cell proliferation and crypt hyperplasia during infection. Additionally, miR-92a targets BIM, a pro-apoptotic protein. The upregulation of miR-92a typically leads to BIM downregulation and reduced apoptosis. Although the decrease in BIM was not statistically significant in our results, this pattern of reduced apoptosis is consistent with observations in infections with uropathogenic *E. coli* (Zhang et al. 2016), indicating a potentially similar mechanism in *C. rodentium* infection.

In summary, the upregulation of the miR-17-92 cluster appears to play a crucial role in *C. rodentium* pathogenesis, promoting cell proliferation and suppressing apoptosis, which contributes to the development of hyperplasia. The modulation of miRNA expression by *C. rodentium* likely enhances its ability to induce cellular changes and evade host defences, highlighting the complex interactions between the pathogen and host.

6.4.2 [Argonaute proteins and *C. rodentium*.](#)

Our findings also revealed a reduction in the abundance of the RISC proteins Ago1 and Ago2 during *in vivo* infection, observed at the proteome level but not at the transcriptome level (**Figure 6.7**). *In vitro* experiments with infected CMT93 cells revealed that HA-Ago1 levels decreased during infection with the WT but not with the T3SS-deficient mutant. This suggests that T3SS effector proteins are essential for this regulation, highlighting the role of T3SS in modulating host miRNA by targeting Ago1.

Similar mechanisms are seen in other pathogens, such as *H. pylori*, which utilises a type 4 secretion system (T4SS) to interfere with host signalling pathways. Belair et al. (2011) demonstrated that *H. pylori* infection represses miR-371-372-373 expression in human cell lines by translocating its virulence factor CagA. Other bacteria like *Legionella pneumophila* and *Salmonella* also manipulate host miRNA systems through various mechanisms. *L. pneumophila* releases extracellular vesicles containing RNA that target specific mRNAs, mimicking eukaryotic miRNAs (Sahr et al. 2022). Similarly, *Salmonella* produces miRNA-like functional RNA to facilitate intracellular survival (Gu et al. 2017). These examples suggest

that *C. rodentium* might use a similar strategy, potentially injecting effector proteins or miRNA-like RNA into host cells to modulate Argonaute proteins and miRNA regulation.

To explore this further, future investigations could involve studying CMT93 cells expressing HA-Ago1 along with mutants lacking individual T3SS genes. This approach could help identify the specific effector proteins responsible for the reduced abundance of Ago1 and elucidate the mechanisms by which *C. rodentium* modulates host miRNA and Argonaute proteins during infection.

Interestingly, HA-Ago2 levels remained unchanged in infected CMT93 cells despite its reduced abundance in vivo. This discrepancy suggests that different regulatory mechanisms may be at play in regulating Ago2 during in vivo infection. The in vivo environment includes various cell types and complex interactions not fully replicated in vitro with CMT93 cells. Factors such as immune responses, cytokine signalling, and interactions with other cell types and microbiota might influence protein stability and abundance differently than in vitro conditions. Additionally, Ago2 undergoes various post-translational modifications, such as phosphorylation, ubiquitination, and degradation by the proteasome (Adams et al. 2009; Smibert et al. 2013; Müller et al. 2020), which can affect protein stability and localisation. In vivo infection might enhance these modifications, leading to decreased Ago2 levels, whereas the in vitro conditions might not induce the same level of post-translational modifications, resulting in stable Ago2 levels.

Interestingly, RNA levels of EGFR, a transmembrane glycoprotein stimulated by mmu-miR-92a (upregulated during *C. rodentium* infection), are increased during infection. This protein targets Ago2 in cancer, promoting its phosphorylation (Lin and Gregory 2015), which may change its localisation within the cell, increasing the difficulty of its detection with proteomic analysis, and explaining the reduced abundance detected in vivo. Moreover, ZSWIM8, an E3 ubiquitin ligase that targets Ago proteins (Shi et al. 2020), could also play a role in Ago protein degradation during infection. While its levels do not change in the transcriptome and proteome of infected enterocytes, it could mediate Ago degradation during *C. rodentium* infection.

Our study underscores the significant role of T3SS in regulating Ago1 during *C. rodentium* infection and highlights the potential involvement of post-translational modifications and

other cellular factors in modulating Ago2 levels. Further research is needed to identify the specific mechanisms and effector proteins involved in modulating Ago proteins during *C. rodentium* infection.

6.5 Conclusions.

The main conclusions following the investigation of miRNA modulation during infection were as follows:

- There is a notable disconnect between miRNA expression, gene expression and protein abundance of targets during *C. rodentium* infection.
- The abundance of Argonaute proteins 1 and 2 decreases during infection in vivo despite RNA levels being unaltered, suggesting post-translational processes are enhanced during infection.
- The type three secretion system plays an important role in inducing a reduction of Ago1 during in vitro infection. However, this effect was not observed for Ago2, indicating that the in vitro conditions may not fully replicate the in vivo post-translational modifications, thereby maintaining stable Ago2 levels.
- These results emphasise the importance of integrating transcriptomic and proteomic analysis to understand gene regulation mechanisms during infection.

These findings highlight the complex interplay between *C. rodentium* and the host miRNA system, revealing potential strategies employed by the pathogen to manipulate host gene regulation. The observed disconnect between miRNA levels and their target mRNA/protein abundance highlights the need for comprehensive multi-omics approaches to fully decipher the regulatory networks during infection.

CHAPTER 7: General conclusions and future directions

7 CHAPTER 7: General conclusions and future directions.

7.1 General conclusions.

This PhD aimed to elucidate the molecular responses of IECs to *C. rodentium* infection. The infection induces significant changes in the host IECs, including antimicrobial response, alterations in the colonic microbiome, changes in cellular metabolism, and modifications in the miRNome profile. Through transcriptomic and proteomic analyses, complex regulatory mechanisms and pathways activated during infection were revealed, highlighting the interplay between RNA, protein, post-transcriptional processes and post-translational modifications (PTM).

The key conclusions from this PhD study are summarised as follows:

1) Characterisation of the transcriptome profile of infected cells (Chapter 3): The transcriptome analysis elucidated the dynamics of bacteria-host interactions, confirming the involvement of well-known pathways related to immune response, inflammation, and metabolism. Additionally, it identified previously unknown altered pathways during infection, such as the Pentose Phosphate Pathway (PPP) and the ubiquitin-proteasome system (UPS). These findings confirm that *C. rodentium* targets multiple host pathways for its pathogenicity. Some UPS genes with increased expression during infection promote tumour growth, potentially contributing to colonic crypt hyperplasia, while other genes with unchanged expression play an important role in host defence. The dual function of the UPS emphasises its complex role in balancing pathogen support while ensuring host protection. The PPP is a metabolic pathway that converts glucose-6-phosphate into ribose-5-phosphate and generates NADPH, both of which are crucial for nucleotide synthesis and cellular proliferation. Its increased activity supports the rapid cell division and DNA repair needed during *C. rodentium* infection, providing the necessary resources for IECs to adapt to the infection-induced proliferation and crypt hyperplasia.

Additionally, the use of transcriptome analysis offered the advantage of identifying secreted proteins which could have been challenging to detect with other traditional

proteomic techniques, underscoring the importance of using multiple analytical methods.

2) Comparative analysis of transcriptome and proteome of infected epithelial cells

(Chapter 4): The comparative analysis revealed a poor correlation between gene expression and protein levels, highlighting the significant role of post-transcriptional and post-translational regulation in response to *C. rodentium* infection. While transcriptomic analysis indicated changes in molecules associated with the proteasome complex, these changes did not correspond with alterations in the proteome. This disconnection highlights the complexity of post-transcriptional and post-translational control, where increased gene expression does not necessarily lead to a proportional increase in protein abundance. It remains unclear whether this lack of correlation reflects a host strategy to modulate proteasome activity differently or a bacterial strategy to influence host protein degradation processes.

The integration of transcriptomics and proteomics approaches not only confirmed known pathways altered by *C. rodentium* infection but also demonstrated that the bacteria actively degraded microvilli and mitochondria in infected IECs. Additionally, transcriptomics detected a broader range of genes and unique pathways, such as prostaglandin metabolism, that proteomics alone could miss. This reinforces the value of employing both omics approaches to achieve a thorough understanding of the molecular changes and their implications during infection.

3) Prostaglandin biosynthesis regulation (Chapter 5): Transcriptome pathway analysis

showed that prostaglandin biosynthesis was affected during infection, suggesting a shift towards a pro-inflammatory environment and the stabilisation of pro-inflammatory prostaglandins. While the transcriptomic data showed clear alterations in prostaglandin biosynthesis, the proteomic profile did not reflect significant changes and failed to detect relevant enzymes. This discrepancy highlights the limitations of relying solely on proteomics to understand the full range of metabolic changes and underscores the importance of using multiple analytical techniques. The integration of transcriptomics and proteomics provided a comprehensive overview of the infection, revealing

pathways that may not have been identified with a single technique, ensuring a fuller understanding of the underlying molecular dynamics.

Furthermore, the results did not support the hypothesis that reducing prostaglandin synthesis with aspirin would mitigate inflammation and colonic crypt hyperplasia. The lack of significant changes in infection pathogenicity with low-dose aspirin treatment suggested that prostaglandins may not be central to the inflammation pathogenesis of *C. rodentium*, or that the inhibition was insufficient to impact these processes. While aspirin did not affect colonisation, colonic crypt hyperplasia, or lipocalin-2 production, it did promote weight loss in infected mice, likely due to potential side effects like gastrointestinal irritation or microbiota disruption. These findings suggest that the relationship between prostaglandin biosynthesis and *C. rodentium* infection is more complex than initially thought and may involve alternative pathways and mechanisms.

- 4) Regulation of RNA-induced silencing complex (RISC) (Chapter 6):** The investigation of RISC regulation during infection revealed a significant discrepancy between miRNA expression, target gene expression, and the corresponding protein levels. The findings demonstrate that the relationship between miRNA levels and their target mRNAs or proteins is complex and not necessarily linear. Alterations in miRNA expression during infection do not always result in the anticipated changes in the expression of their target mRNAs or proteins, highlighting the intricate regulatory mechanisms at play.

A key finding is that the levels of Argonaute proteins, which are essential for miRNA function, decrease during *C. rodentium* infection, even though the corresponding RNA levels remain the same. This suggests that the pathogen might be using post-translational modifications to affect these proteins, potentially disrupting miRNA regulation and influencing host cell functions. Additionally, the T3SS of *C. rodentium* plays a crucial role in reducing the levels of one of these Argonaute proteins, Ago1, in vitro. The T3SS seems to help the pathogen interfere with miRNA pathways by injecting proteins that affect Argonaute levels, potentially manipulating host gene regulation to its advantage.

7.2 Overall discussion.

This PhD study has provided significant insights into the molecular responses of IECs to *C. rodentium* infection, revealing how this pathogen manipulates critical cellular pathways to its advantage. Among the mechanisms discovered are the UPS, PPP, prostaglandin biosynthesis, and the miRNA system. These findings reflect larger strategies employed by various pathogens, illustrating the complexity and interconnection of host-pathogen interactions.

7.2.1 Manipulation of the Ubiquitin-Proteasome System

C. rodentium manipulates the UPS likely to promote its survival and contribute to colonic crypt hyperplasia, a tactic mirrored by other pathogens. The UPS, essential for protein degradation and regulation, is a common target for pathogens which frequently exploit PTMs to subvert host defences. For instance, Human Papillomavirus (HPV) exploits the UPS to degrade the tumour suppressor protein p53, facilitating viral persistence and oncogenesis (Scheffner et al. 1990). Similarly, *Salmonella enterica* manipulates the UPS via the delivery of several bacterial effectors to aid in immune evasion (Wang et al. 2018). In addition to ubiquitination, other PTMs, such as phosphorylation and acetylation, are also targeted by pathogens to control host cell functions. Human Cytomegalovirus (HCMV) and Human Immunodeficiency Virus (HIV) manipulate host phosphorylation pathways to evade immune detection and enhance viral replication (Vossen et al. 2002; Johnson et al. 2022), while *L. monocytogenes* modulate host histone acetylation to alter gene expression and facilitate bacterial survival within cells (Hamon et al. 2007).

These examples emphasise the complexity with which pathogens subvert PTMs to hijack host cellular machinery, promoting their survival, replication, and pathogenesis. This suggests that the UPS manipulation by *C. rodentium* is likely to evade immune defences and promote cell proliferation, mirroring a broader strategy seen across pathogens to promote pathogen survival and pathogenesis.

7.2.2 Exploitation of the Pentose Phosphate Pathway.

The upregulation of the PPP in IEC of mice during *C. rodentium* infection is also a strategy observed across various pathogens, including intracellular bacteria such as *Mycobacterium tuberculosis* and *Chlamydia trachomatis*. While *M. tuberculosis* enhances PPP activity in

infected macrophages likely to induce the antimycobacterial metabolite itaconate (Chandra et al. 2022), in *C. trachomatis*-infected cells glucose is directed through the PPP to generate sufficient NADPH, which is essential for the increased lipid biosynthesis required for the bacterium's growth and development within the host cell (Eisenreich et al. 2013).

Although the effects of altering the PPP of hosts vary across infections, these similarities suggest that the PPP is a crucial metabolic pathway commonly exploited by bacterial pathogens to meet their energy and biosynthetic needs in the infected cell. In *C. rodentium* infection, the upregulation of the PPP likely has a similar purpose, supporting survival in proliferating cells by meeting the metabolic demands of the infection.

7.2.3 Prostaglandins in pathogen-mediated immune modulation.

Prostaglandin biosynthesis is a pathway significantly altered during *C. rodentium* infection and similar modulation of prostaglandin profiles is observed in infections by other pathogens. For example, the Influenza virus upregulates PGE₂ to suppress immune responses, thereby facilitating viral persistence (Coulombe et al. 2014). Similarly, *H. pylori* modulates PGE₂ levels in the context of gastric cancer by upregulating Cox2, which increases PGE₂ synthesis, and downregulating 15-PGDH, which reduces PGE₂ degradation. This mechanism is comparable to our findings with *C. rodentium*. In *H. pylori* infection, the resulting elevation of PGE₂ contributes to the development of gastric cancer by promoting inflammation and aiding in bacterial survival (Zhao et al. 2017). While *C. rodentium* infection does not induce cancer, it induces cell proliferation. Thereby, it can be speculated that the increased PGE₂ biosynthesis observed during infection helps in bacterial persistence by promoting inflammation, similar to the observed effects during *H. pylori* infection.

The ability of diverse pathogens to manipulate prostaglandin pathways highlights the role of PGE₂ in immune regulation and pathogenesis. While these studies suggest that prostaglandins may be critical for inflammation and cell proliferation during *C. rodentium* infection, the limited efficacy of Cox inhibitors in altering *C. rodentium* outcomes suggests that these molecules are not the unique modulators of the immune response, suggesting the involvement of multiple alternative immune pathways.

7.2.4 miRNA system in host-pathogen interactions.

The miRNA system, which plays a crucial role in gene regulation, is another target for *C. rodentium* and other diverse pathogens. For instance, HIV interacts with a wide range of host miRNAs, modulating their activity to either suppress or maintain viral replication and contributing to viral latency (Rashid et al. 2023). Notably, miR-34a targets three host proteins essential for HIV-1 pathogenesis, highlighting its potential for therapeutic intervention (Rashid et al. 2023). Similarly, *H. pylori* manipulates host miRNA expression by upregulating pro-inflammatory miRNAs, such as miR-155, while downregulating tumour-suppressive miRNAs, which promotes inflammation and contributes to the progression of chronic gastritis and gastric cancer (Xu et al. 2024).

Additionally, the parasite *Trypanosoma cruzi*, the causative agent of Chagas disease, upregulates inflammatory miRNA such as miR-21, miR-146a, and miR-155 in both acutely and chronically infected mice. This upregulation contributes to the progression of the disease by promoting inflammation and immune system dysregulation (Ballinas-Verdugo et al. 2021; Rego et al. 2023).

These examples highlight that the manipulation of host miRNA expression is a strategy that many pathogens use to modulate immune responses and promote inflammation. In *C. rodentium*'s case, targeting the miRNA system potentially has a similar role, contributing to altering the immune signalling pathways, sustaining infection and improving bacterial survival.

7.3 Future directions.

This study provides a comprehensive analysis of molecular dynamics involved in *C. rodentium* infection. Given the complexity of host-pathogen interactions disclosed, future research should build on these findings to deepen our understanding of these interactions. The intricate interplay between transcriptomic and proteomic changes highlights the need for a multifaceted approach to investigating infection dynamics. Integrating additional omics techniques is crucial in advancing our knowledge of host-pathogen interactions and developing targeted therapeutic strategies.

To achieve these goals, future research should focus on the following areas:

- 1) Investigate post-transcriptional and post-translational regulation:** Chapters 4 and 6 revealed discrepancies between gene expression and protein levels, as well as complex interactions between miRNAs, their target RNAs, and corresponding proteins. Future research should focus on understanding the precise mechanisms behind these post-transcriptional and post-translational processes. Investigating how *C. rodentium* manipulates these pathways, including miRNAs, phosphorylation, ubiquitination, and acetylation processes, could provide critical insights into protein dynamics and regulation during infection, explaining the observed discrepancies between transcriptome and proteome data. Understanding how *C. rodentium* manipulates these processes will be crucial for understanding their roles in protein stability and function, and will be critical in deciphering their role in pathogenesis, immune evasion and host cell manipulation.
- 2) Integrate metabolomics approaches to complement transcriptomics and proteomics:** The use of transcriptomics and proteomics in this research has helped understand the molecular responses and metabolic changes of IEC to *C. rodentium* infection, however, certain gaps remain. The addition of metabolomics could fill these gaps by analysing metabolites and metabolic pathways that are altered during infection. For example, exploring the PPP and prostaglandin biosynthesis could reveal how changes in cellular metabolism contribute to host-pathogen interactions and how these changes influence disease pathology.
- 3) Conduct long-term studies on aspirin:** Given the minimal impact of low-dose aspirin on *C. rodentium* infection outcomes, long-term studies with different administration routes and varying dosages could provide a more complete understanding of their impact. Those studies should investigate the prolonged effects of aspirin on inflammation, infection dynamics, and host recovery.
- 4) Evaluate different therapeutic strategies and dosages:** In addition to the Cox inhibitor aspirin, future studies should investigate the efficacy of higher doses or alternative administration routes of different Cox inhibitors to better understand their therapeutic potential and limitations. Evaluating different delivery methods or formulations could

reveal more effective ways to modulate prostaglandin levels and improve therapeutic outcomes.

- 5) Explore alternative pathways:** The role of prostaglandins in *C. rodentium* pathogenesis may not be as central as initially hypothesised. Investigating alternative immune-modulating pathways that contribute to inflammation and hyperplasia during infection could provide new insights into how the pathogen manipulates the host environment. Discovering these non-prostaglandin-related pathways could lead to new therapeutic targets and strategies to manage infections caused by *C. rodentium* and other similar pathogens.
- 6) Mutant studies to understand the role of T3SS effectors in miRNA regulation:** The role of the T3SS in modulating Argonaute proteins, highlighted in Chapter 6, questions about the specific bacterial effectors responsible for these interactions. Conducting mutant studies with *C. rodentium* strains lacking specific T3SS effectors could help identify which bacterial effectors are responsible for manipulating the host miRNA machinery. Comparing infection outcomes and Argonaute protein status in wild type versus mutant strains should reveal key effectors involved in miRNA regulation.

These comprehensive approaches will be crucial in deciphering the complex mechanisms underlying host-pathogen interactions. This could help identify new targets for therapeutic intervention, ultimately improving treatment outcomes not only for *C. rodentium* infections but also for managing other bacterial pathogens that exploit similar infection strategies, such as EPEC and EHEC.

7.4 Final summary.

In summary, this study has significantly advanced our understanding of the molecular responses of intestinal epithelial cells to *C. rodentium* infection. By integrating transcriptomic and proteomic analyses, we have uncovered complex regulatory mechanisms and pathways involved in infection dynamics. The findings highlight the importance of post-transcriptional and post-translational regulation, particularly the role of miRNAs and Argonaute proteins. The study also underscores the value of using a multi-omics approach to fully understand the complexities of host-pathogen interactions. Future research building on these insights will be essential for developing more effective therapeutic strategies to combat infections caused by AE pathogens.

References

REFERENCES

- Adams, B. D., Claffey, K. P. and White, B. A. 2009. Argonaute-2 expression is regulated by epidermal growth factor receptor and mitogen-activated protein kinase signaling and correlates with a transformed phenotype in breast cancer cells. *Endocrinology* 150(1), pp. 14-23. doi: 10.1210/en.2008-0984
- Agard, M., Asakrah, S. and Morici, L. 2013. PGE2 suppression of innate immunity during mucosal bacterial infection. *Frontiers in Cellular and Infection Microbiology* 3, doi: 10.3389/fcimb.2013.00045
- Ahmed, I., Chandrakesan, P., Tawfik, O., Xia, L., Anant, S. and Umar, S. 2012. Critical Roles of Notch and Wnt/ β -Catenin Pathways in the Regulation of Hyperplasia and/or Colitis in Response to Bacterial Infection. *Infection and Immunity* 80(9), pp. 3107-3121. doi: 10.1128/iai.00236-12
- Al-Amrani, S., Al-Jabri, Z., Al-Zaabi, A., Alshekaili, J. and Al-Khabori, M. 2021. Proteomics: Concepts and applications in human medicine. *World J Biol Chem* 12(5), pp. 57-69. doi: 10.4331/wjbc.v12.i5.57
- Al-Nakhle, H. H. 2024. Unraveling the Multifaceted Role of the miR-17-92 Cluster in Colorectal Cancer: From Mechanisms to Biomarker Potential. *Current Issues in Molecular Biology* 46(3), pp. 1832-1850. doi: 10.3390/cimb46030120
- Allaj, V., Guo, C. and Nie, D. 2013. Non-steroid anti-inflammatory drugs, prostaglandins, and cancer. *Cell & Bioscience* 3(1), p. 8. doi: 10.1186/2045-3701-3-8
- Aoki, T. and Narumiya, S. 2012. Prostaglandins and chronic inflammation. *Trends in Pharmacological Sciences* 33(6), pp. 304-311. doi: 10.1016/j.tips.2012.02.004
- Armstrong, G. L., Hollingsworth, J. and Morris, J. G. 1996. Emerging Foodborne Pathogens: *Escherichia coli* O157:H7 as a Model of Entry of a New Pathogen into the Food Supply of the Developed World. *Epidemiologic Reviews* 18(1), pp. 29-51. doi: 10.1093/oxfordjournals.epirev.a017914
- Aslam, B., Basit, M., Nisar, M. A., Khurshid, M. and Rasool, M. H. 2017. Proteomics: Technologies and Their Applications. *J Chromatogr Sci* 55(2), pp. 182-196. doi: 10.1093/chromsci/bmw167
- Babbin, B. A. et al. 2008. Annexin A1 regulates intestinal mucosal injury, inflammation, and repair. *J Immunol* 181(7), pp. 5035-5044. doi: 10.4049/jimmunol.181.7.5035
- Backlund, M. G. et al. 2005. 15-Hydroxyprostaglandin dehydrogenase is down-regulated in colorectal cancer. *J Biol Chem* 280(5), pp. 3217-3223. doi: 10.1074/jbc.M411221200

- Ballinas-Verdugo, M. A. et al. 2021. Circulating miR-146a as a possible candidate biomarker in the indeterminate phase of Chagas disease. *Biological Research* 54(1), doi: 10.1186/s40659-021-00345-3
- Bard, J. A. M., Goodall, E. A., Greene, E. R., Jonsson, E., Dong, K. C. and Martin, A. 2018. Structure and Function of the 26S Proteasome. *Annual Review of Biochemistry* 87(1), pp. 697-724. doi: 10.1146/annurev-biochem-062917-011931
- Barker, N., van de Wetering, M. and Clevers, H. 2008. The intestinal stem cell. *Genes Dev* 22(14), pp. 1856-1864. doi: 10.1101/gad.1674008
- Bartel, D. P. 2004. MicroRNAs: Genomics, Biogenesis, Mechanism, and Function. *Cell* 116(2), pp. 281-297. doi: 10.1016/s0092-8674(04)00045-5
- Belair, C., Baud, J., Chabas, S., Sharma, C. M., Vogel, J., Staedel, C. and Darfeuille, F. 2011. *Helicobacter pylori* interferes with an embryonic stem cell micro RNA cluster to block cell cycle progression. *Silence* 2(1), p. 7. doi: 10.1186/1758-907x-2-7
- Berger, C. N., Crepin, V. F., Baruch, K., Mousnier, A., Rosenshine, I. and Frankel, G. 2012. EspZ of enteropathogenic and enterohemorrhagic *Escherichia coli* regulates type III secretion system protein translocation. *mBio* 3(5), doi: 10.1128/mBio.00317-12
- Berger, C. N., Crepin, V. F., Jepson, M. A., Arbeloa, A. and Frankel, G. 2009. The mechanisms used by enteropathogenic *Escherichia coli* to control filopodia dynamics. *Cellular Microbiology* 11(2), pp. 309-322. doi: 10.1111/j.1462-5822.2008.01254.x
- Berger, C. N. et al. 2017. *Citrobacter rodentium* Subverts ATP Flux and Cholesterol Homeostasis in Intestinal Epithelial Cells In Vivo. *Cell Metabolism* 26(5), pp. 738-752.e736. doi: 10.1016/j.cmet.2017.09.003
- Berger, C. N. et al. 2018. The *Citrobacter rodentium* type III secretion system effector EspO affects mucosal damage repair and antimicrobial responses. *PLOS Pathogens* 14(10), p. e1007406. doi: 10.1371/journal.ppat.1007406
- Bergstrom, K. S. et al. 2008. Modulation of intestinal goblet cell function during infection by an attaching and effacing bacterial pathogen. *Infect Immun* 76(2), pp. 796-811. doi: 10.1128/IAI.00093-07
- Bergstrom, K. S. B. et al. 2010. Muc2 Protects against Lethal Infectious Colitis by Disassociating Pathogenic and Commensal Bacteria from the Colonic Mucosa. *PLOS Pathogens* 6(5), p. e1000902. doi: 10.1371/journal.ppat.1000902
- Bhavsar, A. P., Guttman, J. A. and Finlay, B. B. 2007. Manipulation of host-cell pathways by bacterial pathogens. *Nature* 449(7164), pp. 827-834. doi: 10.1038/nature06247

- Bindea, G. et al. 2009. ClueGO: a Cytoscape plug-in to decipher functionally grouped gene ontology and pathway annotation networks. *Bioinformatics* 25(8), pp. 1091-1093. doi: 10.1093/bioinformatics/btp101
- Bogdan, D. et al. 2018. Fatty acid-binding protein 5 controls microsomal prostaglandin E synthase 1 (mPGES-1) induction during inflammation. *Journal of Biological Chemistry* 293(14), pp. 5295-5306. doi: 10.1074/jbc.ra118.001593
- Breschi, A., Gingeras, T. R. and Guigó, R. 2017. Comparative transcriptomics in human and mouse. *Nature Reviews Genetics* 18(7), pp. 425-440. doi: 10.1038/nrg.2017.19
- Broering, M. F. et al. 2022. Development of Annexin A1-surface-functionalized metal-complex multi-wall lipid core nanocapsules and effectiveness on experimental colitis. *Eur J Pharm Biopharm* 181, pp. 49-59. doi: 10.1016/j.ejpb.2022.10.022
- Brüser, A. et al. 2017. Prostaglandin E2 glyceryl ester is an endogenous agonist of the nucleotide receptor P2Y6. *Scientific Reports* 7(1), doi: 10.1038/s41598-017-02414-8
- Buchschacher, G. L., Yu, L., Murai, F., Friedmann, T. and Miyanochara, A. 1999. Association of Murine Leukemia Virus Pol with Virions, Independent of Gag-Pol Expression. *Journal of Virology* 73(11), pp. 9632-9637. doi: 10.1128/jvi.73.11.9632-9637.1999
- Burke, J. E. and Dennis, E. A. 2009. Phospholipase A2 Biochemistry. *Cardiovascular Drugs and Therapy* 23(1), pp. 49-59. doi: 10.1007/s10557-008-6132-9
- Caballero-Flores, G., Pickard, J. M. and Nunez, G. 2021. Regulation of *Citrobacter rodentium* colonization: virulence, immune response and microbiota interactions. *Curr Opin Microbiol* 63, pp. 142-149. doi: 10.1016/j.mib.2021.07.003
- Carson, D. et al. 2020. *Citrobacter rodentium* induces rapid and unique metabolic and inflammatory responses in mice suffering from severe disease. *Cellular Microbiology* 22(1), doi: 10.1111/cmi.13126
- Casamassimi, A., Federico, A., Rienzo, M., Esposito, S. and Ciccodicola, A. 2017. Transcriptome Profiling in Human Diseases: New Advances and Perspectives. *International Journal of Molecular Sciences* 18(8), p. 1652. doi: 10.3390/ijms18081652
- Cepeda-Molero, M. et al. 2017. Attaching and effacing (A/E) lesion formation by enteropathogenic *E. coli* on human intestinal mucosa is dependent on non-LEE effectors. *PLOS Pathogens* 13(10), p. e1006706. doi: 10.1371/journal.ppat.1006706
- Chan, J. M., Bhinder, G., Sham, H. P., Ryz, N., Huang, T., Bergstrom, K. S. and Vallance, B. A. 2013. CD4+ T Cells Drive Goblet Cell Depletion during *Citrobacter rodentium* Infection. *Infection and Immunity* 81(12), pp. 4649-4658. doi: 10.1128/iai.00655-13

- Chandra, P., Coullon, H., Agarwal, M., Goss, C. W. and Philips, J. A. 2022. Macrophage global metabolomics identifies cholestenone as host/pathogen cometabolite present in human *Mycobacterium tuberculosis* infection. *Journal of Clinical Investigation* 132(3), doi: 10.1172/jci152509
- Chen, W. et al. 2016. MicroRNA-361-3p suppresses tumor cell proliferation and metastasis by directly targeting SH2B1 in NSCLC. *Journal of Experimental & Clinical Cancer Research* 35(1), doi: 10.1186/s13046-016-0357-4
- Chen, Y. and Wang, X. 2020. miRDB: an online database for prediction of functional microRNA targets. *Nucleic Acids Research* 48(D1), pp. D127-D131. doi: 10.1093/nar/gkz757
- Chen, Z. et al. 2021. Foxo1 controls gut homeostasis and commensalism by regulating mucus secretion. *Journal of Experimental Medicine* 218(9), doi: 10.1084/jem.20210324
- Cheng, Y., Duan, C. and Zhang, C. 2020. New perspective on SH2B1: An accelerator of cancer progression. *Biomed Pharmacother* 121, p. 109651. doi: 10.1016/j.biopha.2019.109651
- Cho, E. S., Cha, Y. H., Kim, H. S., Kim, N. H. and Yook, J. I. 2018. The Pentose Phosphate Pathway as a Potential Target for Cancer Therapy. *Biomolecules & Therapeutics* 26(1), pp. 29-38. doi: 10.4062/biomolther.2017.179
- Clare, S. et al. 2013. Enhanced Susceptibility to *Citrobacter rodentium* Infection in MicroRNA-155-Deficient Mice. *Infection and Immunity* 81(3), pp. 723-732. doi: 10.1128/iai.00969-12
- Collins, J. W. et al. 2014a. Fermented Dairy Products Modulate *Citrobacter rodentium*-Induced Colonic Hyperplasia. *The Journal of Infectious Diseases* 210(7), pp. 1029-1041. doi: 10.1093/infdis/jiu205
- Collins, J. W., Keeney, K. M., Crepin, V. F., Rathinam, V. A. K., Fitzgerald, K. A., Finlay, B. B. and Frankel, G. 2014b. *Citrobacter rodentium*: infection, inflammation and the microbiota. *Nature Reviews Microbiology* 12(9), pp. 612-623. doi: 10.1038/nrmicro3315
- Coulombe, F. et al. 2014. Targeted Prostaglandin E2 Inhibition Enhances Antiviral Immunity through Induction of Type I Interferon and Apoptosis in Macrophages. *Immunity* 40(4), pp. 554-568. doi: 10.1016/j.immuni.2014.02.013
- Crepin, V. F., Shaw, R., Abe, C. M., Knutton, S. and Frankel, G. 2005. Polarity of enteropathogenic *Escherichia coli* EspA filament assembly and protein secretion. *J Bacteriol* 187(8), pp. 2881-2889. doi: 10.1128/JB.187.8.2881-2889.2005
- Croxen, M. A. and Finlay, B. B. 2010. Molecular mechanisms of *Escherichia coli* pathogenicity. *Nature Reviews Microbiology* 8(1), pp. 26-38. doi: 10.1038/nrmicro2265

- Croxen, M. A., Law, R. J., Scholz, R., Keeney, K. M., Wlodarska, M. and Finlay, B. B. 2013. Recent Advances in Understanding Enteric Pathogenic *Escherichia coli*. *Clinical Microbiology Reviews* 26(4), pp. 822-880. doi: 10.1128/cmr.00022-13
- Das, K., Garnica, O. and Dhandayuthapani, S. 2016. Modulation of Host miRNAs by Intracellular Bacterial Pathogens. *Frontiers in Cellular and Infection Microbiology* 6, doi: 10.3389/fcimb.2016.00079
- de Jong, T. V., Moshkin, Y. M. and Guryev, V. 2019. Gene expression variability: the other dimension in transcriptome analysis. *Physiol Genomics* 51(5), pp. 145-158. doi: 10.1152/physiolgenomics.00128.2018
- Dean, P., Maresca, M., Ller, S., S., Phillips, A. D. and Kenny, B. 2006. Potent diarrheagenic mechanism mediated by the cooperative action of three enteropathogenic *Escherichia coli*-injected effector proteins. *Proceedings of the National Academy of Sciences* 103(6), pp. 1876-1881. doi: 10.1073/pnas.0509451103
- Dejani, N. N. et al. 2018. Intestinal host defense outcome is dictated by PGE2 production during efferocytosis of infected cells. *Proceedings of the National Academy of Sciences* 115(36), pp. E8469-E8478. doi: 10.1073/pnas.1722016115
- Delacour, D., Salomon, J., Robine, S. and Louvard, D. 2016. Plasticity of the brush border — the yin and yang of intestinal homeostasis. *Nature Reviews Gastroenterology & Hepatology* 13(3), pp. 161-174. doi: 10.1038/nrgastro.2016.5
- Denamur, E., Clermont, O., Bonacorsi, S. and Gordon, D. 2021. The population genetics of pathogenic *Escherichia coli*. *Nature Reviews Microbiology* 19(1), pp. 37-54. doi: 10.1038/s41579-020-0416-x
- Deng, W. et al. 2005. Regulation of Type III Secretion Hierarchy of Translocators and Effectors in Attaching and Effacing Bacterial Pathogens. *Infection and Immunity* 73(4), pp. 2135-2146. doi: 10.1128/iai.73.4.2135-2146.2005
- Deng, W. et al. 2004. Dissecting virulence: Systematic and functional analyses of a pathogenicity island. *Proceedings of the National Academy of Sciences* 101(10), pp. 3597-3602. doi: 10.1073/pnas.0400326101
- Dennis, E. A. and Norris, P. C. 2015. Eicosanoid storm in infection and inflammation. *Nature Reviews Immunology* 15(8), pp. 511-523. doi: 10.1038/nri3859
- Dong, N., Liu, L. and Shao, F. 2010. A bacterial effector targets host DH-PH domain RhoGEFs and antagonizes macrophage phagocytosis. *The EMBO Journal* 29(8), pp. 1363-1376. doi: 10.1038/emboj.2010.33

Donowitz, M. et al. 2010. Alterations in the proteome of the NHERF1 knockout mouse jejunal brush border membrane vesicles. *Physiol Genomics* 42A(3), pp. 200-210. doi: 10.1152/physiolgenomics.00001.2010

Dorris, S. L. and Peebles, R. S. 2012. PGI₂ as a Regulator of Inflammatory Diseases. *Mediators of Inflammation* 2012, pp. 1-9. doi: 10.1155/2012/926968

Dupree, E. J., Jayathirtha, M., Yorkey, H., Mihasan, M., Petre, B. A. and Darie, C. C. 2020. A Critical Review of Bottom-Up Proteomics: The Good, the Bad, and the Future of This Field. *Proteomes* 8(3), p. 14. doi: 10.3390/proteomes8030014

Eckmann, L. et al. 1997. Role of intestinal epithelial cells in the host secretory response to infection by invasive bacteria. Bacterial entry induces epithelial prostaglandin h synthase-2 expression and prostaglandin E2 and F2alpha production. *Journal of Clinical Investigation* 100(2), pp. 296-309. doi: 10.1172/jci119535

Eisenreich, W., Heesemann, J., Rudel, T. and Goebel, W. 2013. Metabolic host responses to infection by intracellular bacterial pathogens. *Frontiers in Cellular and Infection Microbiology* 3, doi: 10.3389/fcimb.2013.00024

Elliott, S. J. et al. 2000. The Locus of Enterocyte Effacement (LEE)-Encoded Regulator Controls Expression of Both LEE- and Non-LEE-Encoded Virulence Factors in Enteropathogenic and Enterohemorrhagic *Escherichia coli*. *Infection and Immunity* 68(11), pp. 6115-6126. doi: 10.1128/iai.68.11.6115-6126.2000

Elliott, S. J. et al. 1998. The complete sequence of the locus of enterocyte effacement (LEE) from enteropathogenic *Escherichia coli* E2348/69. *Molecular Microbiology* 28(1), pp. 1-4. doi: 10.1046/j.1365-2958.1998.00783.x

Escoll, P. and Buchrieser, C. 2018. Metabolic reprogramming of host cells upon bacterial infection: Why shift to a Warburg-like metabolism? *The FEBS Journal* 285(12), pp. 2146-2160. doi: 10.1111/febs.14446

Eulalio, A., Huntzinger, E. and Izaurralde, E. 2008. Getting to the Root of miRNA-Mediated Gene Silencing. *Cell* 132(1), pp. 9-14. doi: 10.1016/j.cell.2007.12.024

Fan, Y., Wang, Y. and Wang, K. 2015. Prostaglandin E2 stimulates normal bronchial epithelial cell growth through induction of c-Jun and PDK1, a kinase implicated in oncogenesis. *Respiratory Research* 16(1), doi: 10.1186/s12931-015-0309-0

Fitzhenry, R. J. 2002. Intimin type influences the site of human intestinal mucosal colonisation by enterohaemorrhagic *Escherichia coli* O157:H7. *Gut* 50(2), pp. 180-185. doi: 10.1136/gut.50.2.180

- Frankel, G. and Phillips, A. D. 2008. Attaching effacing *Escherichia coli* and paradigms of Tir-triggered actin polymerization: getting off the pedestal. *Cellular Microbiology* 10(3), pp. 549-556. doi: 10.1111/j.1462-5822.2007.01103.x
- Frankel, G., Phillips, A. D., Rosenshine, I., Dougan, G., Kaper, J. B. and Knutton, S. 1998. Enteropathogenic and enterohaemorrhagic *Escherichia coli*: more subversive elements. *Molecular Microbiology* 30(5), pp. 911-921. doi: 10.1046/j.1365-2958.1998.01144.x
- Franzin, F. M. and Sircili, M. P. 2015. Locus of enterocyte effacement: a pathogenicity island involved in the virulence of enteropathogenic and enterohemorrhagic *Escherichia coli* subjected to a complex network of gene regulation. *Biomed Res Int* 2015, p. 534738. doi: 10.1155/2015/534738
- Fujiwara, M. et al. 2022. microRNA-92a promotes CNS autoimmunity by modulating the regulatory and inflammatory T cell balance. *Journal of Clinical Investigation* 132(10), doi: 10.1172/jci155693
- Furniss, R. C. D. and Clements, A. 2018. Regulation of the Locus of Enterocyte Effacement in Attaching and Effacing Pathogens. *J Bacteriol* 200(2), doi: 10.1128/JB.00336-17
- Garmendia, J., Frankel, G. and Crepin, V. R. F. 2005. Enteropathogenic and Enterohemorrhagic *Escherichia coli* Infections: Translocation, Translocation, Translocation. *Infection and Immunity* 73(5), pp. 2573-2585. doi: 10.1128/iai.73.5.2573-2585.2005
- Gaytan, M. O., Martinez-Santos, V. I., Soto, E. and Gonzalez-Pedrajo, B. 2016. Type Three Secretion System in Attaching and Effacing Pathogens. *Front Cell Infect Microbiol* 6, p. 129. doi: 10.3389/fcimb.2016.00129
- Ghazalpour, A. et al. 2011. Comparative Analysis of Proteome and Transcriptome Variation in Mouse. *PLoS Genetics* 7(6), p. e1001393. doi: 10.1371/journal.pgen.1001393
- Gibson, D. L. et al. 2010. Interleukin-11 reduces TLR4-induced colitis in TLR2-deficient mice and restores intestinal STAT3 signaling. *Gastroenterology* 139(4), pp. 1277-1288. doi: 10.1053/j.gastro.2010.06.057
- Gomes, T. A. T., Ooka, T., Hernandez, R. T., Yamamoto, D. and Hayashi, T. 2020. *Escherichia albertii* Pathogenesis. *EcoSal Plus* 9(1), doi: 10.1128/ecosalplus.ESP-0015-2019
- Goosney, D. L., Gruenheid, S. and Finlay, B. B. 2000. Gut Feelings: Enteropathogenic *E. coli* (EPEC) Interactions with the Host. *Annual Review of Cell and Developmental Biology* 16(1), pp. 173-189. doi: 10.1146/annurev.cellbio.16.1.173
- Goshe, M. B. and Smith, R. D. 2003. Stable isotope-coded proteomic mass spectrometry. *Curr Opin Biotechnol* 14(1), pp. 101-109. doi: 10.1016/s0958-1669(02)00014-9
- Greco, T. M. and Cristea, I. M. 2017. Proteomics Tracing the Footsteps of Infectious Disease. *Mol Cell Proteomics* 16(4 suppl 1), pp. S5-S14. doi: 10.1074/mcp.O116.066001

- Gu, H. et al. 2017. *Salmonella* produce microRNA-like RNA fragment Sal-1 in the infected cells to facilitate intracellular survival. *Scientific Reports* 7(1), doi: 10.1038/s41598-017-02669-1
- Haider, S. and Pal, R. 2013. Integrated Analysis of Transcriptomic and Proteomic Data. *Current Genomics* 14(2), pp. 91-110. doi: 10.2174/1389202911314020003
- Hall, G. A., Dorn, C. R., Chanter, N., Scotland, S. M., Smith, H. R. and Rowe, B. 1990. Attaching and effacing lesions in vivo and adhesion to tissue culture cells of Vero-cytotoxin-producing *Escherichia coli* belonging to serogroups O5 and O103. *Journal of General Microbiology* 136(4), pp. 779-786. doi: 10.1099/00221287-136-4-779
- Hamon, M. A., Batsché, E., Régnault, B., Tham, T. N., Seveau, S., Muchardt, C. and Cossart, P. 2007. Histone modifications induced by a family of bacterial toxins. *Proceedings of the National Academy of Sciences* 104(33), pp. 13467-13472. doi: 10.1073/pnas.0702729104
- Holmes, A., MüHlen, S., Roe, A. J. and Dean, P. 2010. The EspF Effector, a Bacterial Pathogen's Swiss Army Knife. *Infection and Immunity* 78(11), pp. 4445-4453. doi: 10.1128/iai.00635-10
- Home Office. 2014. *Guidance on the Operation of the Animals (Scientific Procedures) Act 1986 (ASPAs)*. Government of the United Kingdom. Available at: <https://www.gov.uk/guidance/guidance-on-the-operation-of-the-animals-scientific-procedures-act-1986> [Accessed: 7/8/2024].
- Hood, M. I. and Skaar, E. P. 2012. Nutritional immunity: transition metals at the pathogen–host interface. *Nature Reviews Microbiology* 10(8), pp. 525-537. doi: 10.1038/nrmicro2836
- Hopkins, E. G. D. and Frankel, G. 2021. Overview of the Effect of *Citrobacter rodentium* Infection on Host Metabolism and the Microbiota. Springer US, pp. 399-418.
- Hopkins, E. G. D., Roumeliotis, T. I., Mullineaux-Sanders, C., Choudhary, J. S. and Frankel, G. 2019. Intestinal Epithelial Cells and the Microbiome Undergo Swift Reprogramming at the Inception of Colonic *Citrobacter rodentium* Infection. *mBio* 10(2), doi: 10.1128/mBio.00062-19
- Horsley, V. and Pavlath, G. K. 2003. Prostaglandin F₂ α stimulates growth of skeletal muscle cells via an NFATC2-dependent pathway. *Journal of Cell Biology* 161(1), pp. 111-118. doi: 10.1083/jcb.200208085
- Hsu, K.-L., Tsuboi, K., Adibekian, A., Pugh, H., Masuda, K. and Cravatt, B. F. 2012. DAGL β inhibition perturbs a lipid network involved in macrophage inflammatory responses. *Nature Chemical Biology* 8(12), pp. 999-1007. doi: 10.1038/nchembio.1105
- Hu, S. S. J., Bradshaw, H. B., Chen, J. S. C., Tan, B. and Walker, J. M. 2008. Prostaglandin E₂ glycerol ester, an endogenous COX-2 metabolite of 2-arachidonoylglycerol, induces hyperalgesia and modulates NF κ B activity. *British Journal of Pharmacology* 153(7), pp. 1538-1549. doi: 10.1038/bjp.2008.33

- Hua, Y., Yan, K. and Wan, C. 2018. Clever Cooperation: Interactions Between EspF and Host Proteins. *Frontiers in Microbiology* 9, doi: 10.3389/fmicb.2018.02831
- Huang, B. et al. 2022. Development and validation of a novel ubiquitination-related gene prognostic signature based on tumor microenvironment for colon cancer. *Transl Cancer Res* 11(10), pp. 3724-3740. doi: 10.21037/tcr-22-607
- Hunt, J. M. 2010. Shiga toxin-producing *Escherichia coli* (STEC). *Clin Lab Med* 30(1), pp. 21-45. doi: 10.1016/j.cll.2009.11.001
- Huntzinger, E. and Izaurralde, E. 2011. Gene silencing by microRNAs: contributions of translational repression and mRNA decay. *Nature Reviews Genetics* 12(2), pp. 99-110. doi: 10.1038/nrg2936
- Iguchi, A. et al. 2009. Complete Genome Sequence and Comparative Genome Analysis of Enteropathogenic *Escherichia coli* O127:H6 Strain E2348/69. *Journal of Bacteriology* 191(1), pp. 347-354. doi: 10.1128/jb.01238-08
- Iizumi, Y. et al. 2007. The enteropathogenic *E. coli* effector EspB facilitates microvillus effacing and antiphagocytosis by inhibiting myosin function. *Cell Host Microbe* 2(6), pp. 383-392. doi: 10.1016/j.chom.2007.09.012
- Iwanaga, K. et al. 2014. Mast cell-derived prostaglandin D2 inhibits colitis and colitis-associated colon cancer in mice. *Cancer Res* 74(11), pp. 3011-3019. doi: 10.1158/0008-5472.CAN-13-2792
- Jabri, B. and Abadie, V. 2015. IL-15 functions as a danger signal to regulate tissue-resident T cells and tissue destruction. *Nature Reviews Immunology* 15(12), pp. 771-783. doi: 10.1038/nri3919
- Jiang, X. et al. 2021. Mechanism of action and potential applications of selective inhibition of microsomal prostaglandin E synthase-1-mediated PGE2 biosynthesis by sonlicromanol's metabolite KH176m. *Scientific Reports* 11(1), doi: 10.1038/s41598-020-79466-w
- Johnson, J. R. et al. 2022. Global post-translational modification profiling of HIV-1-infected cells reveals mechanisms of host cellular pathway remodeling. *Cell Rep* 39(2), p. 110690. doi: 10.1016/j.celrep.2022.110690
- Jokiranta, T. S. 2017. HUS and atypical HUS. *Blood* 129(21), pp. 2847-2856. doi: 10.1182/blood-2016-11-709865
- Kaper, J. B., Nataro, J. P. and Mobley, H. L. T. 2004. Pathogenic *Escherichia coli*. *Nature Reviews Microbiology* 2(2), pp. 123-140. doi: 10.1038/nrmicro818
- Kaur, P. and Dudeja, P. K. 2023. Pathophysiology of Enteropathogenic *Escherichia coli*-induced Diarrhea. *Newborn (Clarksville)* 2(1), pp. 102-113. doi: 10.5005/jp-journals-11002-0056

- Khan, S. A. and Ilies, M. A. 2023. The Phospholipase A2 Superfamily: Structure, Isozymes, Catalysis, Physiologic and Pathologic Roles. *International Journal of Molecular Sciences* 24(2), p. 1353. doi: 10.3390/ijms24021353
- Kim, M., Otsubo, R., Morikawa, H., Nishide, A., Takagi, K., Sasakawa, C. and Mizushima, T. 2014. Bacterial Effectors and Their Functions in the Ubiquitin-Proteasome System: Insight from the Modes of Substrate Recognition. *Cells* 3(3), pp. 848-864. doi: 10.3390/cells3030848
- Kim, Y. G., Kamada, N., Shaw, M. H., Warner, N., Chen, G. Y., Franchi, L. and Nunez, G. 2011. The Nod2 sensor promotes intestinal pathogen eradication via the chemokine CCL2-dependent recruitment of inflammatory monocytes. *Immunity* 34(5), pp. 769-780. doi: 10.1016/j.immuni.2011.04.013
- Kingsley, P. J., Rouzer, C. A., Morgan, A. J., Patel, S. and Marnett, L. J. 2019. Aspects of Prostaglandin Glycerol Ester Biology. Springer International Publishing, pp. 77-88.
- Knutton, S. 1998. A novel EspA-associated surface organelle of enteropathogenic *Escherichia coli* involved in protein translocation into epithelial cells. *The EMBO Journal* 17(8), pp. 2166-2176. doi: 10.1093/emboj/17.8.2166
- Kodama, T., Akeda, Y., Kono, G., Takahashi, A., Imura, K., Iida, T. and Honda, T. 2002. The EspB protein of enterohaemorrhagic *Escherichia coli* interacts directly with alpha-catenin. *Cellular Microbiology* 4(4), pp. 213-222. doi: 10.1046/j.1462-5822.2002.00176.x
- Köhler, C.-D. and Dobrindt, U. 2011. What defines extraintestinal pathogenic *Escherichia coli*? *International Journal of Medical Microbiology* 301(8), pp. 642-647. doi: 10.1016/j.ijmm.2011.09.006
- Kolobkov, D. S., Sviridova, D. A., Abilev, S. K., Kuzovlev, A. N. and Salnikova, L. E. 2022. Genes and Diseases: Insights from Transcriptomics Studies. *Genes* 13(7), p. 1168. doi: 10.3390/genes13071168
- Koroleva, E. P., Halperin, S., Gubernatorova, E. O., Macho-Fernandez, E., Spencer, C. M. and Tumanov, A. V. 2015. *Citrobacter rodentium*-induced colitis: A robust model to study mucosal immune responses in the gut. *J Immunol Methods* 421, pp. 61-72. doi: 10.1016/j.jim.2015.02.003
- Kramer, A., Green, J., Pollard, J., Jr. and Tugendreich, S. 2014. Causal analysis approaches in Ingenuity Pathway Analysis. *Bioinformatics* 30(4), pp. 523-530. doi: 10.1093/bioinformatics/btt703
- Law, R. J., Gur-Arie, L., Rosenshine, I. and Finlay, B. B. 2013. In Vitro and In Vivo Model Systems for Studying Enteropathogenic *Escherichia coli* Infections. *Cold Spring Harbor Perspectives in Medicine* 3(3), pp. a009977-a009977. doi: 10.1101/cshperspect.a009977
- Lawo, S. et al. 2009. HAUS, the 8-Subunit Human Augmin Complex, Regulates Centrosome and Spindle Integrity. *Current Biology* 19(10), pp. 816-826. doi: 10.1016/j.cub.2009.04.033

- Lee, H. S. and Kim, W. J. 2022. The Role of Matrix Metalloproteinase in Inflammation with a Focus on Infectious Diseases. *International Journal of Molecular Sciences* 23(18), p. 10546. doi: 10.3390/ijms231810546
- Lee, Y., Jeon, K., Lee, J.-T., Kim, S. and Kim, V. N. 2002. MicroRNA maturation: stepwise processing and subcellular localization. *The EMBO Journal* 21(17), pp. 4663-4670. doi: 10.1093/emboj/cdf476
- Leoni, G. et al. 2013. Annexin A1, formyl peptide receptor, and NOX1 orchestrate epithelial repair. *Journal of Clinical Investigation* 123(1), pp. 443-454. doi: 10.1172/jci65831
- Letellier, E. et al. 2014. Identification of SOCS2 and SOCS6 as biomarkers in human colorectal cancer. *British Journal of Cancer* 111(4), pp. 726-735. doi: 10.1038/bjc.2014.377
- Li, H. and Stillman, B. 2012. *The Origin Recognition Complex: A Biochemical and Structural View*. Springer Netherlands, pp. 37-58.
- Li, Z., Wang, Z., Shen, B., Chen, C., Ding, X. and Song, H. 2020. Effects of aspirin on the gastrointestinal tract: Pros vs. cons (Review). *Oncology Letters* 20(3), pp. 2567-2578. doi: 10.3892/ol.2020.11817
- Lin, S. and Gregory, R. I. 2015. MicroRNA biogenesis pathways in cancer. *Nature Reviews Cancer* 15(6), pp. 321-333. doi: 10.1038/nrc3932
- Liu, L., Wong, C. C., Gong, B. and Yu, J. 2018. Functional significance and therapeutic implication of ring-type E3 ligases in colorectal cancer. *Oncogene* 37(2), pp. 148-159. doi: 10.1038/onc.2017.313
- Luo, J., Yang, H. and Song, B.-L. 2020. Mechanisms and regulation of cholesterol homeostasis. *Nature Reviews Molecular Cell Biology* 21(4), pp. 225-245. doi: 10.1038/s41580-019-0190-7
- Lupp, C., Robertson, M. L., Wickham, M. E., Sekirov, I., Champion, O. L., Gaynor, E. C. and Finlay, B. B. 2007. Host-Mediated Inflammation Disrupts the Intestinal Microbiota and Promotes the Overgrowth of Enterobacteriaceae. *Cell Host & Microbe* 2(2), pp. 119-129. doi: 10.1016/j.chom.2007.06.010
- Lyle, C. et al. 2019. c-Cbl targets PD-1 in immune cells for proteasomal degradation and modulates colorectal tumor growth. *Scientific Reports* 9(1), doi: 10.1038/s41598-019-56208-1
- Ma, C. et al. 2006. *Citrobacter rodentium* infection causes both mitochondrial dysfunction and intestinal epithelial barrier disruption in vivo: role of mitochondrial associated protein (Map). *Cellular Microbiology* 8(10), pp. 1669-1686. doi: 10.1111/j.1462-5822.2006.00741.x
- Maculins, T., Fiskin, E., Bhogaraju, S. and Dikic, I. 2016. Bacteria-host relationship: ubiquitin ligases as weapons of invasion. *Cell Research* 26(4), pp. 499-510. doi: 10.1038/cr.2016.30

- Markovic, M. A. and Brubaker, P. L. 2019. The roles of glucagon-like peptide-2 and the intestinal epithelial insulin-like growth factor-1 receptor in regulating microvillus length. *Scientific Reports* 9(1), doi: 10.1038/s41598-019-49510-5
- Maseda, D. et al. 2019. Nonsteroidal Anti-inflammatory Drugs Alter the Microbiota and Exacerbate *Clostridium difficile* Colitis while Dysregulating the Inflammatory Response. *mBio* 10(1), doi: 10.1128/mBio.02282-18
- Matsuzawa, T., Kuwae, A., Yoshida, S., Sasakawa, C. and Abe, A. 2004. Enteropathogenic *Escherichia coli* activates the RhoA signaling pathway via the stimulation of GEF-H1. *The EMBO Journal* 23(17), pp. 3570-3582. doi: 10.1038/sj.emboj.7600359
- Maudet, C., Mano, M. and Eulalio, A. 2014. MicroRNAs in the interaction between host and bacterial pathogens. *FEBS Letters* 588(22), pp. 4140-4147. doi: 10.1016/j.febslet.2014.08.002
- Mccarthy, M. K. et al. 2013. Prostaglandin E2 Induction during Mouse Adenovirus Type 1 Respiratory Infection Regulates Inflammatory Mediator Generation but Does Not Affect Viral Pathogenesis. *PLoS ONE* 8(10), p. e77628. doi: 10.1371/journal.pone.0077628
- Melchior, K., Gerner, R. R., Hossain, S., Nuccio, S. P., Moreira, C. G. and Raffatellu, M. 2024. IL-22-dependent responses and their role during *Citrobacter rodentium* infection. *Infect Immun*, p. e0009924. doi: 10.1128/iai.00099-24
- Michas, A., Michas, V., Anagnostou, E., Galanopoulos, M., Tolia, M. and Tsoukalas, N. 2023. The Clinical Significance of MicroRNAs in Colorectal Cancer Signaling Pathways: A Review. *Global Medical Genetics* 10(04), pp. 315-323. doi: 10.1055/s-0043-1777094
- Mo, C., Zhao, R., Vallejo, J., Igwe, O., Bonewald, L., Wetmore, L. and Brotto, M. 2015. Prostaglandin E2 promotes proliferation of skeletal muscle myoblasts via EP4 receptor activation. *Cell Cycle* 14(10), pp. 1507-1516. doi: 10.1080/15384101.2015.1026520
- Müller, M., Fazi, F. and Ciaudo, C. 2020. Argonaute Proteins: From Structure to Function in Development and Pathological Cell Fate Determination. *Frontiers in Cell and Developmental Biology* 7, doi: 10.3389/fcell.2019.00360
- Mullineaux-Sanders, C., Sanchez-Garrido, J., Hopkins, E. G. D., Shenoy, A. R., Barry, R. and Frankel, G. 2019. *Citrobacter rodentium*–host–microbiota interactions: immunity, bioenergetics and metabolism. *Nature Reviews Microbiology* 17(11), pp. 701-715. doi: 10.1038/s41579-019-0252-z
- Mundy, R., MacDonald, T. T., Dougan, G., Frankel, G. and Wiles, S. 2005. *Citrobacter rodentium* of mice and man. *Cell Microbiol* 7(12), pp. 1697-1706. doi: 10.1111/j.1462-5822.2005.00625.x
- Mundy, R., Pickard, D., Wilson, R. K., Simmons, C. P., Dougan, G. and Frankel, G. 2003. Identification of a novel type IV pilus gene cluster required for gastrointestinal colonization of *Citrobacter rodentium*. *Molecular Microbiology* 48(3), pp. 795-809. doi: 10.1046/j.1365-2958.2003.03470.x

- Murata, T. and Maehara, T. 2016. Discovery of anti-inflammatory role of prostaglandin D2. *Journal of Veterinary Medical Science* 78(11), pp. 1643-1647. doi: 10.1292/jvms.16-0347
- Mutz, K. O., Heilkenbrinker, A., Lonne, M., Walter, J. G. and Stahl, F. 2013. Transcriptome analysis using next-generation sequencing. *Curr Opin Biotechnol* 24(1), pp. 22-30. doi: 10.1016/j.copbio.2012.09.004
- Myung, S. J. et al. 2006. 15-Hydroxyprostaglandin dehydrogenase is an in vivo suppressor of colon tumorigenesis. *Proc Natl Acad Sci U S A* 103(32), pp. 12098-12102. doi: 10.1073/pnas.0603235103
- Na, H.-K., Park, J.-M., Lee, H. G., Lee, H.-N., Myung, S.-J. and Surh, Y.-J. 2011. 15-Hydroxyprostaglandin dehydrogenase as a novel molecular target for cancer chemoprevention and therapy. *Biochemical Pharmacology* 82(10), pp. 1352-1360. doi: 10.1016/j.bcp.2011.08.005
- Nagai, T., Abe, A. and Sasakawa, C. 2005. Targeting of Enteropathogenic *Escherichia coli* EspF to Host Mitochondria Is Essential for Bacterial Pathogenesis. *Journal of Biological Chemistry* 280(4), pp. 2998-3011. doi: 10.1074/jbc.m411550200
- Nancy L. Freeman et al. 2000. Interaction of the Enteropathogenic *Escherichia coli* Protein, Translocated Intimin Receptor (Tir), With Focal Adhesion Proteins. *Cell Motility and the Cytoskeleton* 47, pp. 307-318.
- Nataro, J. P. and Kaper, J. B. 1998. Diarrheagenic *Escherichia coli*. *Clinical Microbiology Reviews* 11(1), pp. 142-201. doi: 10.1128/cmr.11.1.142
- Niaz, S. and Hussain, M. U. 2018. Role of GW182 protein in the cell. *The International Journal of Biochemistry & Cell Biology* 101, pp. 29-38. doi: 10.1016/j.biocel.2018.05.009
- Nolfi-Donagan, D., Braganza, A. and Shiva, S. 2020. Mitochondrial electron transport chain: Oxidative phosphorylation, oxidant production, and methods of measurement. *Redox Biol* 37, p. 101674. doi: 10.1016/j.redox.2020.101674
- Nougayrede, J.-P. and Sonnenberg, M. S. 2004. Enteropathogenic *Escherichia coli* EspF is targeted to mitochondria and is required to initiate the mitochondrial death pathway. *Cellular Microbiology* 6(11), pp. 1097-1111. doi: 10.1111/j.1462-5822.2004.00421.x
- O'Neill, G. P. and Ford-Hutchinson, A. W. 1993. Expression of mRNA for cyclooxygenase-1 and cyclooxygenase-2 in human tissues. *FEBS Letters* 330(2), pp. 157-160. doi: 10.1016/0014-5793(93)80263-t
- Oyesola, O. O. and Tait Wojno, E. D. 2021. Prostaglandin regulation of type 2 inflammation: From basic biology to therapeutic interventions. *European Journal of Immunology* 51(10), pp. 2399-2416. doi: 10.1002/eji.202048909

- Pakbin, B., Brück, W. M. and Rossen, J. W. A. 2021. Virulence Factors of Enteric Pathogenic *Escherichia coli*: A Review. *International Journal of Molecular Sciences* 22(18), p. 9922. doi: 10.3390/ijms22189922
- Palmer, B. R. and Marinus, M. G. 1994. The dam and dcm strains of *Escherichia coli*-a review. *Gene* 143(1), pp. 1-12. doi: 10.1016/0378-1119(94)90597-5
- Palmer, L. D. and Skaar, E. P. 2019. Cuts Both Ways: Proteases Modulate Virulence of Enterohemorrhagic *Escherichia coli*. *mBio* 10 (1), pp. e00115-00119. doi: 10.1128/mbio.00115-19
- Papapietro, O. et al. 2013. R-Spondin 2 signalling mediates susceptibility to fatal infectious diarrhoea. *Nature Communications* 4(1), p. 1898. doi: 10.1038/ncomms2816
- Papatheodorou, P., Domanska, G., Oxle, M., Mathieu, J., Selchow, O., Kenny, B. and Rassow, J. 2006. The enteropathogenic *Escherichia coli* (EPEC) Map effector is imported into the mitochondrial matrix by the TOM/Hsp70 system and alters organelle morphology. *Cellular Microbiology* 8(4), pp. 677-689. doi: 10.1111/j.1462-5822.2005.00660.x
- Patel, F. A. and Challis, J. R. 2002. Cortisol/progesterone antagonism in regulation of 15-hydroxysteroid dehydrogenase activity and mRNA levels in human chorion and placental trophoblast cells at term. *J Clin Endocrinol Metab* 87(2), pp. 700-708. doi: 10.1210/jcem.87.2.8245
- Perna, N. T., Mayhew, G. F., Pósfai, G. R., Elliott, S., Sonnenberg, M. S., Kaper, J. B. and Blattner, F. R. 1998. Molecular Evolution of a Pathogenicity Island from Enterohemorrhagic *Escherichia coli* O157:H7. *Infection and Immunity* 66(8), pp. 3810-3817. doi: 10.1128/iai.66.8.3810-3817.1998
- Pettus, B. J. et al. 2003. The sphingosine kinase 1/phingosine-1-phosphate pathway mediates COX-2 induction and PGE2 production in response to TNF- α . *The FASEB Journal* 17(11), pp. 1411-1421. doi: 10.1096/fj.02-1038com
- Petty, N. K. et al. 2010. The *Citrobacter rodentium* Genome Sequence Reveals Convergent Evolution with Human Pathogenic *Escherichia coli*. *Journal of Bacteriology* 192(2), pp. 525-538. doi: 10.1128/jb.01144-09
- Pfanner, N., Warscheid, B. and Wiedemann, N. 2019. Mitochondrial proteins: from biogenesis to functional networks. *Nature Reviews Molecular Cell Biology* 20(5), pp. 267-284. doi: 10.1038/s41580-018-0092-0
- Piscatelli, H. et al. 2011. The EHEC Type III Effector NleL Is an E3 Ubiquitin Ligase That Modulates Pedestal Formation. *PLoS ONE* 6(4), p. e19331. doi: 10.1371/journal.pone.0019331
- Platenkamp, A. and Mellies, J. L. 2018. Environment Controls LEE Regulation in Enteropathogenic *Escherichia coli*. *Frontiers in Microbiology* 9, doi: 10.3389/fmicb.2018.01694

- Popov, G. et al. 2023. Distinct Molecular Features of NleG Type 3 Secreted Effectors Allow for Different Roles during *Citrobacter rodentium* Infection in Mice. *Infect Immun* 91(1), p. e0050522. doi: 10.1128/iai.00505-22
- Public Health England. 2024. *Shiga toxin-producing Escherichia coli (STEC) data: 2021*. Available at: <https://www.gov.uk/government/publications/escherichia-coli-e-coli-o157-annual-totals/shiga-toxin-producing-escherichia-coli-stec-data-2021> [Accessed: 17/06/2024].
- Ramachandran, R. P. et al. 2020. Mitochondrial Targeting of the Enteropathogenic *Escherichia coli* Map Triggers Calcium Mobilization, ADAM10-MAP Kinase Signaling, and Host Cell Apoptosis. *mBio* 11(5), doi: 10.1128/mBio.01397-20
- Rashid, F., Zaongo, S. D., Song, F. and Chen, Y. 2023. The diverse roles of miRNAs in HIV pathogenesis: Current understanding and future perspectives. *Frontiers in Immunology* 13, doi: 10.3389/fimmu.2022.1091543
- Raymond, B., Crepin, V. F., Collins, J. W. and Frankel, G. 2011. The WxxxE effector EspT triggers expression of immune mediators in an Erk/JNK and NF- κ B-dependent manner. *Cellular Microbiology* 13(12), pp. 1881-1893. doi: 10.1111/j.1462-5822.2011.01666.x
- Rego, N., Libisch, M. G., Rovira, C., Tosar, J. P. and Robello, C. 2023. Comparative microRNA profiling of *Trypanosoma cruzi* infected human cells. *Frontiers in Cellular and Infection Microbiology* 13, doi: 10.3389/fcimb.2023.1187375
- Ricciotti, E. and Fitzgerald, G. A. 2011. Prostaglandins and Inflammation. *Arteriosclerosis, Thrombosis, and Vascular Biology* 31(5), pp. 986-1000. doi: 10.1161/atvbaha.110.207449
- Robins-Browne, R. M., Holt, K. E., Ingle, D. J., Hocking, D. M., Yang, J. and Tauschek, M. 2016. Are *Escherichia coli* Pathotypes Still Relevant in the Era of Whole-Genome Sequencing? *Frontiers in Cellular and Infection Microbiology* 6, doi: 10.3389/fcimb.2016.00141
- Rodrigues, D. M. et al. 2012. Matrix metalloproteinase 9 contributes to gut microbe homeostasis in a model of infectious colitis. *BMC Microbiology* 12(1), p. 105. doi: 10.1186/1471-2180-12-105
- Rojas-Lopez, M., Monterio, R., Pizza, M., Desvaux, M. and Rosini, R. 2018. Intestinal Pathogenic *Escherichia coli*: Insights for Vaccine Development. *Front Microbiol* 9, p. 440. doi: 10.3389/fmicb.2018.00440
- Roy, B. C. et al. 2015. Role of bacterial infection in the epigenetic regulation of Wnt antagonist WIF1 by PRC2 protein EZH2. *Oncogene* 34(34), pp. 4519-4530. doi: 10.1038/onc.2014.386
- Ruano-Gallego, D. et al. 2021. Type III secretion system effectors form robust and flexible intracellular virulence networks. *Science* 371(6534), p. eabc9531. doi: 10.1126/science.abc9531

- Ryu, J., Otsubo, R., Ashida, H., Iida, T., Abe, A., Sasakawa, C. and Mimuro, H. 2021. CBL-C E3 ubiquitin ligase acts as a host defense to mediate ubiquitin-proteasomal degradation of enteropathogenic *Escherichia coli* Tir protein. bioRxiv: Cold Spring Harbor Laboratory.
- Sahr, T., Escoll, P., Rusniok, C., Bui, S., Pehau-Arnaudet, G., Lavieu, G. and Buchrieser, C. 2022. Translocated *Legionella pneumophila* small RNAs mimic eukaryotic microRNAs targeting the host immune response. *Nature Communications* 13(1), doi: 10.1038/s41467-022-28454-x
- Saliminejad, K., Khorram Khorshid, H. R., Soleymani Fard, S. and Ghaffari, S. H. 2019. An overview of microRNAs: Biology, functions, therapeutics, and analysis methods. *Journal of Cellular Physiology* 234(5), pp. 5451-5465. doi: 10.1002/jcp.27486
- Sander, W. J., O'Neill, H. G. and Pohl, C. H. 2017. Prostaglandin E2 As a Modulator of Viral Infections. *Front Physiol* 8, p. 89. doi: 10.3389/fphys.2017.00089
- Scaletsky, I. C., Pedroso, M. Z. and Fagundes-Neto, U. 1996. Attaching and effacing enteropathogenic *Escherichia coli* O18ab invades epithelial cells and causes persistent diarrhea. *Infection and Immunity* 64(11), pp. 4876-4881. doi: 10.1128/iai.64.11.4876-4881.1996
- Schauer, D. B. and Falkow, S. 1993. Attaching and effacing locus of a *Citrobacter freundii* biotype that causes transmissible murine colonic hyperplasia. *Infect Immun* 61(6), pp. 2486-2492. doi: 10.1128/iai.61.6.2486-2492.1993
- Scheffner, M., Werness, B. A., Huibregtse, J. M., Levine, A. J. and Howley, P. M. 1990. The E6 oncoprotein encoded by human papillomavirus types 16 and 18 promotes the degradation of p53. *Cell* 63(6), pp. 1129-1136. doi: 10.1016/0092-8674(90)90409-8
- Schwanhäusser, B. et al. 2011. Global quantification of mammalian gene expression control. *Nature* 473(7347), pp. 337-342. doi: 10.1038/nature10098
- Serapio-Palacios, A. and Finlay, B. B. 2020. Dynamics of expression, secretion and translocation of type III effectors during enteropathogenic *Escherichia coli* infection. *Current Opinion in Microbiology* 54, pp. 67-76. doi: 10.1016/j.mib.2019.12.001
- Shames, S. R., Croxen, M. A., Deng, W. and Finlay, B. B. 2011. The type III system-secreted effector EspZ localizes to host mitochondria and interacts with the translocase of inner mitochondrial membrane 17b. *Infect Immun* 79(12), pp. 4784-4790. doi: 10.1128/IAI.05761-11
- Shames, S. R. et al. 2010. The pathogenic *E. coli* type III effector EspZ interacts with host CD98 and facilitates host cell prosurvival signalling. *Cellular Microbiology* 12(9), pp. 1322-1339. doi: 10.1111/j.1462-5822.2010.01470.x
- Sharba, S. et al. 2019. Formyl peptide receptor 2 orchestrates mucosal protection against *Citrobacter rodentium* infection. *Virulence* 10(1), pp. 610-624. doi: 10.1080/21505594.2019.1635417

- Shen, A. et al. 2022. Down-Regulating HAUS6 Suppresses Cell Proliferation by Activating the p53/p21 Pathway in Colorectal Cancer. *Frontiers in Cell and Developmental Biology* 9, doi: 10.3389/fcell.2021.772077
- Shenoy, A. R., Furniss, R. C. D., Goddard, P. J. and Clements, A. 2018. Modulation of Host Cell Processes by T3SS Effectors. *Curr Top Microbiol Immunol* 416, pp. 73-115. doi: 10.1007/82_2018_106
- Shi, C. Y., Kingston, E. R., Kleaveland, B., Lin, D. H., Stubna, M. W. and Bartel, D. P. 2020. The ZSWIM8 ubiquitin ligase mediates target-directed microRNA degradation. *Science* 370(6523), doi: 10.1126/science.abc9359
- Silberger, D. J., Zindl, C. L. and Weaver, C. T. 2017. *Citrobacter rodentium*: a model enteropathogen for understanding the interplay of innate and adaptive components of type 3 immunity. *Mucosal Immunology* 10(5), pp. 1108-1117. doi: 10.1038/mi.2017.47
- Slater, S. L. and Frankel, G. 2020. Advances and Challenges in Studying Type III Secretion Effectors of Attaching and Effacing Pathogens. *Frontiers in Cellular and Infection Microbiology* 10, doi: 10.3389/fcimb.2020.00337
- Slater, S. L., Sagfors, A. M., Pollard, D. J., Ruano-Gallego, D. and Frankel, G. 2018. The Type III Secretion System of Pathogenic *Escherichia coli*. *Curr Top Microbiol Immunol* 416, pp. 51-72. doi: 10.1007/82_2018_116
- Smibert, P., Yang, J.-S., Azzam, G., Liu, J.-L. and Lai, E. C. 2013. Homeostatic control of Argonaute stability by microRNA availability. *Nature Structural & Molecular Biology* 20(7), pp. 789-795. doi: 10.1038/nsmb.2606
- Sobah, M. L., Liongue, C. and Ward, A. C. 2021. SOCS Proteins in Immunity, Inflammatory Diseases, and Immune-Related Cancer. *Frontiers in Medicine* 8, doi: 10.3389/fmed.2021.727987
- Sora, V. M., Meroni, G., Martino, P. A., Soggiu, A., Bonizzi, L. and Zecconi, A. 2021. Extraintestinal Pathogenic *Escherichia coli*: Virulence Factors and Antibiotic Resistance. *Pathogens* 10(11), p. 1355. doi: 10.3390/pathogens10111355
- Stecher, B. and Hardt, W. D. 2011. Mechanisms controlling pathogen colonization of the gut. *Curr Opin Microbiol* 14(1), pp. 82-91. doi: 10.1016/j.mib.2010.10.003
- Stevens, M. P. and Frankel, G. M. 2015. The Locus of Enterocyte Effacement and Associated Virulence Factors of Enterohemorrhagic *Escherichia coli*. *Enterohemorrhagic Escherichia coli and Other Shiga Toxin-Producing E. coli*. pp. 97-130.
- Stewart, S. A. et al. 2003. Lentivirus-delivered stable gene silencing by RNAi in primary cells. *RNA* 9(4), pp. 493-501. doi: 10.1261/rna.2192803

- Stockinger, B. 2021. T cell subsets and environmental factors in *Citrobacter rodentium* infection. *Current Opinion in Microbiology* 63, pp. 92-97. doi: 10.1016/j.mib.2021.06.006
- Strzalka, W. and Ziemienowicz, A. 2011. Proliferating cell nuclear antigen (PCNA): a key factor in DNA replication and cell cycle regulation. *Ann Bot* 107(7), pp. 1127-1140. doi: 10.1093/aob/mcq243
- Sun, A., Chen, Y., Tian, X. and Lin, Q. 2023. The Role of HECT E3 Ubiquitin Ligases in Colorectal Cancer. *Biomedicines* 11(2), p. 478. doi: 10.3390/biomedicines11020478
- Szrok-Jurga, S., Czumaj, A., Turyn, J., Hebanowska, A., Swierczynski, J., Sledzinski, T. and Stelmanska, E. 2023. The Physiological and Pathological Role of Acyl-CoA Oxidation. *International Journal of Molecular Sciences* 24(19), p. 14857. doi: 10.3390/ijms241914857
- Tang, B. et al. 2012. Compromised autophagy by MIR30B benefits the intracellular survival of *Helicobacter pylori*. *Autophagy* 8(7), pp. 1045-1057. doi: 10.4161/auto.20159
- Tenaillon, O., Skurnik, D., Picard, B. and Denamur, E. 2010. The population genetics of commensal *Escherichia coli*. *Nature Reviews Microbiology* 8(3), pp. 207-217. doi: 10.1038/nrmicro2298
- Teslaa, T., Ralser, M., Fan, J. and Rabinowitz, J. D. 2023. The pentose phosphate pathway in health and disease. *Nature Metabolism* 5(8), pp. 1275-1289. doi: 10.1038/s42255-023-00863-2
- Tobelaim, W. S. et al. 2015. Tumour-promoting role of SOCS1 in colorectal cancer cells. *Scientific Reports* 5(1), p. 14301. doi: 10.1038/srep14301
- Tomson, F. L. et al. 2005. Enteropathogenic *Escherichia coli* EspG disrupts microtubules and in conjunction with Orf3 enhances perturbation of the tight junction barrier. *Molecular Microbiology* 56(2), pp. 447-464. doi: 10.1111/j.1365-2958.2005.04571.x
- Tong, T., Zhou, Y., Huang, Q., Xiao, C., Bai, Q., Deng, B. and Chen, L. 2023. The regulation roles of miRNAs in *Helicobacter pylori* infection. *Clinical and Translational Oncology* 25(7), pp. 1929-1939. doi: 10.1007/s12094-023-03094-9
- Trabulsi, L. R., Keller, R., Gomes, T.A.T. 2002. Typical and Atypical Enteropathogenic *Escherichia coli*. *Emerging Infectious Diseases* 8, 508–513, doi: 10.3201/eid0805.010385
- Tran, S.-L., Jenkins, C., Livrelli, V. and Schüller, S. 2018. Shiga toxin 2 translocation across intestinal epithelium is linked to virulence of Shiga toxin-producing *Escherichia coli* in humans. *Microbiology* 164(4), pp. 509-516. doi: 10.1099/mic.0.000645
- Tu, X., Nisan, I., Yona, C., Hanski, E. and Rosenshine, I. 2003. EspH, a new cytoskeleton-modulating effector of enterohaemorrhagic and enteropathogenic *Escherichia coli*. *Molecular Microbiology* 47(3), pp. 595-606. doi: 10.1046/j.1365-2958.2003.03329.x

- Vainio, P. et al. 2011. Arachidonic acid pathway members PLA2G7, HPGD, EPHX2, and CYP4F8 identified as putative novel therapeutic targets in prostate cancer. *Am J Pathol* 178(2), pp. 525-536. doi: 10.1016/j.ajpath.2010.10.002
- Vallance, B. A. and Finlay, B. B. 2000. Exploitation of host cells by enteropathogenic *Escherichia coli*. *Proceedings of the National Academy of Sciences* 97(16), pp. 8799-8806. doi: 10.1073/pnas.97.16.8799
- Vander Heiden, M. G., Cantley, L. C. and Thompson, C. B. 2009. Understanding the Warburg Effect: The Metabolic Requirements of Cell Proliferation. *Science* 324(5930), pp. 1029-1033. doi: 10.1126/science.1160809
- Varet, H., Brillet-Guéguen, L., Coppée, J.-Y. and Dillies, M.-A. 2016. SARTools: A DESeq2- and EdgeR-Based R Pipeline for Comprehensive Differential Analysis of RNA-Seq Data. *PLoS ONE* 11(6), p. e0157022. doi: 10.1371/journal.pone.0157022
- Vitale, S., Picascia, S. and Gianfrani, C. 2016. The cross-talk between enterocytes and intraepithelial lymphocytes. *Molecular and Cellular Pediatrics* 3(1), doi: 10.1186/s40348-016-0048-4
- Vogel, C. and Marcotte, E. M. 2012. Insights into the regulation of protein abundance from proteomic and transcriptomic analyses. *Nature Reviews Genetics* 13(4), pp. 227-232. doi: 10.1038/nrg3185
- Vossen, M. T., Westerhout, E. M., Söderberg-Nauclér, C. and Wiertz, E. J. 2002. Viral immune evasion: a masterpiece of evolution. *Immunogenetics* 54(8), pp. 527-542. doi: 10.1007/s00251-002-0493-1
- Wahid, F., Shehzad, A., Khan, T. and Kim, Y. Y. 2010. MicroRNAs: synthesis, mechanism, function, and recent clinical trials. *Biochim Biophys Acta* 1803(11), pp. 1231-1243. doi: 10.1016/j.bbamcr.2010.06.013
- Wales, A. D., Woodward, M. J. and Pearson, G. R. 2005. Attaching-effacing bacteria in animals. *J Comp Pathol* 132(1), pp. 1-26. doi: 10.1016/j.jcpa.2004.09.005
- Wang, B. et al. 2021. Metabolism pathways of arachidonic acids: mechanisms and potential therapeutic targets. *Signal Transduction and Targeted Therapy* 6(1), doi: 10.1038/s41392-020-00443-w
- Wang, D. and Dubois, R. N. 2010. Eicosanoids and cancer. *Nature Reviews Cancer* 10(3), pp. 181-193. doi: 10.1038/nrc2809
- Wang, L., Yan, J., Niu, H., Huang, R. and Wu, S. 2018. Autophagy and Ubiquitination in *Salmonella* Infection and the Related Inflammatory Responses. *Frontiers in Cellular and Infection Microbiology* 8, doi: 10.3389/fcimb.2018.00078

- Wang, W. S., Guo, C. M. and Sun, K. 2020. Cortisol Regeneration in the Fetal Membranes, A Coincidental or Requisite Event in Human Parturition? *Front Physiol* 11, p. 462. doi: 10.3389/fphys.2020.00462
- Wautier, J.-L. and Wautier, M.-P. 2023. Pro- and Anti-Inflammatory Prostaglandins and Cytokines in Humans: A Mini Review. *International Journal of Molecular Sciences* 24(11), p. 9647. doi: 10.3390/ijms24119647
- Welinder-Olsson, C. and Kaijser, B. 2005. Enterohemorrhagic *Escherichia coli* (EHEC). *Scandinavian Journal of Infectious Diseases* 37(6-7), pp. 405-416. doi: 10.1080/00365540510038523
- Wen, B., Tokar, T., Taibi, A., Chen, J., Jurisica, I. and Comelli, E. M. 2019. *Citrobacter rodentium* alters the mouse colonic miRNome. *Genes Immun* 20(3), pp. 207-213. doi: 10.1038/s41435-018-0026-z
- WHO. 2018. *E. coli*. Available at: <https://www.who.int/newsroom/fact-sheets/detail/e-coli> [Accessed: 05/12/2023].
- WHO. 2022. *Food safety*. Available at: <https://www.who.int/news-room/fact-sheets/detail/food-safety> [Accessed: 05/12/2023].
- WHO. 2023. *Immunization, Vaccines and Biologicals department*. Available at: <https://www.who.int/teams/immunization-vaccines-andbiologicals/diseases> [Accessed: 06/12/2023].
- WHO. 2024. *Diarrhoeal disease*. Available at: <https://www.who.int/news-room/fact-sheets/detail/diarrhoeal-disease> [Accessed: 01/09/2024].
- Wong, A. R. C. et al. 2011. Enteropathogenic and enterohaemorrhagic *Escherichia coli*: even more subversive elements. *Molecular Microbiology* 80(6), pp. 1420-1438. doi: 10.1111/j.1365-2958.2011.07661.x
- Xiao, Y. et al. 2019. Interleukin-33 Promotes REG3 γ Expression in Intestinal Epithelial Cells and Regulates Gut Microbiota. *Cellular and Molecular Gastroenterology and Hepatology* 8(1), pp. 21-36. doi: 10.1016/j.jcmgh.2019.02.006
- Xicohtencatl-Cortes, J. et al. 2007. Intestinal adherence associated with type IV pili of enterohemorrhagic *Escherichia coli* O157:H7. *Journal of Clinical Investigation* 117(11), pp. 3519-3529. doi: 10.1172/jci30727
- Xu, H. et al. 2024. MicroRNAs in *Helicobacter pylori*-infected gastric cancer: Function and clinical application. *Pharmacol Res* 205, p. 107216. doi: 10.1016/j.phrs.2024.107216
- Yan, M. et al. 2004. 15-Hydroxyprostaglandin dehydrogenase, a COX-2 oncogene antagonist, is a TGF-beta-induced suppressor of human gastrointestinal cancers. *Proc Natl Acad Sci U S A* 101(50), pp. 17468-17473. doi: 10.1073/pnas.0406142101

Yang, Y. H., Morand, E. and Leech, M. 2013. Annexin A1: potential for glucocorticoid sparing in RA. *Nat Rev Rheumatol* 9(10), pp. 595-603. doi: 10.1038/nrrheum.2013.126

Yerushalmi, G., Litvak, Y., Gur-Arie, L. and Rosenshine, I. 2014. Dynamics of Expression and Maturation of the Type III Secretion System of Enteropathogenic *Escherichia coli*. *Journal of Bacteriology* 196(15), pp. 2798-2806. doi: 10.1128/jb.00069-14

Zhang, Z., Wang, M., Eisel, F., Tchatalbachev, S., Chakraborty, T., Meinhardt, A. and Bhushan, S. 2016. Uropathogenic *Escherichia coli* Epigenetically Manipulate Host Cell Death Pathways. *J Infect Dis* 213(7), pp. 1198-1207. doi: 10.1093/infdis/jiv569

Zhao, J., Wen, S., Wang, X. and Zhang, Z. 2017. *Helicobacter pylori* modulates cyclooxygenase-2 and 15-hydroxy prostaglandin dehydrogenase in gastric cancer. *Oncology Letters*, doi: 10.3892/ol.2017.6843

Zhou, X., Li, X. and Wu, M. 2018. miRNAs reshape immunity and inflammatory responses in bacterial infection. *Signal Transduction and Targeted Therapy* 3(1), doi: 10.1038/s41392-018-0006-9

Zou, M., Zeng, Q.-S., Nie, J., Yang, J.-H., Luo, Z.-Y. and Gan, H.-T. 2021. The Role of E3 Ubiquitin Ligases and Deubiquitinases in Inflammatory Bowel Disease: Friend or Foe? *Frontiers in Immunology* 12, doi: 10.3389/fimmu.2021.769167